UNIVERSITY OF LIVERPOOL

Morphology Control in Colloidal Metal Nanoparticle Synthesis and their Application to Catalysis

This dissertation is submitted in accordance with the requirements of the University of Liverpool for the degree of Doctor of Philosophy

by

Romen Herrera Padilla

April 2018

Acknowledgments

First and foremost, I would like to thank Dr Priecel and Dr Zhong for their massive contribution, without them, I would have walked out of any clear direction. Their guidance and continuous help have been crucial, and I will forever be grateful for their kindness and encouragement. It has been a true honour to work with such professional and brilliant scientists like you, and very enriching to share all these years. Thank you so much!

Very special thanks go to Eduardo and specially the most beautiful, kind and smart girl from Cordoba, Mi Arma. Your contribution has been priceless, and I wish you all the best for the brilliant future you have ahead. I would also like to thank all the members PhD students, Master students, Post-Docs, etc… in Liverpool for their friendliness, stories and good times shared. I also want to give a big thanks to all the people in Singapore who made my time over there unforgettable.

Dr Cuñado, sabes lo enormemente agradecido que te estoy y solo espero que la amistad que hemos creado durante estos años dure para siempre.

A mi familia, Mama, Papa… no se que haria sin vosotros, os quiero mucho!

A mi abuela Maruca, siempre te voy a llevar en el corazon!

Por ultimo y mas importante, Tony, no creo que haya forma de expresarte lo agradecido que te estoy. Todavia recuerdo como si fuera ayer mismo la primera vez que te vi. Estare eternamente en deuda contigo y no creo que haya forma de pagarte esta oportunidad que me has dado. El respeto que te tengo como el excelente cientifico que eres no es ni por asomo comparable al aprecio y admiracion que te tengo como persona. Tu calidad humana, bondad e integridad estan fuera del alcance de la mayoria de mortales y si hubieran unas pocas personas mas como tu, el mundo seria definitivamente un lugar mejor. Ha sido un verdadero honor, GRACIAS!

Abstract

In this thesis, new synthesis methodologies for colloidal metal spherical and anisotropic nanoparticles have been probed in order to study their size-shape effect and to test their catalytic capability.

There is a growing amount of studies of the properties, structure and catalytic capabilities of noble metal nanoparticles such as gold (Au), silver (Ag), palladium (Pd) or platinum (Pt) that have formed the basis for preparation of new heterogeneous catalysts that can be used to improve reactivity in chemical reactions such as selective oxidations, selective reductions or photocatalysis.

If we are capable to understand the effects that size and shape will have on the properties of metal nanoparticles and establish a correlation between these and the catalytic activity, we would be able to develop catalysts supporting a specific reaction with great yield (high conversion and selectivity). Hence, the scope of this project has been to understand the synthesis methods of different nanoparticle morphologies, using mainly first, sonication-assisted method for spherical nanoparticles, and particularly gold anisotropic nanoparticles such as gold nanorods (AuNRs) and gold nanostars (AuNSs) methods, to finally support these noble metal nanoparticles and find out their catalytic activity. This should lead to new heterogeneous catalysts that can show enhanced activity in a number of important reactions, such as selective oxidations or reductions, photocatalysis and other future applications.

This work aims to develop a rapid and efficient strategy for preparing supported metal catalysts for catalytic applications. The sonication-assisted reduction-precipitation method was employed to prepare the heterogeneous mono- and bi-metallic catalysts for photocatalytic degradation of Methyl Orange (MO) and preferential oxidation (PROX) of CO in H_2-rich gas. In general, there are three advantages for the sonication-assisted method as compared with the conventional methods, including high dispersion of metal nanoparticles on the catalyst support, the much higher deposition efficiency (DE) than those of the deposition-precipitation (DP) and co-precipitation (CP) methods, and the very fast preparation, which only lasts 10-20 seconds for the

deposition. In the AuPd/TiO_2 catalysts series, the AuPd(3:1)/TiO_2 catalyst is the most active for MO photocatalytic degradation; while for PROX reaction, Ru/TiO_2, Au-Cu/SBA-15 and Pt/γ-Al_2O_3 catalysts are very active, and the last one showed high stability in the lifetime test. The structural characterization revealed that in the AuPd(3:1)/TiO_2 catalyst, Au-Pd alloy particles were formed and a high percentage of Au atoms was located at the surface. Therefore, this sonication-assisted method is efficient and rapid in the preparation of supported metal catalysts with obvious structural characteristics for various catalytic applications.

The aim of this project has been to understand the synthesis of various morphologies of noble metal nanoparticles. These and their specific properties can be then explored in supported form in different chemical transformations. Thus, colloidal synthesis methods provide us with optimum control of nanoparticles morphologies for different shapes with a narrow particle size distribution. So, we will use the advantages of these methods to immobilize the different nanoparticles synthesized using the sol-immobilization method for this purpose.

Finally, this study has demonstrated that anisotropic gold nanoparticles nanorods (AuNRs) and nanostars (AuNSs) possess catalytic activity for reactions such as reduction of 4-nitrophenol in the case of AuNSs, selective oxidation of hydroxymethylfurfural (HMF) for AuNRs and photodegradation of Methyl Orange (MO) for both anisotropic structures. We have also supported them for the first time on titania via sol-immobilization method, showing that supported nanoparticles are stable and can be used long term.

Table of Contents

Chapter 1

Literature Overview

1 Literature Overview

1.1 Introduction

In a world of exponential growth in energy demand and high consumption of non-renewable resources, catalysis will need to play an indispensable part in materials science, chemical production, energy storage, and environmental remediation. Conventional heterogeneous catalysis heavily relies on high operating temperatures because of large activation energy barriers and thus suffers from numerous negative side effects: low energy efficiencies for inherent exothermic reactions, rapid deactivation of catalytic centres, poor selectivity for most partial redox reactions, and sometimes harsh operating conditions (1-3). Recent developments in nanotechnology affords the synthesis of well-defined metal nanoparticles for catalysts that could provide tools to improve this situation in chemocatalytic applications.

Nanoscience is the scientific area that is dedicated to the creation and study of nano-scale materials. It has required the development of innovative design and manipulation techniques of these systems, known today as nanotechnology (4), to understand and explore all the possibilities that nanotechnology could provide scientific society. The interest in this science lies in the new possibilities offered by the miniaturization of the systems and in the novel properties that these present (5-8).

Currently, the most studied nanometric systems have been those composed of metals, semiconductors (9, 10) and magnetic materials (11-13). In relation to metals, gold and silver are noteworthy due to their high stability and the ease with which they can be functionalized on the surface (14-17).

The reason for the boom in study of these systems (specifically gold) was due to the promising applications that have both in the energy field and in catalysis (18-23), like in biological (13, 24, 25) and biomedical (5, 26-28) applications. Most of the possible applications of these systems are based on the understanding of the properties that gold presents at the nanometre scale in comparison to bulk gold. According to band theory (29, 30), when gold is in bulk form, the electrons that are in the conduction band are highly delocalised (not confined), because the energy levels are very close to each

other, imparting these electrons with the ability to absorb electromagnetic radiation in a multitude of energy ranges. However, this property changes with reduction of particle size down to the nanometre scale (3, 31, 32), because the superficial electrons experience quantum confinement (**Figure 1.1**). This effect occurs when the wavelength associated with these electrons is of the same order as the particle size (the de Broglie wavelength), since at this point, the particles behave like quantum potential boxes, where the electrons get trapped.

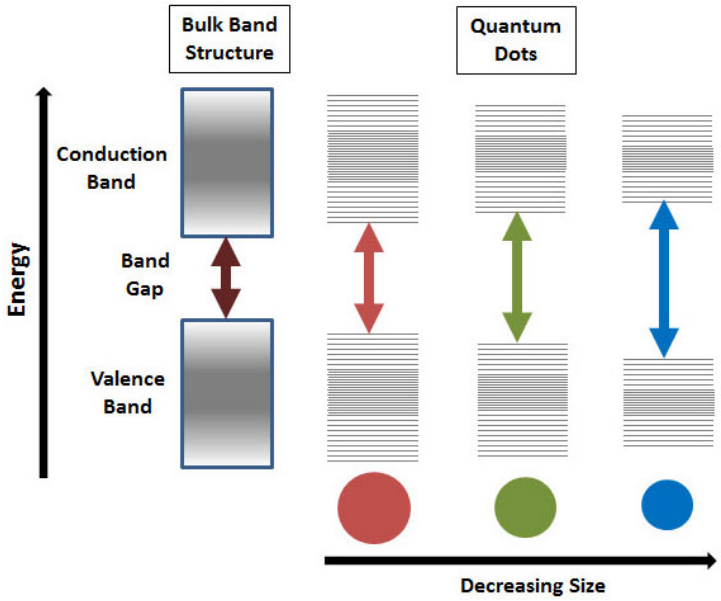

Figure 1.1. Schematic representation of the phenomenon of quantum confinement.

The direct consequence of the decrease in particle size is an increase of the energy gap between consecutive energy states up to a critical size, where energy levels take discrete values. In summary, how much smaller the space in which the movement of electrons is allowed, the greater the energy separation between the allowed energies due to quantum confinement (33).

As a consequence of this confinement, when light falls on a gold nanoparticle, the electric field of the radiation excites the electrons in the conduction band causing them

to be displaced from their original position. This phenomenon can be seen in **Figure 1.2**:

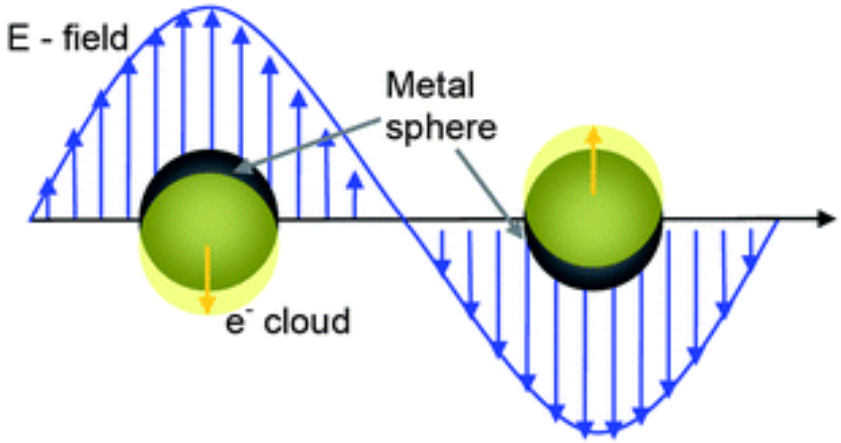

Figure 1.2. Schematic representation of the interaction between the conduction electrons of the nanoparticles and the electric field of light.

When the electrons are displaced from the nucleus a dipole is created in which the equilibrium restoring force is a Coulomb type of force between the electrons and the nucleus so that these surface electrons begin to oscillate coherently with the electric field of light, producing what is known as surface plasmon resonance (SPR) (23, 34-36). For this reason, an absorption of energy by the surface of the nanoparticle giving rise to an absorption band known as the plasmonic band takes place (37-40). The position and width of this plasmonic band depends to a large extent on parameters such as the refractive index of the solvent (26, 41) and the size and morphology of the particle (21, 22, 42).

In 1908, this phenomenon was explained theoretically by solving Maxwell's equations on electromagnetic absorption and radiation dispersion by spherical particles (43-45). This theory allowed the calculation of the extinction spectra of spherical nanoparticles (from now on they will be called simply nanoparticles), where the function dielectric material was known, and the particles were much smaller than the wavelength of the incident radiation.

Under these conditions, the electric field of light (46-48) can be considered constant, and therefore, the interaction between the two is governed by electrostatics rather than by electrodynamics (approximation quasi-static). For example, small particles (less

than 20 nm) produce dipoles that absorb in the UV-Vis spectrum region (around 520 nm). Experimentally it is observed that as the size of the particle is increased, the intensity of the SPR decreases while increasing the width of the band. A slight displacement is also observed at lower wavelengths (29, 49, 50). In addition, in these particles the dispersion produced by the surface of the nanoparticles is important, since the mean free path of the electrons in conduction is in the range of tens of nanometres, and in this case, is limited by the particle size (26, 49, 51). Nanocylinders have optical properties different from nanoparticles, and therefore, to predict the theoretical spectra of these nanostructures the development of Mie's (52, 53) theory was necessary for ellipsoid nanoparticles (from now on they will be called nanocylinders) by Gans (54-56). The results obtained explained the splitting of the plasmonic band (SPR), producing a band in the UV-Vis region similar to that observed in the nanoparticles, and another generally more intense one in the NIR region. It was determined that the first one was due to the excitation of electrons of the transverse axis of the nanocylinders (TSPR), and the second one to the excitation of the superficial electrons along the longitudinal axis of the nanocylinder (LSPR), (**Figure 1.3**).

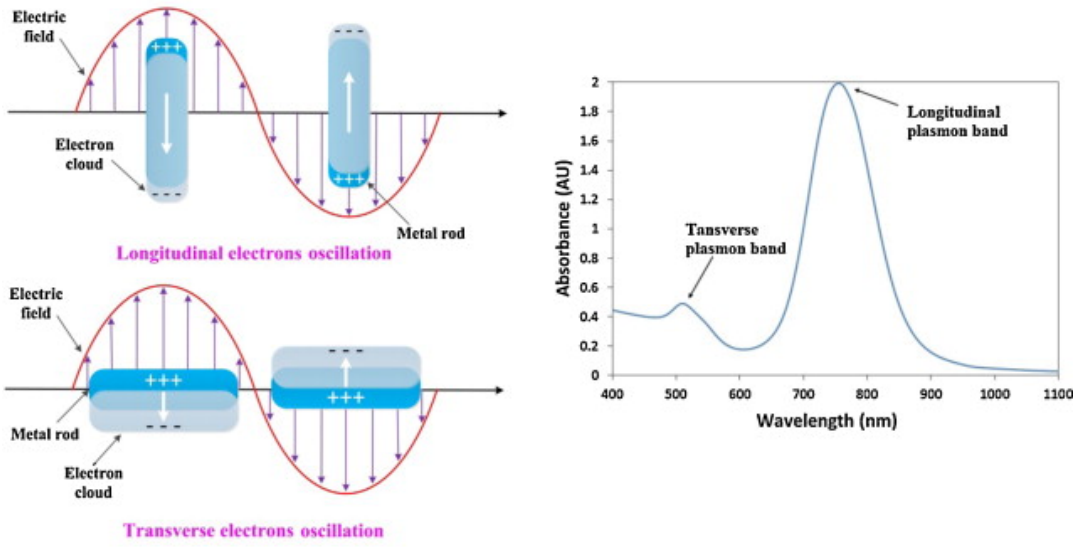

Figure 1.3. Schematic representation of the resonance of surface electrons throughout of the longitudinal and transverse axis of the nanocylinders (a). Typical UV-Vis spectra of gold nanorods where peaks show both SPR (b).

It should be noted that the plasmonic band corresponding to the longitudinal axis experiences a shift to longer wavelengths as the aspect ratio increases, with the aspect ratio being defined as the ratio of length of the nanocylinder to its width (37, 57, 58).

The work presented in this thesis describes the preparation and characterization of gold nanoparticles using different colloidal synthesis methods for several morphologies, as well as the synthesis and characterization of different samples of gold nanocylinders by the method of seed growth (59) with different aspect ratio and thus, differences in the optical properties.

Special attention will be directed to gold nanocylinders because of their ability to absorb different wavelengths controlled by the aspect ratio, which gives great versatility and properties suitable for use in large applications. For example, in the field of medicine, with the aim of reducing side effects from current cancer treatments, researchers are studying the feasibility of optical hyperthermia as a possible alternative or complementary therapy (26, 60-62).

This technique is based on when the nanoparticles are irradiated with a beam of light tuned to their surface plasmon resonance (SPR), they absorb the light and quickly dissipate it to the medium in the form of localized heat. This characteristic can therefore be used to raise the temperature of tumour cells to exceed thresholds at which cell death would occur (60, 63). In addition, there are studies that demonstrate that nanorods have anti-angiogenic power since they interact selectively with certain growth factors, inhibiting thus the vascularization and, therefore, the proliferation of tumours (27, 60, 64, 65).

Another application of great interest of gold nanorods directly related to their optical properties, is their use in solar energy devices to improve the collection of the solar spectrum in solar cells sensitized with colorant (66-68). In these solar cells, the peak absorption of most of the conventional dye molecules is usually centred around 500-600 nm, while gold nanostars additionally have a very intense plasmonic band in the NIR region. In this way, an increase in photocurrent density is produced because the surface plasmon traps low-energy sunlight. In addition, it is possible to vary the wavelengths absorbed by adjusting the aspect ratio of the nanorods (69, 70).

1.2 Nanoparticle synthesis

1.2.1 The colloidal method

Colloids are individual particles, which are larger than atomic dimensions, but small enough to exhibit Brownian motion. If the particles are large enough, then their dynamic behaviour in suspension as a function of time will be governed by the forces of gravity and the sedimentation phenomenon will occur. If they are small enough to be colloids, then their irregular movement in suspension could be attributed to collective bombardments of a multitude of thermally agitated molecules in a liquid suspension. This range of particle size in a colloidal solution usually oscillate in the nanometre range, hence the colloidal method is an efficient method of nanoparticle production (71-73). This method consists of dissolving a salt of the metallic precursor or the oxide, a reducer and a stabilizer in a continuous or dispersing phase (a liquid in this case). The latter can play the role of the reducer, the stabilizer or both. In principle the average size, the size distribution and the shape or morphology of nanoparticles can be controlled by varying the concentration of the reactants, the reducing agent and the stabilizer and the nature of the dispersant medium. By this method, dispersions can be formed which are stable very long for periods. For example, Michael Faraday, in 1857, created colloidal dispersions of gold, which today still remain stable (74, 75). In the 1950s, Turkevitch reported the first standard and reproducible method for the preparation of metal colloids (particles of 20 nm gold by means of the reduction of [$AuCl_4^-$] with sodium citrate). Additionally, he was the first to propose a step-by-step mechanism for training nanoclusters based on nucleation and growth (76, 77).

1.2.2 Photochemical and radiochemical methods

Reduction synthesis of metallic nanoparticles modifying the chemical system by means of high energies is associated with the generation of highly active strong reducing species such as electrons, radicals and excited species. Photochemical reduction (photolysis) and chemical radiation (radiolysis) differ on the nature of the energy used. Photochemical synthesis is characterized by energies below 60 eV, while radiolysis uses energies of 103-104 eV. The methods of photochemical reduction and

radiochemistry possess advantages over the method of chemical reduction. Due to the absence of impurities found when useing chemical reducers, these methods produce high purity nanoparticles. Further, photochemical and radiochemical reduction allow the production of nanoparticles under solid state conditions and at low temperatures. Photochemical reduction in solution is often used to sinter noble metal particles. These particles are obtained from the corresponding salts in water, alcohol or organic solvents. Due to its availability and reproducibility, reduction by radiation to synthesize nanoparticles is of wide interest. In the liquid phase, the stages associated with the spatial distribution of the intermediary products play an essential role in the production of nanoparticles metallic cells. In contrast to photolysis, the distribution of intermediates generated during the synthesis process is more uniform, resulting in particles with narrower size distributions. The pulsed radiolysis method allows the synthesis of active metal particles with unusual oxidation states (78-80).

1.2.3 Microwave irradiation method

The irradiation technique with microwaves produces nanoparticles with very low size dispersion, although precise control in morphology is not always achieved, as happens in the majority of the "bottom up" techniques. The microwave acts as a high frequency electric field, capable of heating any material containing electrical charges such as polar molecules in a solvent or ions in a solid. Polar solvents are heated, and their component molecules are forced to rotate with the field and lose energy in collisions. The conductive and semiconducting samples are heated when ions and electrons within them form an electric current and the energy is lost due to the electrical resistance of the material. In recent years, the process of assisted heating by microwaves has been used as an attractive alternative for the synthesis of nanoscale materials, given that it is a fast, uniform and effective method, increasing the kinetics of reaction by one or two orders of magnitude. Colloidal nanoparticles of Pt, Ru, Ag and Pd stabilized by polymers have been prepared from the precursor salts of the dissolved metals in ethylene glycol solutions using microwave heating (78, 81). On the other hand, microwave heating of liquid samples decreases temperature fluctuations in the reaction medium, providing, as a consequense, a more homogeneous environment for nucleation and growth of metallic particles (17).

1.2.4 Use of dendrimers

The synthesis of nanoparticles has also been carried out using micelles, emulsions and dendrimers as nanoreactors that allow the synthesis of particles with a defined shape and size. This is achieved by altering the nature of the dendrimers. Dendrimers are highly branched molecules, which include a central nucleus, repetitive intermediary units and terminal functional groups (82-84). Dendrimers represent new types of macromolecules that combine the high molecular weight and low viscosity of their solutions with their three-dimensional molecular structure and the presence of a spatial structure. The size of the dendrimers ranges from 2 to 15 nm and they represent natural nanoreactors. Dendrimers with a small number of intermediary units exist in an "open" manner while those involving many units form three-dimensional spherical structures. The terminal groups of the dendrimers can be modified with hydroxides, carboxyls, hydroxycarboxyls, among others. Dendrimers of different generations with several terminal functional groups have proved to be suitable templates for the synthesis of monometallic and bimetallic nanoparticles. Different polyamidoamines have been very popular as dendrimers for the synthesis of nanoparticles. With these dendrimers sintered gold nanoparticles of 1-3 nm have been prepared (85-87). Other studies, for example, have reported that this method is useful for the synthesis of nanoparticles of platinum and palladium with particle sizes between 1 and 2 nm incorporated in poly dendrimers (amidoamines) functionalized with amino groups. The dendrimers have also been actively used for the synthesis of bimetallic nanoparticles (88, 89) .

1.2.5 Solvothermal synthesis method

Solvothermal synthesis is a grouping of a series of techniques. A metal precursor dissolved in a liquid, in a closed container, is heated above its boiling point, which generates a, normally moderate, pressure higher than atmospheric pressure. The liquid applied is usually water, and hence the name "hydrothermal synthesis" is employed when it is applied; however, increasingly other liquid media are used: organic solvents, liquid ammonia, hydrazine, etc., and then the general term “solvothermal synthesis” is employed. In these types of techniques, the reaction times are long (compared to other chemical methods). Hydrothermal synthesis refers to heterogeneous reactions in an aqueous medium above 100 ° C and 1 bar. A distinctive feature of hydrothermal

synthesis is that reagents that are poorly soluble in water pass to dissolution by the action of the solvent itself or of mineralizers. The objective of this technique is to achieve a better dissolution of the components of a system and thus manage to dissolve, or make react, species which are sparingly soluble under usual conditions (eg, silica, aluminosilicates, titanates, sulfides).

1.2.6 Sol-gel method

The sol-gel method is a wet phase chemical process widely used in material science. This method is mainly used for the manufacture of nanomaterials (usually metal oxides). The typical precursors of the sol-gel process are the alkoxides of metals and metal chlorides, which undergo hydrolysis and polycondensation reactions to form a colloidal dispersion, which after limited polymerization forms a gel. In general, alkoxides are very sensitive to moisture (dehydrated they rehydrate very readily), that is why the hydrolysis for the formation of the gel is carried out using alcohols as a common solvent for the different immiscible liquids. A polymeric gel is an infinite macromolecular network, which is swollen by solvent. A gel can be created when the concentration of the dispersed species increases. The solvent is trapped in the particle network and thus the polymer network prevents the liquid from separating, while the liquid prevents the solid collapses into a compact mass. The partial dehydration of a gel produces an elastic solid residue that is known as xerogel. Finally, this material is completely dehydrated and eventually thermally treated in gas flow to obtain the final nanostructured material (71, 90).

The sol-gel method has been used in recent years to prepare a broad variety of nanostructured materials. The method is attractive because it involves low temperature processes. Also, the high purity and homogeneity are attributable to its form of preparation in multicomponent systems (71).

1.3 Deposition methods of nanoparticles on metal oxides

1.3.1 Impregnation

Impregnation consists of filling the pores of the support with a solution of the metal precursor (usually a salt). The volume of solution may be that necessary to fill the volume of pores or an excess that after a period is removed by evaporation, in such a way that the metal precursor and its counter ion remain on the surface of the support. This is a simple and cheap method; therefore, it is the classic method of catalyst preparation at the industrial level; nevertheless, it possesses the disadvantage of little control the metal precursor interacts with the support, also the counter ion of the metal precursor. Is not readily lost Once the interaction of the metal precursors with the support is achieved, the material obtained is subjected to thermal treatment in reducing or oxidising gas mixtures, to obtain the nanoparticles deposited in the support (91).

1.3.2 Ionic adsorption

In this method, the adsorption of anions as well as cations can be employed. Cations can be adsorbed through electrostatic interaction with negatively charged surface groups, this is achieved when the pH of the solution in which it is suspended the support is higher than the isoelectric point of the support (IEP). Anionic species can be adsorbed on the positively charged surface support groups, when the pH of the solution is lower than IEP (91, 92). The surfaces of oxides or hydroxides can be protonated or deprotonated depending of the pH of the solution. The value at which the total electric charge of the surface is zero is the zero-load point, which has the same pH value as the IEP.

1.3.3 Deposition-Precipitation (DP)

This method consists of the deposition of a hydrated oxide or of a hydroxide on the surface of a support, as a result of a gradual and homogeneous increase of the pH of the solution in which the support is suspended. Typical basifying agents are hydroxides, such as NaOH, or KOH, carbonates or weak bases such as urea (91). The precipitate can be nucleated by the surface of the support, and when the deposition of

the entire active phase is carried out correctly it is linked to the support without it remaining floating in the solution. This method, as well as ionic adsorption, presents the advantage over impregnation that most of the counter ions of the metallic precursor can be removed efficiently by means of repeated washings of the samples after the deposition of the metal precursor. As in the previous methods, deposited nanoparticles are obtained after treatment of the metal precursor in interaction with the support, under reducing or oxidising atmospheres, depending on the chemical properties of the deposited species and the desired oxidation state of the deposited material. The size and morphology of supported particles is highly dependent on the synthesis parameters used (temperature, contact time, pH, type of gas and temperature used during heat treatment), of the support used (electronic characteristics, morphology, surface defect structure, etc.), and the metal precursor (91).

1.3.4 Deposition of colloids

In principle, the average size and distribution of particle size can be controlled by selecting properly the conditions of synthesis. The advantage of using a colloidal route to prepare supported metal materials lies in the fact that the conditions of preparation can be manipulated to obtain particles with a narrow size distribution around the desired size. A wide range of methods for the synthesis of metal colloids, in which a large number of reducers have been used such as sodium citrate, sodium thiocyanate, polyethylene imine, tetrakis [hydroxymethyl] phosphonium and sodium borohydride have been reported in the literature (76, 89). As mentioned above, also stabilizers can be used. Metal nanoparticles can be immobilized on the support by submerging it in the colloidal suspension, followed by a washing and drying process. In a successful preparation the particles, once supported, should not be significantly larger than the obtained in the solution. To achieve this, it is necessary to maintain a delicate balance between various parameters such as the nature and concentration of stabilizer, the metal / stabilizer ratio and, of course, the nature of the support (89). In principle, the deposition of colloidal particles is not a problem (93) unless it is necessary to remove the stabilizer by thermal treatment.

1.3.5 Photochemical deposition

This method is based on the fact that certain metal cations with potential appropriate redox properties can be deposited on the support and reduced by photoelectrons created by illumination of semiconductor, such as oxides of zinc, tungsten and titanium. The photoreduction mechanism has been widely studied (94). In this method organic stabilizers such as PVA and PVP can be employed to limit particle growth (95). Supports that do not have a suitable bandgap (Fe_2O_3 and SnO_2) usually are not suitable for use as supports in this method (87). The disadvantage of this method is that its effectiveness is very sensitive to the characteristics of both the bulk and the surface of the support. The biggest advantage is that it is not necessary to treat the samples thermally since during the preparation the metal precursor is reduced by UV irradiation.

The two main anisotropic nanoparticles studied in this project have been gold nanorods and nanostars.

1.4 Gold nanorods (AuNRs)

Nanorods are not as easily synthesized as nanospheres since they require anisotropic growth, a process which does not happen spontaneously. Several different methods have been used to overcome this issue. Some of the most popular ones are synthesis in templates, seed-mediated growth in solution and non-seeded growth in solution. Synthesis in templates can be subdivided into two different categories; synthesis in hard templates and synthesis in soft templates. Hard templates are ready made nanoporous materials, commonly aluminium oxide membranes. The nanoparticle is produced either by chemically reducing the gold precursor inside the template pores or by electrochemical deposition of the gold precursor on the templates. Soft templates are, for instance, rod-like micelles and certain surfactants. The shape of the rod-like micelle, and the specific binding behaviour of the surfactants promotes the anisotropic growth of the nanoparticles (96).

Seed-mediated growth and non-seeded growth are both wet chemistry methods. The difference is that in the seed mediated growth method gold seed particles are produced first and are then used to catalyse the synthesis of gold nanorods whereas the non-seeded methods synthesize the rods in a single step. In short, both these methods mix

the gold precursor with some capping agent that promotes anisotropic growth. For gold, cetyl trimethyl ammonium bromide (CTAB) is commonly used. CTAB promotes anisotropic growth because it is less likely to stick to the edges than to the sides of the growing nanorod, allowing more gold ions to assemble at the ends of the rod. The reason for this preference is that the spacing of the gold atoms is closer to the size of the CTA^+ headgroup that binds to the gold at the (1,0,0) plane than at the close-packed (1,1,1) plane of the Au NP (97). In the seed mediated growth method relatively weak reducing agents, such as ascorbic acid, are sufficient for the seed-mediated growth mechanism since the gold seeds act as a catalyst. In the non-seeded method, the strong reducing agent $NaBH_4$ is commonly used to induce nucleation and a weaker reducing agent is used to promote growth as in the seed-mediated growth method. In addition, it has been shown that adding silver nitrate to the growth solution promotes the synthesis of higher aspect nanorods. It was long believed that this effect was due in some way to the effect of the silver ions. However, it is now understood that it is due to electrostatic screening of the CTA^+ ends of the CTAB molecules by the NO_3^- ions, making the binding of additional CTAB molecules to the gold particle more thermodynamically favourable (98). The CTAB capping process is illustrated in **Figure 1.4**.

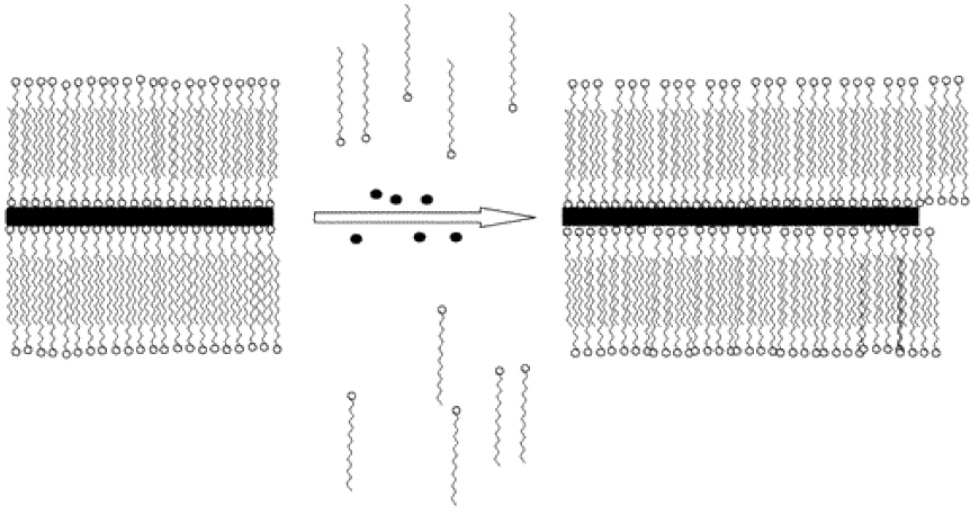

Fig. 1.4 Cartoon illustrating "zipping": the formation of the bilayer of CTAB (squiggles) on the nanorod (black rectangle) surface may assist nanorod formation as more gold ions (black dots) are introduced (99).

The seed mediated method was used in the experiments as it has many advantages including the one that comes with the wet chemistry approach; no prefabricated templates are necessary. In addition, it has been shown to give a good yield of nearly mono-disperse nanoparticles (97).

1.5 Gold nanostars (AuNS)

The physical, chemical and optical properties of nanoscale colloids depend on their composition, size and shape. There is a great interest in using nano-colloids for photo-thermal ablation, drug delivery and many other biomedical applications. Gold is particularly used because of its low toxicity (40, 100). The peak of the surface plasmon resonance mode depends on the structure and composition of the metal nano-colloids. Since the surface plasmon resonance mode is stimulated with light there is a need to have the peak absorbance in the near infrared region where biological tissue transmission is maximal. The typical gold nanostar synthesis method is based on a solution containing silver seeds that are used as the nucleating agent for anisotropic growth of gold colloids, where normally, about the 70 % of the nanostructures are nanostars and the other 30 % of the particles are amorphous clusters (101). The

absorbance peak of the nanostars is typically detected in the near infrared range depending on the synthesis procedure employed (102).

1.6 Aims of project

The aim of this project was to understand the synthesis of various morphologies of noble metal nanoparticles so that specific properties can be then explored in supported form in different chemical transformations (86). Colloidal synthesis methods provide an optimum control of nanoparticle morphologies with a narrow particle size.

Chapter 2

Experimental: Materials and Methods

2 Experimental: Materials and Methods

2.1 Introduction

In the experimental chapter, materials used, experiments undertaken including synthesis of nanoparticles and catalysts, reaction procedures and characterization techniques are described. Characterization techniques have been used in order to identify catalyst's properties such a plasmon band resonance peak, real metal loading, particle size, etc.

2.2 Materials

Metal precursors such as hydrogen tetrachloroaurate trihydrate ($HAuCl_4.3H_2O$; 99%), palladium(II) chloride ($PdCl_2$, 99.99 %), rhodium chloride, and sodium borohydride ($NaBH_4$; 99%), L-lysine (≥98%), sodium hydroxide (NaOH ≥98%), tetraethylammonium hydroxide (TEAOH), aluminum nitrate, zinc oxide and cerium oxide and other chemicals such as Methyl Orange were purchased from Sigma Aldrich, and Titanium (IV) dioxide P25 (TiO_2 ≥99.5 %) and γ-Al_2O_3 (Puralox, UR-160, with a surface area of ca 160 m^2/g) were gifts of Degussa and SASOL, respectively.

Cetyltrimethylammonium bromide (CTAB), L-ascorbic acid (AA), silver nitrate ($AgNO_3$; 99%), and TiO_2 P25 were used for the synthesis of supported gold nanorods and the following reagents for the oxidative reactions: 5-hydroxymethyl-2-furfural, 2,5-furandicarboxylic acid 5-hydroxymethyl-2-furan carboxylic acid, levulinic acid, formic acid and sodium hydroxide. All products were obtained from Sigma-Aldrich. All glassware was cleaned with aqua regia (HCl/HNO_3, 3:1 v/v), followed by a thoroughly rinse with double distilled MilliQ water prior to use

2.3 Nanoparticle and catalyst preparation

2.3.1 Preparation of the one-dimensional (1D) Al_2O_3 and CeO_2 nanorods

The synthesis of Al_2O_3 and CeO_2 nanorods followed the hydrothermal method for the synthesis of 1D Fe_2O_3 except using $Al(NO_3)_3$ or $Ce(NO_3)_4$ respectively as the precursor. Typically, 5.0 g of $Al(NO_3)_3.9H_2O$ was added to 30 ml of 20 wt. % aqueous TEAOH solution in an autoclave, which was then heated in an oven at a temperature of 80 ^oC for 10 h. After the reaction, the precipitate was washed with DI water four times, dried in a vacuum oven at 100 ^oC overnight and calcined at 500 ^oC for 3 h (103, 104).

2.3.2 Sonication preparation of supported catalysts

The sonication-assisted catalyst preparation has been carried out following the previous work reported (105) using lysine as the capping agent and $NaBH_4$ as the reducing agent, and the used catalyst supports used were TiO_2-P25, γ-Al_2O_3 and CeO_2 nanorods, the commercial γ-Al_2O_3 from SASOL, ZnO, CeO_2, etc. In a typical catalyst preparation method, 0.5 g of TiO_2 was put in 10 ml deionized water, and 5.08 ml of 0.01 M $HAuCl_4$ and 5.08 ml of 0.01 M lysine (Lys) were added subsequently. The pH of the suspension was adjusted to 5–6 with 0.1 M NaOH.

The suspension was then subjected to sonication (Vibracell 500-Watt Ultrasonic processor, 20 kHz, 39 % energy efficiency) for 20 s, and during the sonication freshly prepared $NaBH_4$ (0.1 M, 5–10 times the Au molar number) was injected instantly and the pH value at the end point was measured. The suspension immediately turned dark in color and was washed with deionized water four times by using centrifuge. In the case of Pd catalysts, $PdCl_2$ was used as precursor and a low pH value below 3 was used because $PdCl_2$ was not dissolved well in water at high pH values. **Figure 3.1** (next chapter) shows a schematic representation of sonication-assisted method.

2.3.3 Gold and Silver spherical nanoparticles (AuNP)

Synthesis of Noble Metal Nanospheres

In a typical synthesis of supported noble metal nanoparticles, water solution of the metal salt(s) ($HAuCl_4$, $AgNO_3$, etc.) of desired concentration is prepared in a round bottom flask and then mixed with the appropriate stabilising agent solution under vigorous stirring. Three different stabilizers with their respective synthesis method as polyvinylpyrrolidone with average molecular weight of 10,000 $g.mol^{-1}$ (PVP^{10}) (106), polyvinyl alcohol (PVA) (107, 108) and Pluronic P-123 (109) were used in order to study their effect on the particle size and catalytic activity once the nanoparticles are supported. At that time, an aqueous solution of the reducing agent $NaBH_4$ 0.1 M was prepared and transferred into the flask dropwise (slowly) ($NaBH_4$/metal=5 molar ratio) in all cases. The addition of $NaBH_4$ leads to an alteration in the colour of the solution from colourless or pale colours (in the case of gold, very pale-yellow solution) to the corresponding colour depending on the nanoparticle size and composition. The as-obtained solution was allowed to stir for 30 min.

Immobilization of Colloidal Noble Metal Nanospheres

The desired amount of titania was suspended in 25 ml of water and acidified to pH 1 with sulfuric acid and added to the metal solution, using another 25 ml of water to wash down the glassware. After 2 h of stirring the solution was then filtered and washed with distilled water until a neutral pH value was achieved (checked with indicator pH paper). The solid was dried overnight at RT or in the vacuum oven. The powders were filtered and then refluxed with 50 ml of water at 80°C for 2 h to remove the excess of ligand and reducing agent (in the case of PVA synthesis (110)). The catalyst was then filtered, washed with water again, dried overnight and finally ground.

2.3.4 Synthesis of Gold Nanorods (AuNRs)

A- Synthesis of colloidal Gold Nanorods:

Gold nanorods (AuNRs) with various aspect ratios (AR) were synthesized through the well-known method of El-Sayed (59) with modifications. Seed preparation was carried out mixing $HAuCl_4 \cdot 3H_2O$ (5 ml, 1 mM) with CTAB (5 ml, 0.2 M) solution, followed by addition of freshly made, ice cold, $NaBH_4$ (600 μl, 10 mM) under rapid stirring for 1 min. $NaBH_4$ is a strong reducing agent and its addition resulted in a brownish-yellow coloured solution. The mixture was then allowed to stand without disturbance at 28-30°C for at least 1 hour before use.

To make gold nanorods, the seeds were then added to a growth solution and incubated at 30°C overnight to allow complete rod growth. The growth solution was typically prepared as follows: the desired amount of gold solution ($HAuCl_4.3H_2O$ 1 mM), in order to achieve the desired metal loading, was first mixed with CTAB solution (0.2 M). Then, it was acidified with HCl to reach a pH about 3. According to the rod dimension and longitudinal plasmon wavelength required, an appropriate amount of $AgNO_3$ (1 mM) was added to the mixture, followed by the rapid addition of L-ascorbic acid (AA) solution (78.8 mM). The mixture turned colourless instantly and finally the rod growth process was initiated due to the addition of the seed solution as prepared above. The colour of the mixture would usually change within minutes, suggesting successful growth of seed particles. This method typically produces short nanorods (rods with aspect ratio (AR) up to 4-5).

B- Immobilization of Colloidal Gold Nanorods:

Before AuNR in colloidal solution can be immobilised, they must be purified by centrifugation in order to remove the excess of reagents, especially the surfactant CTAB. Typically, the solution was centrifuged at a speed of 14,500 rpm for 15 min to separate the gold nanorods. The colourless supernatant was very carefully discarded. The resultant solid pellet was then re-dispersed in an amount of deionised (DI) water

depending on the quantity of the residue. The centrifugation was repeated 2-3 times and finally the solid residue was re-dispersed in DI water.

In the next step, the colloidal suspension was transferred to a 250 ml round bottom flask followed by the procedure outlined above with modifications (110). 25 ml of titania water solution was acidified to pH 1 with sulfuric acid and was added to the colloidal nanoparticle solution (and 25 ml more used to wash down the glassware) and it was left for 2 hours under vigorous stirring and then filtered and washed with distilled water until a neutral pH value was obtained. The solid was dried overnight in a vacuum oven at 60 °C and finally ground. No further treatments were performed.

2.3.5 Synthesis of seed-mediated multipod Au nanoparticles (DMF/PVP)

In this first method, gold nanostars were synthesised using the method reported in (101) where in a typical synthesis, an aqueous solution of chloroauric acid was mixed with different concentrations of PVP (average MW = 10 000) solution in *N*,*N*-dimethylformamide (DMF), followed by the rapid addition of PVP-coated Au seeds in ethanol (111) under stirring. Within 15 min, the colour of the solution changed from pink to colourless and finally turned blue indicating the formation of gold nanostars in solution.

These nanoparticles were not supported due to difficulties removing the polymers and lower catalytic activity compared to surfactant-free AuNSs.

2.3.6 Synthesis CTAB-coated AuNSs

CTAB-coated AuNSs were synthesized using a modified procedure (112, 113) . In a typical synthesis, Au seeds were first prepared mixing a solution of chloroauric acid 0.25 mM with trisodium citrate 0.1 M in 20 mL of Millipore water. Then, freshly prepared, 60 μL of ice-cold sodium borohydride 0.1 M was quickly added under moderate stirring. Immediately, the solution turned brown-pink and slowly developed into its final red colour due to formation of spherical gold nanoparticles approximately 4–5 nm in diameter. The sample was stored overnight in the dark in ambient conditions.

AuNSs samples were synthesized using CTAB as a template. A solution of CTAB 5 mM was mixed with solutions of chloroauric acid 10 mM and silver nitrate 0.01 M under vigorous stirring for 1 minute. Then, 0.1 mL of L-ascorbic acid 0.1 M was added dropwise. Upon addition of the last drop of L-ascorbic acid, the solution turned clear, and the appropriate volume of gold nanoseed was immediately added. Samples were left in the dark under ambient conditions until use.

2.3.7 Synthesis of Surfactant-Free AuNSs

Finally, free-surfactant method (102), gold nanostars (AuNSs) were prepared by a seed-mediated growth method. The seed preparation consists of the addition of 15 ml of 1 % citrate solution to 100 ml of boiling 1 mM $HAuCl_4$ solution under vigorous stirring. After 15 min of boiling while keeping the solution volume stable, the solution was cooled and filtered using a 0.22 μm nitrocellulose membrane, and then kept at 4 °C for long-term storage. For nanostar synthesis, 956 μl of the above citrate-stabilized seed solution was added to 96 ml of 0.25 mM auric chloride ($HAuCl_4$) solution (with 96 μl of 1 M HCl) in a 250 ml round bottom flask at room temperature under moderate stirring (700 rpm). Quickly, 956 μl of silver nitrate ($AgNO_3$) of different concentrations (1–2 mM) and 480 μl of ascorbic acid (AA; 100 mM) were added simultaneously. The solution was stirred for 30 s as its colour rapidly turned from light red to blue or greenish-black.

2.3.8 Surfactant-Free AuNSs Immobilization

Immediately after synthesis, surfactant-free AuNSs were immobilized onto titania TiO_2 using two different approaches. The procedure was exactly the same as the one described previously for the gold nanorods in Chapter 4; colloidal suspension was transferred to a 250 ml round bottom flask followed by the procedure outlined previously with modifications (110). 25 ml of titania water solution was acidified to pH 1 with sulfuric acid and was added to the colloidal nanoparticles solution (and 25 ml more used to wash down the glassware). It was left for 2 hours under vigorous stirring and then filtered and washed with distilled water until a neutral pH value was

obtained. The solid was dried overnight in the vacuum oven at 60 °C and finally ground. No further treatments were performed.

2.4 Catalytic Reactions

2.4.1 Photocatalytic degradation of Methyl Orange (MO)

The photocatalytic degradation of methyl orange (MO) was carried out at 25 ^{o}C using 10 ml MO solution (40 mg/l) and 20 mg of solid catalyst under irradiation of the visible light (400-800 nm) with a chiller. The MO concentration was measured using a UV-visible spectrophotometer by comparing the peak intensity at 465 nm. Prior to the reaction, the solution containing the photocatalyst was stirred for 2 h in the absence of any light to saturate the adsorption of MO on the catalyst surface.

Figure 2.1 Photoreactor LuzChem ICH2. (16 UVA and 16 VIS lamps, 110 VAC, 50/60 Hz cycle, 4 Amps.)

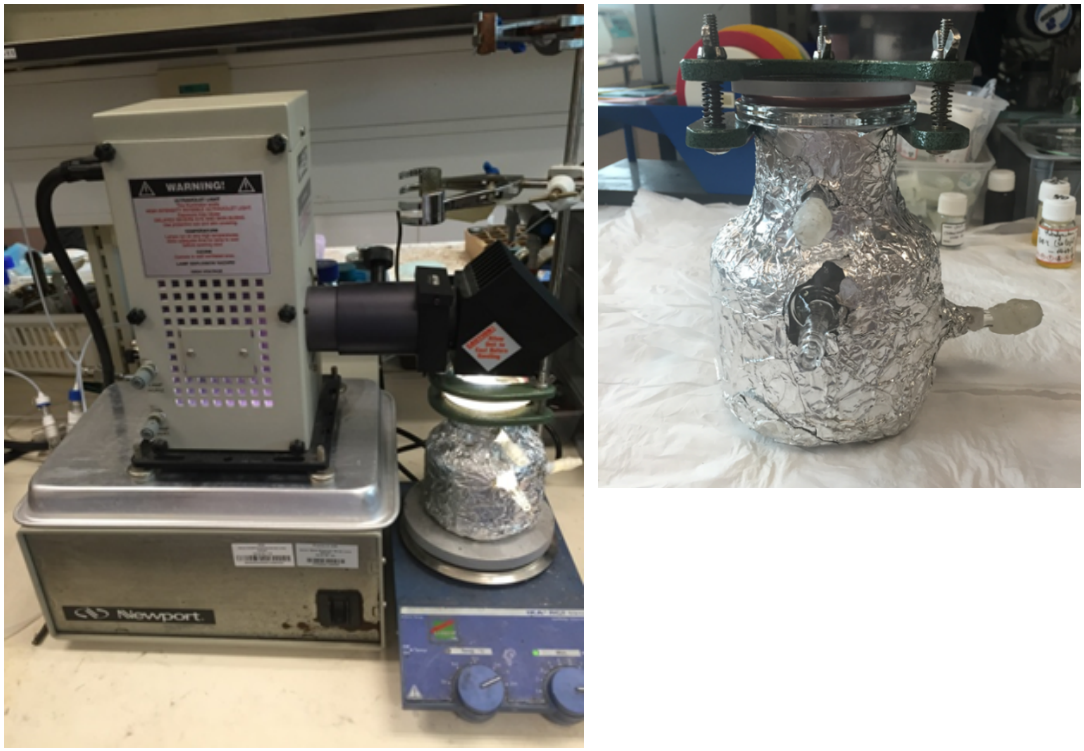

Figure 2.2. (Left) Photoreactor set up with 50 - 200 W research Arc Lamp Sources (Hg), produce collimated or focused output. (Right) photoreactor used in experiments for sonication-assisted nanoparticles.

2.4.2 PROX reactions

The PROX reaction was carried out in a fixed bed reactor at atmospheric pressure using a gas mixture of 1 % CO, 1 % O_2, 78 % H_2, 20 % He at a GHSV of 5000 h^{-1}, or a mixture of 100 ppm CO, 100 ppm O_2, 99.78 % H_2, 0.2 % He at a GHSV of 50 h^{-1}. The reactant and product gases were analyzed with a GC Shimadzu-14B equipped with both TCD and FID detectors.

2.4.3 Selective Oxidation of 5-Hydroxymethyl-2-furfural (HMF)

The oxidation of 5-hydroxymethyl-2-furfural (HMF) was carried out using an autoclave (Parr Instruments) reactor of 100 mL capacity. This reactor was equipped with a magnetic stirrer (0-1500 rpm), specifically was used a cross-magnetic stirrer

bar to achieve a homogeneous mixture of oxygen gas in solution. It was also equipped with measuring and control equipment of temperature and pressure.

The reactor was charged with an aqueous solution (10 ml water) containing the appropriate amount of HMF, metal catalyst and base (NaOH) (molar ratio [1:0.01:4]). The temperature was increased to 60 ◦C and the reaction mixture was stirred at ca. 1500 rpm for 4 h. The autoclave was purged 3 times with O_2 (5 bar) and then pressurized at 20 bar. At the end of the reaction, the reactor was cooled into ice and the solution was filtered under vacuum using a filter paper of 0.2 μm PTPE.

Then, the solution was diluted before analysis with a HPLC using a 0.01M H_2SO_4 solution as the mobile phase. The identification of compounds was achieved by calibration using commercial samples. This reaction was conducted in collaboration with a visiting researcher and Erasmus student resident in the group, Susana Guadix Montero.

2.4.4 4-Nitrophenol Reduction

The catalytic properties of AuNSs both in colloidal suspension and immobilized nanoparticles were examined for the reduction of 4-nitrophenol to 4-aminophenol reaction in the presence of excess $NaBH_4$. The reaction conditions reported by Ye et al (114) were adopted as we will indicate later on. 4-nitrophenol [4-NP] reduction was carried out in situ at room temperature in a standard quartz cell with a path length of 1 cm.

A- *Colloidal:* The aqueous solution of sodium borohydride ($NaBH_4$) 0.1 M was freshly prepared (and kept ice-cold). First, 0.3 mL of a $NaBH_4$ solution was mixed with 3 mL of 0.1 mM [4-NP]. Then, a volume of 25 μL gold nanoparticles was immediately injected.

B- *Solid:* samples (10 mg) were added in the cuvette. Immediately following this, the same volume of [4-NP] was introduced and finally the $NaBH_4$.

2.5 Characterization

The equipment used to analyse and characterize the synthesized nanoparticles and catalysts is described below.

2.5.1 UV-Vis Spectrophotometer

UV-Vis absorption spectra of colloidal suspension of nanoparticles and methyl orange were recorded using a Thermo Scientific Evolution 220 UV-Vis spectrophotometer, while measurement of UV-Vis diffuse reflectance spectra of titania supported nanoparticles was carried out with a Shimadzu UV-2550 UV-Vis spectrophotometer.

2.5.2 Transmission Electron Microscopy (TEM)

The TEM images were obtained with a TEM Jeol 2100 operated at 200 kV. Sample was mounted on 300 mesh copper grids with a holey carbon film, dispersed in methanol by sonication and added as a drop.

2.5.3 Scanning Electron Microscopy (SEM)

SEM was carried out using Hitachi S-4800 Field –Emission Scanning Electron Microscope Oxford Instruments Inca |Energy EDX detector Meiji MT9430 Polarising Microscope. Samples were mounted on 300 mesh copper grids with holey carbon films, as received and dried in air.

2.5.4 X-ray Powder Diffraction (XRD)

XRD was carried out using a Panalytical X'Pert PRO HTS X-Ray Diffractometer employing Cu Kα radiation ($\lambda = 0.154$ nm). Data were recorded in the 2θ range of 10-90° in a transmission mode with a one-hour scan time. A few milligrams of sample were placed on the metal analysis grid. The equipment was located at the Centre of Materials Discovery (CMD).

2.5.5 ICP-OES

For ICP-OES measurements, 10 mg of catalyst was dissolved in 1 ml of pure aqua regia and stirred under ambient conditions overnight. The noble metals like Au and Ag were dissolved in the suspension which was measured and used to calculate Au and Ag concentrations. Each value of Au and Ag was measured three times and averaged. ICP measurements were performed by the analytical services section within the Department of Chemistry.

2.5.6 X-ray Photo-Electron Spectroscopy (XPS)

XPS measurements were undertaken at The Institute of Chemical Engineering and Sciences (ICES) in Singapore. XPS is useful technique to the study the near-surface chemistry of the catalyst as it provides information on the elemental composition, the oxidation state of the elements and in favourable cases, on the dispersion of one phase over another.

Chapter 3

Sonication-Assisted Deposition-Reduction Method for Preparing Supported Metal Catalysts for Catalytic Applications

3 Sonication-Assisted Deposition-Reduction Method for Preparing Supported Metal Catalysts for Catalytic Applications

3.1 Introduction

In the preparation of heterogeneous catalysts, conventional methods such as impregnation usually lead to difficulties in the control of particle size, local composition, crystal phase and morphologies. Recent developments in nanoscience and nanotechnology may offer better possibilities for designing and preparing heterogeneous catalysts with control even at an atomic level. For example, designed bimetallic Pt-M electrocatalysts (M = V, Ti, Co, Fe, Ni, etc ...) were recently reported to show improved resistance to poisonous substances in comparison with conventional Pt catalysts (115). Also, the so-called "oxide-on-metal inverse catalysts" were prepared with more active coordinatively unsaturated (CUS) centres confined at the interface between a transition metal oxide (TMO) particle and a noble metal (NM) particle for catalytic applications (116).

In addition, although the DP and CP methods work quite well for preparation of some catalysts, particularly for the supported gold catalysts (117), the deposition efficiency (DE, which is defined as the percentage of real metal loading to the theoretical metal loading) is usually below 30% except in the case of using urea as the precipitation agent (91), which means majority of Au is washed off in most of the catalyst preparations.

It has been demonstrated that sonication is an effective tool to generate and facilitate the deposition of metal particles onto support surfaces. During the sonication process, extreme conditions such as high transient temperature (≥ 5000 K), pressure (≥ 20 MPa) and very high cooling rates (≥ 10^{10} KS^{-1}) can be reached (118), which can be utilized to decompose some volatile compounds used in the sonochemical synthesis. Meanwhile, the collapse of the bubbles can generate high speed micro-jets in the liquid medium near the solid surface (119), which can propel the small particles to the solid surface.

Gedanken et al. (120-122) did systematic work on the sonochemical synthesis of supported catalysts. However, most of the preparations need long-term sonication to decompose the precursor compounds and their deposition efficiency is still in doubt. The deposition-reduction process is widely used for the preparation of supported catalysts (93, 122, 123), in which there is involvement of very complicated interactions, e.g., the interaction between metal particle and capping agent when a capping agent is used, the particle-particle interaction and the particle-support interaction, etc. The former often involves chemical bond formation while in the latter two kinds of interactions are often related to the electrostatic interaction and/or chemical bonding formation (124, 125).

The reduction step could be very fast but the deposition step probably not, or with low deposition efficiency. How to control the above-mentioned interactions to realize a highly efficient deposition and dispersion of metal particles onto support is still a big challenge (126).

Previously we investigated the interaction of Au colloids with amino acids such as lysine, and found that, at low pH values, lysine molecules can crosslink Au colloids, and this crosslinking is stronger than the electrostatic repulsion among the Au colloids. In this case, large Au particles or linear Au aggregates will be obtained because of the crosslinking.

However, at high pH values and under sonication, only isolated Au particles are obtained. At the high pH values, the amino acid capped Au colloids become more negatively charged on their surface and their electrostatic repulsion is stronger than that at low pH values, preventing their fast aggregation. Meanwhile, the application of sonication can break the Au linear aggregates and drive the Au colloids to deposit on the support surface with high efficiency.

On the other hand, when the solution pH value is close to the isoelectric point (IEP) of the catalyst support, the electrostatic repulsion between the Au colloids and the catalyst support such as TiO_2 (with an IEP of about 6) becomes weak, which will facilitate deposition of Au colloids (127, 128).

Based on these findings, a sonication-assisted precipitation-reduction for preparation of supported Au catalysts on a series of supports has been carried out by us (105). This method is fast, and is suitable for the deposition of Au onto supports with an isoelectric point (IEP) above 5 with very high dispersion. However, we still wondered whether this method could be extended to the preparation of other supported metal catalysts, in particular, bi-metallic catalysts, as the latter often lead to different catalytic behaviour from the mono-metal catalysts. Also, the influence of some preparation parameters on catalyst preparation and the metal deposition efficiency were still not studied.

In this work, the novel sonication method (105, 129) has been employed to prepare various mono- and bi-metallic catalysts supported on several supports under various experimental conditions. The resultant catalysts have been applied for two types of important reactions: (i) the photo-degradation of methyl orange (MO) and (ii) the preferential oxidation (PROX) of CO in H_2-rich gas. The first reaction is related to the treatment of industrial wastewater and the second to H_2 gas purification for industrial applications.

3.2 Experimental

3.2.1 Preparation of the one-dimensional (1D) Al_2O_3 and CeO_2 nanorods

The synthesis of Al_2O_3 and CeO_2 nanorods followed the hydrothermal method for the synthesis of 1D Fe_2O_3 except for using $Al(NO_3)_3$ or $Ce(NO_3)_4$ as the precursor. Typically, 5.0 g of $Al(NO_3)_3.9H_2O$ was added to 30 ml of 20 wt. % aqueous TEAOH solution in an autoclave, which was then heated in an oven at a temperature of 80 ^oC for 10 h. After the reaction, the precipitate was washed with DI water for four times, dried in a vacuum oven at 100 ^oC overnight and calcined at 500 ^oC for 3 h (103, 104).

3.2.2 Sonication preparation of the supported catalysts

The sonication-assisted catalyst preparation has been carried out following the previous work reported (105) using lysine as the capping agent and $NaBH_4$ as the reducing agent. The used catalyst supports used were TiO_2-P25, γ-Al_2O_3 and CeO_2 nanorods, commercial γ-Al_2O_3 from SASOL, ZnO, CeO_2, etc. In a typical catalyst preparation, 0.5 g of TiO_2 was put in 10 ml deionized water, and 5.08 ml of 0.01 M $HAuCl_4$ and 5.08 ml of 0.01 M lysine (Lys) were added subsequently. The pH of the suspension was adjusted to 5–6 with 0.1 M NaOH.

The suspension was then subjected to sonication (Vibracell 500-Watt Ultrasonic processor, 20 kHz, 39 % energy efficiency) for 20 s, and during the sonication freshly prepared $NaBH_4$ (0.1 M, 5–10 times the Au molar number) was injected instantly and the pH at the end point was measured. The suspension immediately turned dark in colour and was washed with deionized water 4 times by using centrifuge. In the case of Pd catalysts, $PdCl_2$ was used as precursor and a pH below 3 was used because $PdCl_2$ was not fully dissolved in water at high pH values. **Figure 3.1** (next page) shows a schematic representation of sonication-assisted method.

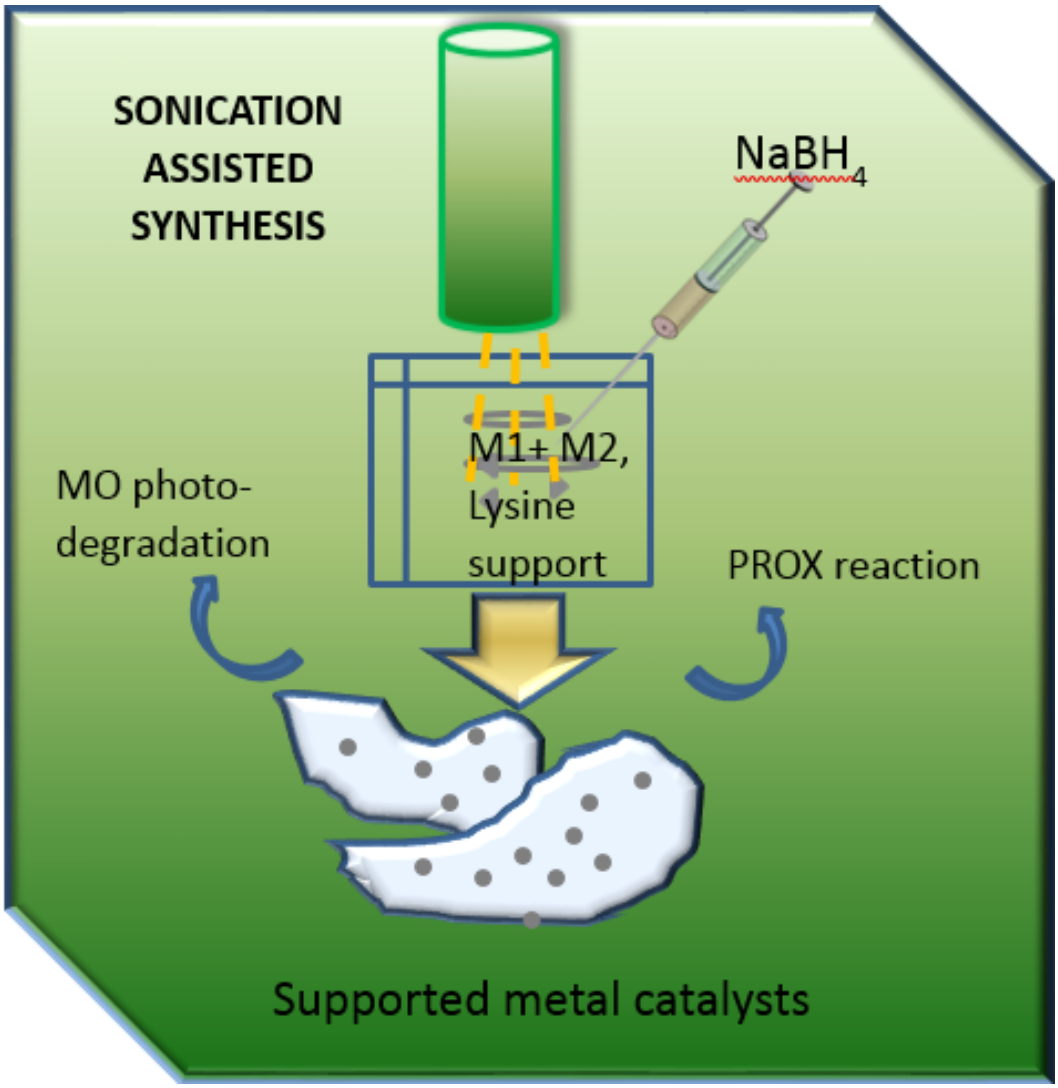

Figure 3.1. Schematic representation of the sonication-assisted method

3.2.3 Photocatalytic degradation of Methyl Orange (MO)

The photocatalytic degradation of methyl orange (MO) was carried out at 25 ^{o}C using 10 ml MO solution (40 mg/l) and 20 mg of solid catalyst under irradiation of the visible light (400-800 nm) with a chiller. The MO concentration was measured using a UV-vis spectrophotometer by comparing the peak intensity at 465nm. Prior to the reaction, the solution containing the photocatalyst was stirred for 2 h in the absence of light to saturate the adsorption of MO on the catalyst surface.

3.2.4 PROX reactions

The PROX reaction was carried out in a fixed bed reactor at atmospheric pressure using a gas mixture of 1 % CO, 1 % O_2, 78 % H_2, 20 % He at a GHSV of 5000 h^{-1}, or a mixture of 100 ppm CO, 100 ppm O_2, 99.78 % H_2, 0.2 % He at a GHSV of 50 h^{-1}. The reactant and product gases were analyzed with a GC Shimadzu-14B equipped with both TCD and FID detectors.

3.3 Results and discussion

In this section, the physical and catalytic properties of the laboratory synthesised metal nanoparticles are presented and discussed in detail. The characterization of prepared catalysts and analysis of their catalytic activities have been conducted using the following techniques; Transmission Electron Microscopy (TEM), X-ray Diffraction (XRD), Inductive Coupled Plasma- Optical Emission Spectroscopy (ICP-OES), UV-Vis Spectroscopy, Gas Chromatography (GC) and X-ray Photoelectron Spectroscopy (XPS).

3.3.1 Sonication-assisted preparation of the supported catalysts and hydrothermal synthesis of the one-dimensional (1D) support

In the sonication-assisted deposition-reduction preparations, experimental parameters such as the types of metal and support, pH value, Au/Pd ratio, solvent, reagent addition sequence were varied. In general, it is found that with this method prepare various supported metal catalysts with high dispersion can be prepared, including Au, Pt, Rh, Ru and Pd supported on Al_2O_3, TiO_2, ZnO and CeO_2, etc. The sizes of most metal particles are usually between 2-6 nm (**Figure 3.2**), varying a little with the change of metal, support as well as the pH (the pH was usually maintained above 6). In the Pd/γ-Al_2O_3 catalyst and Au-Pd bimetallic catalysts, the metal particles are in the range of

5-20 nm in size (the TEM images are not shown here). The large Pd particle size and wide distribution probably are related to the nature of the Pd and the low pH used, because the $PdCl_2$ precursor is not completely dissolved at high pH aqueous solution. TEM images in **Figure 3.2**, show the 1D γ-Al_2O_3 and CeO_2 materials were successfully prepared, the diameter of these nanorods was between 10 and 20 nm, and the aspect ratio between 5 and 20. These 1D nanostructures together with some commercial metal oxides were used as the catalyst supports.

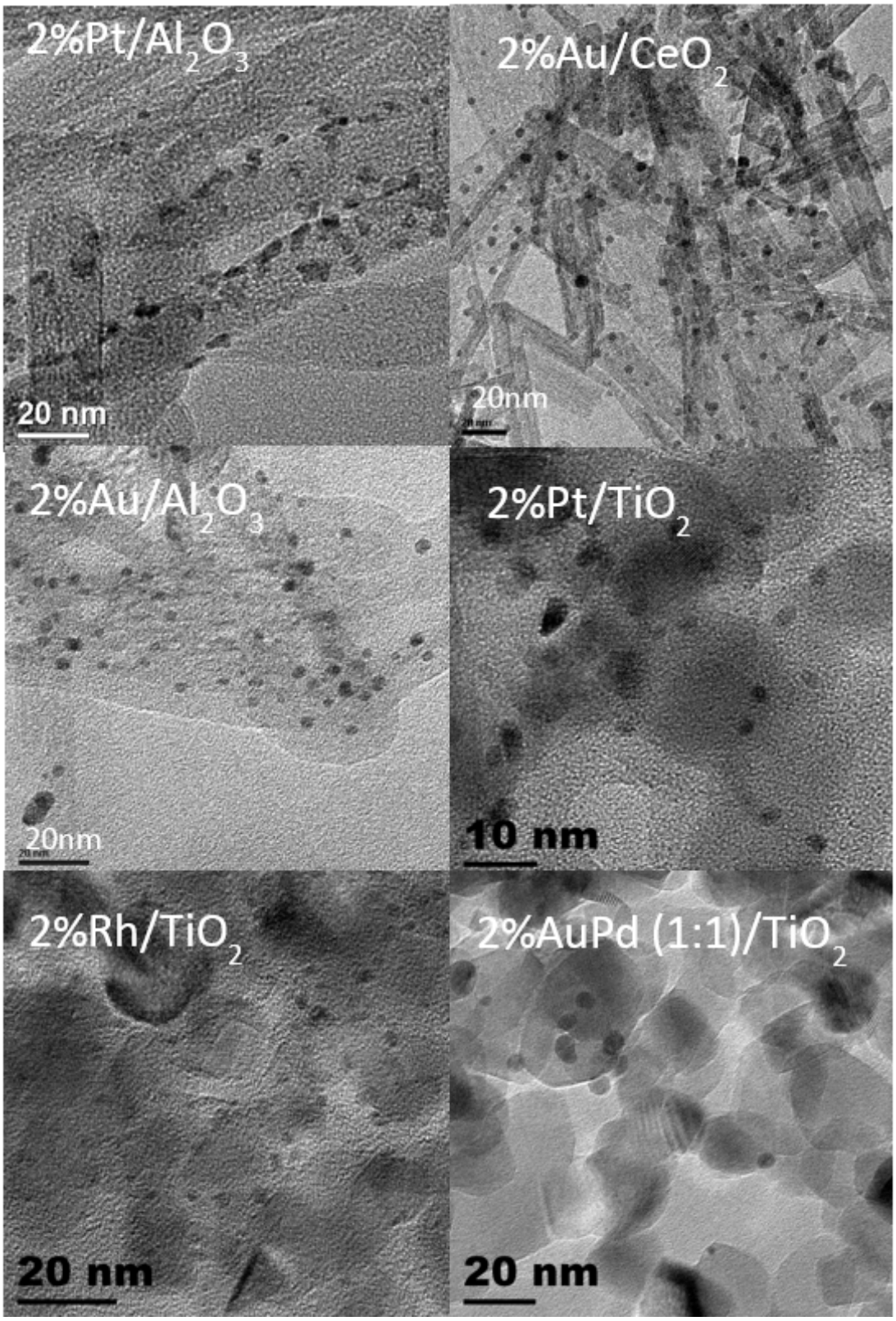

Figure 3.2. TEM images of the supported metal catalysts prepared by the sonication-assisted method.

However, the low pH value leads to the growth of large particles due to the crosslinking of metal particles by lysine molecules (127). Ethanol and ethanol-H_2O mixtures with various ethanol/H_2O ratios were also employed as the solvent. However, it was found that the use of ethanol solvent led to the formation of larger metal particles, including Au and Pd, etc.

The addition sequence of the reagent in the sonication-assisted preparation of Au-Pd catalysts was also varied. For example, to avoid the low solubility problem of $PdCl_2$ in H_2O, $PdCl_2$ or $HAuCl_4$ + $PdCl_2$ was dissolved in water at low pH below 3, followed by addition of $NaBH_4$ and lysine in the solution with sonication. Au was also initially deposited on the support at one pH value followed by the deposition of Pd at another pH on the Au-deposited catalyst (catalyst 6 in table 1), or vice versa (catalyst 7). Unfortunately, these approaches did not lead to the formation of very uniformly dispersed metal catalysts. Their TEM images are shown **Figure 3.3** and their catalytic performance will be outlined later.

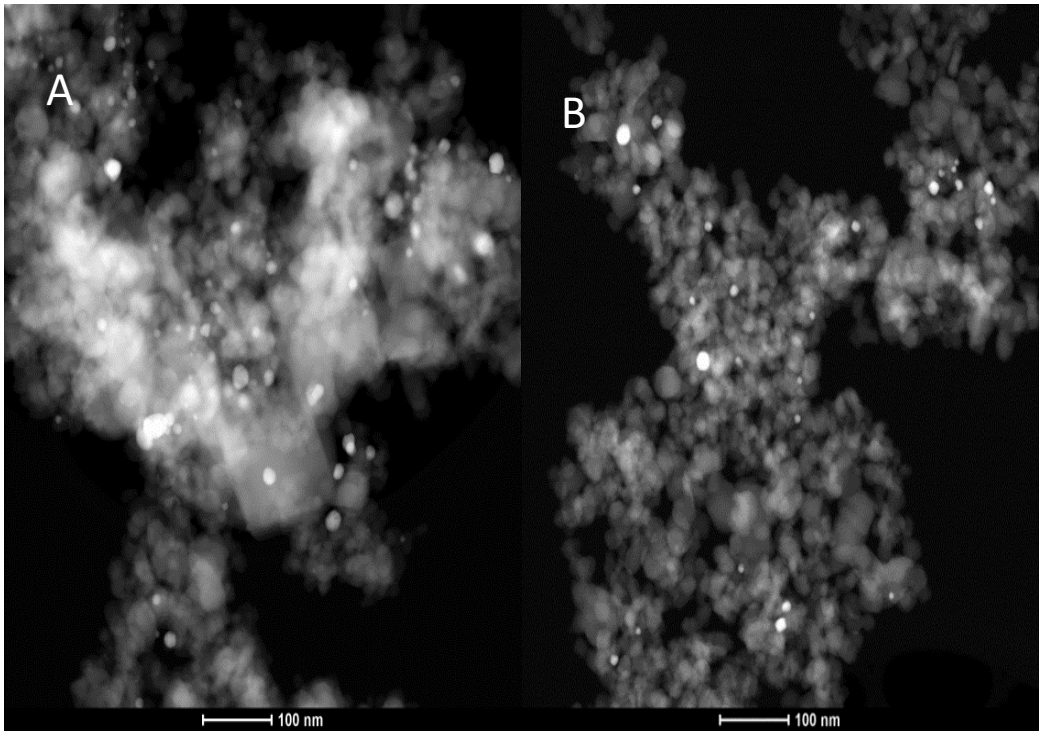

Figure 3.3. TEM images of the two 2wt%AuPd(3:1)/TiO_2 catalysts prepared by changing the deposition sequence of Au and Pd. (A) Pd was first deposited followed by Au deposition (Catalyst 6 in **Table 3.1**), and (B) Au was first deposited followed

by Pd deposition (Catalyst 7 in **Table 3.1**). The catalysts were calcined in air at 300 ^{o}C for 1h. Some large particles were identified in these two samples.

Table 3.1. ICP analysis of the catalyst composition

Catalyst no.	Theoretical atomic ratio of Au/Pd	ICP analysis			DE (%)	pH
		Au (wt%)	Pd (wt%)	Total (%)		
1(2wt%Au/TiO_2)	1:0	1.84	0.0	1.84	92	5.5
2(2wt%AuPd/TiO_2)	3:1	1.55	0.29	1.84	92	1.6
3(2wt%AuPd/TiO_2)	1:1	1.17	0.63	1.79	89	1.4
4(2wt%AuPd/TiO_2)	1:3	0.45	1.05	1.5	75	1.4
5(2wt%AuPd/TiO_2-R)	3:1	1.39	0.21	1.6	80	9.6
6(2wt%Pd-Au/TiO_2)	3:1	1.31	0.16	1.6	74	2.8/1.3
7(2wt%Au-Pd/TiO_2)	3:1	1.29	0.26	1.6	77	3.0/2.8

**Notes: DE = deposition efficiency.*
Catalysts 1–4: $NaBH_4$ was added into the slurry Au and Pd precursors, lysine solution and support.
Catalyst 5(#27): Au and Pd precursor solution was added into slurry containing $NaBH_4$, lysine and the catalyst support (inverse sonochemical method).
Catalyst 6 (#31): Pd was deposited first followed with Au deposition.
Catalyst 7(#32): Au was deposited first followed with Pd deposition.

In addition, it is seen from **Figure 3.2** that the Pt particles supported on the γ-Al_2O_3 nanorods are not spherical but triangular or oval shapes. Upon close inspection, these particles can be seen to be small aggregates composed of 2-3 individual particles each.

The most uniform metal particles are Au supported on various supports, and Rh supported on TiO_2 (**Figure 3.2**). Once the metal particles are deposited on the support, the catalysts were calcined at 300 ^{o}C in air to completely remove the capping lysine molecules on them. Since this calcination temperature is much lower than that required for the other capping agents such as thiols (126), it has little effect on the final metal particle size. This low temperature calcination is one of the merits of the lysine capping agent.

One of the important indicators for successful preparation of the catalysts is the deposition efficiency (DE). **Table 3.1** lists some of the DE values of the prepared catalysts by this sonication method. The highest DE value is observed for catalyst 1 (Au/TiO_2) and 2 (AuPd (3:1)/TiO_2), which is 92 %. With increasing Pd content, the

DE value decreased but was still above 70 %. These DE values are much higher than those of the catalysts prepared by co-precipitation and deposition-precipitation (126). The sonication-assisted method for catalyst preparation which is outlined is fast and versatile and suitable for the preparation of many catalysts with high DE values.

3.3.2 Au-Pd catalysts for the photocatalytic oxidation of MO and their structural characteristics

Photocatalytic reactions are important for environmental remediation because nowadays there is increasing pollution of water resources and air. It is desired to find cheap and sustainable solutions to purify these media (68, 130-132). In this work, photocatalytic degradation of MO was employed to test the photocatalytic property of the catalysts.

A number of mono- and bimetallic catalysts were tested for this reaction, including Au, Cu, Pd, Pt, and Au-Pd, Au-Cu, Au-Fe, Au-Co, Au-Pt and Au-Rh and Au-Ru supported on TiO_2. It was found that the supported Au-Pd series catalysts exhibited high catalytic activities. **Figure 3.4** displays the measured UV-vis spectra of MO after 1 h reaction on some catalysts, from which it can be seen that MO was degraded as its peak intensity at ca. 465 nm was decreased.

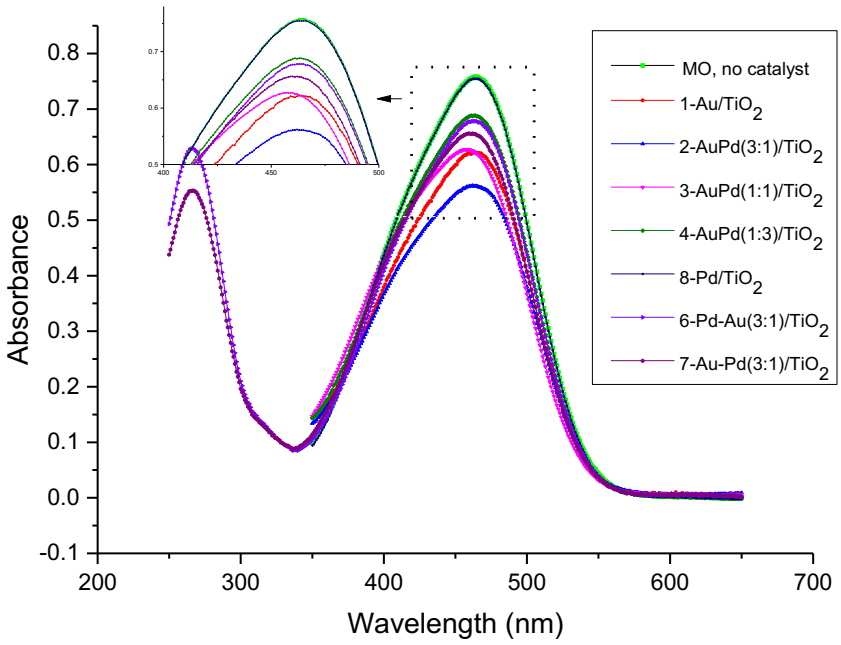

Figure 3.4. Catalytic degradation of MO under visible light at 25 ^{o}C (1 h).

Figure 3.5 shows the calculated MO conversion after 3 h reaction at 25 ^{o}C based on the peak area changes at 465 nm. The oxidized Pd/TiO_2 catalyst shows only a negligible MO conversion of 0.9 % after the 3 h reaction while that on Au/TiO_2 is 10.4 %, indicating that Pd (actually PdO, which will be explained later) is not active for this reaction but Au is. For the Au-Pd/TiO_2 catalysts that have a total theoretical metal loading of 2 wt. %, but with various Au/Pd atomic ratios, the MO conversion is increased with increasing Pd content at the beginning.

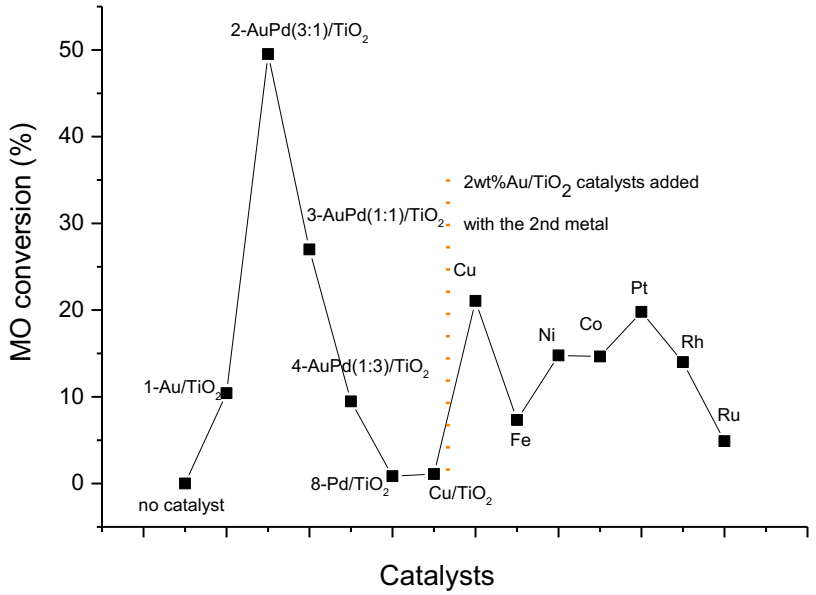

Figure 3.5. Catalytic degradation of MO under visible light after 3 h reaction at 25 ^{o}C.

The maximum MO conversion is achieved on catalyst 2 (2wt%AuPd(3:1)/TiO_2), which is ca. 49.5 % (**Figure 3.5**), although in this catalyst the theoretical Au loading is lower than that in catalyst 1 (Au/TiO_2). It is clear there is a synergetic interaction between Au and Pd which leads to a significant increase in catalytic activity. However, with further increase of the Pd content, the catalytic activity became lower again, probably because of the decrease of the most active Au sites on the catalyst surface. Since the Au component is quite active for this reaction, several catalysts with 2 wt. % Au and 1 wt. % of the 2nd metal were prepared and tested, and the catalytic performances are also shown in **Figure 3.5** (see the area on the right side of the orange dotted line). The addition of Cu, Pt, Ni, Co and Rh leads to an increase of the catalytic activity as compared to Au/TiO_2, but all of the catalysts are still much poorer than catalyst 2 (2wt%AuPd(3:1)/TiO_2), indicating the addition of these metals is not as good as Pd in promoting the catalytic performance of MO degradation. Therefore, in the following, the focus is on AuPd/TiO_2 catalysts only.

2wt%AuPd(3:1)/TiO_2 catalysts were prepared by varying the preparation method or conditions, e.g., by using the impregnation method and inverse sonication method (see

Table 3.1). After the 3 h reaction, the impregnation method prepared 2wt%AuPd(3:1)/TiO_2 catalyst showed only a MO conversion of 12.1 %, while catalysts 5, 6 and 7 in **Table 1** showed MO conversions of 15.9 %, 22.9 % and 9.8 % respectively, all of which are much lower than catalyst 2 (**Figure 3.5**). Why these catalysts were so different in catalytic performance is a point for consideration. As shown in **Table 3.1**, catalyst 2 has a little higher Au loading than catalyst 5, 6 and 7.

The measured XRD patterns are shown in **Figure 3.6**. Unfortunately, no Au and Pd reflections are observed because of the high dispersion and low loading of both Au and Pd. The major diffraction peaks of metallic Au should be located at 2θ = 38.2 and 44.4°, while those of metallic Pd would be at 40.1 and 46.7°. Thus the Au-rich AuPd alloy and Pd-rich AuPd alloy should exhibit reflections between 38.2 and 40.1° and between 44.4 and 46.7° respectively (133).

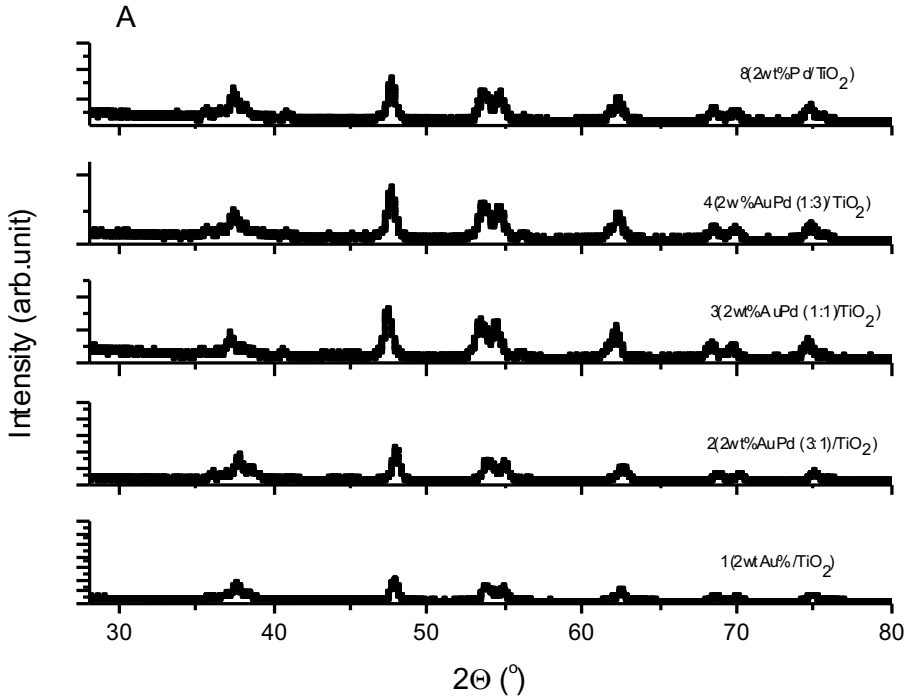

Figure 3.6. XRD patterns of some catalysts.

The UV-vis spectra measured for the catalysts are shown in **Figure 3.7** (next page). The Au nanoparticles have an intristic interband transition around 2.5 eV and thus

exhibit a surface plasmon resonance (SPR) band maximum at around 560 nm for Au/TiO_2 (134). This peak is not seen in the spectra of $AuPd/TiO_2$ catalysts, indicating the suppression of the plasmonic band of Au by Pd and a strong interaction between Au and Pd.

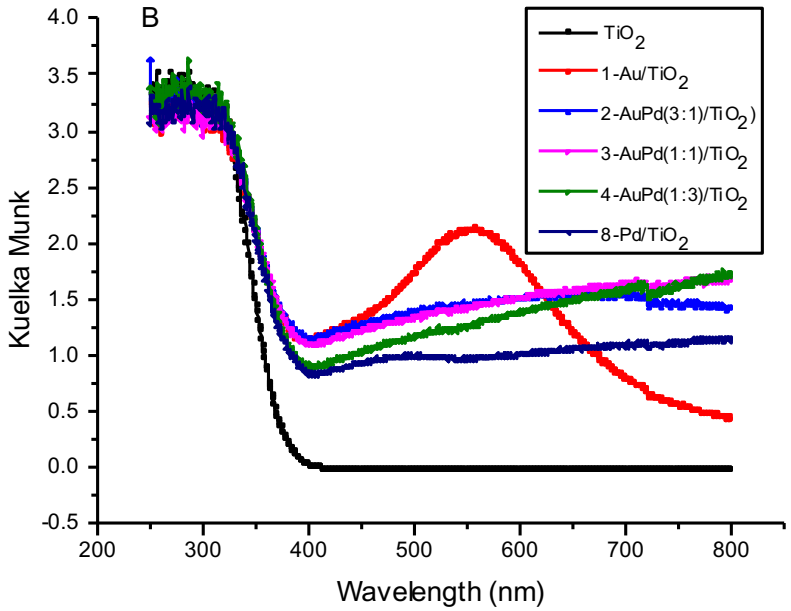

Figure 3.7. UV-Vis diffuse reflectance spectra of some catalysts.

Differing from Au nanoparticles, Pd nanoparticles only exhibit broad optical resonances that have been assigned to the so-called localized surface plasmons (LSPs) due to the fact that the d-band overlaps with the s- and p-bands over the whole range of interest (134). The change of the optical properties of Au after Pd addition is probably related to a change of electronic structure, which can partly confirm alloying of Au and Pd (135-138).

TEM analysis was further carried out for catalyst 2 comprising $2wt\%AuPd(3:1)/TiO_2$ and the results are shown in **Figures 3.8** and **3.9**. Quantification of EDX analysis from large area samples gives a ratio of Au:Pd =65:35. The intensity in HAADF-STEM images is proportional to the atomic number (Z^2) of atoms, and thus it can easily differentiate Au and Pd atoms due to difference between their atomic numbers. **Figure 3.8 (A)** shows a low magnification HAADF-STEM image of $2wt\%AuPd(3:1)/TiO_2$ catalyst. Since Pd nanoparticles have lower contrast than Au, no individual Pd

nanoparticles are observed on the substrate, indicating that the supported metal particles could be the mixture of Pd and Au.

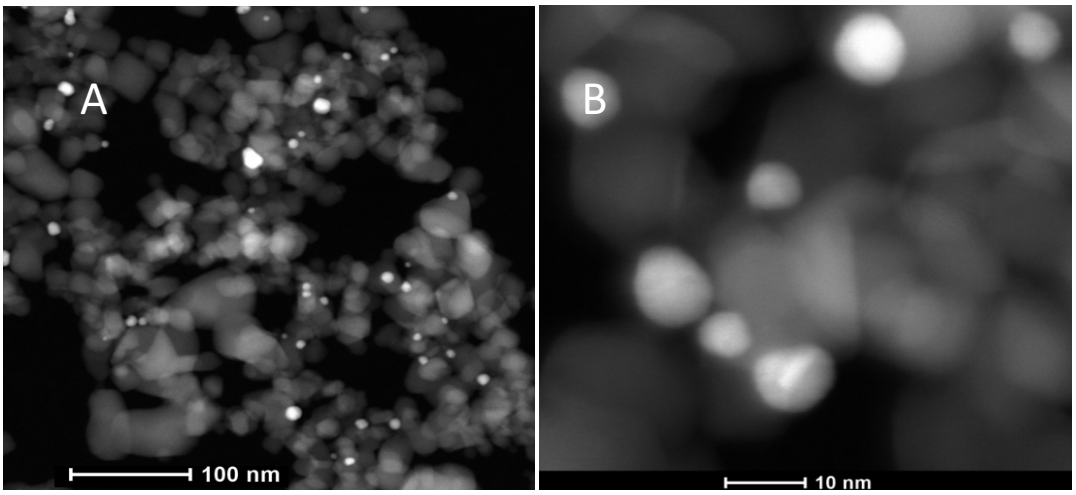

Figure 3.8. HAADF-STEM images of the 2wt%AuPd(3:1)/TiO_2 catalyst after oxidation in air at 300 ^{o}C.

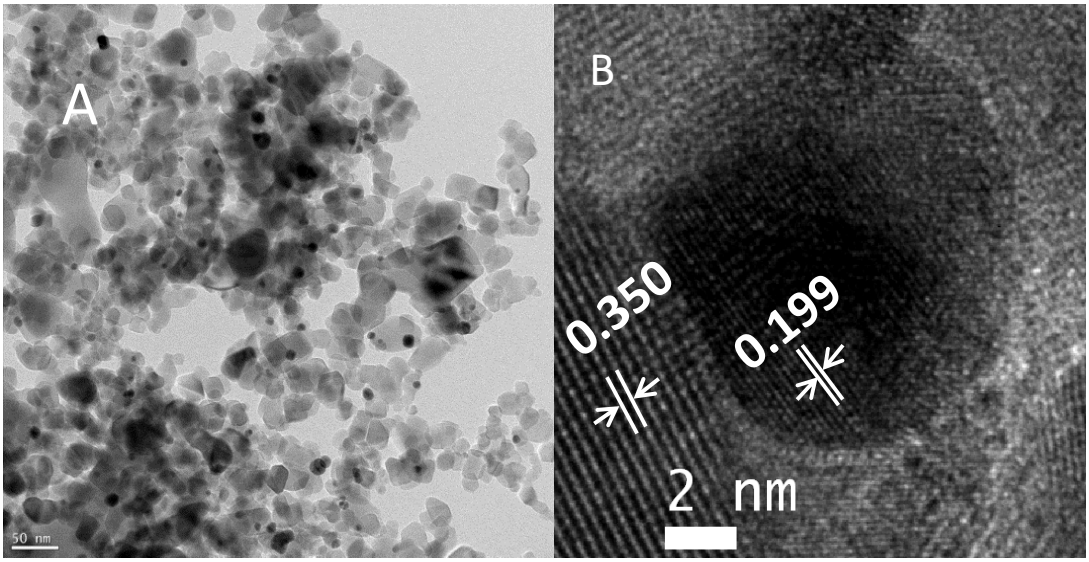

Figure 3.9. Low (A) and high (B) resolution TEM images of the 2-2wt%AuPd(3:1)/TiO_2 catalyst after oxidation in air at 300 ^{o}C.

Figure 3.9 (B) presents a high magnification STEM image of metal particles. The uniform contrast presented by the particle further strongly suggests an alloy structure of Au and Pd, rather than core-shell or bi-particle structures. A point EDX analysis acquired from one nanoparticle gave a composition of Au:Pd =69:31, confirming the alloy structure of particles. The high resolution TEM image (**Figure 3.9 B**) shows a 10-nm sized AuPd nanoparticle on the TiO_2 substrate. The lattice spacing measured for TiO_2 is 0.350 nm, corresponding to TiO_2 (101) plane with a standard value of 0.352 nm. The 0.6% error indicates the TEM instrument was well calibrated. The lattice distance of AuPd nanoparticle is 0.199 nm, which is between 0.195 and 0.204 nm, the distances of Pd(200) and Au (200) planes respectively. This measured distance is close to that of AuPd alloy with a ratio of 3:1 (0.202 nm), suggesting the metal nanoparticles are the alloy of Pd and Au.

XPS analysis was conducted for some catalysts to determine their surface structural features. The measured $Au4f_{7/2}$ binding energy appears in the range of 83.2 to 83.6 eV (**Table 3.2**), which is lower than that of bulk gold. Probably there is a shift of electrons from Pd or the oxygen-vacancies in TiO_2 to Au, leading to the partial negative charging of Au.

Catalyst no.	Theoretic composition	Au BE (eV)	Surface Au/Pd	Surface $Pd^{2+}/(Pd^{2+} + Pd^0)$
1- 2 wt%Au/TiO_2	2(2:0)	83.2	∞	---
2- 2 wt%AuPd/TiO_2	2(3:1)	83.3	1.59	0.059
3- 2 wt%AuPd/TiO_2	2(1:1)	83.5	0.64	0.34
6- 2 wt%Pd–Au/TiO_2	2(3:1)	83.4	1.06	0.052
7- 2 wt%Au–Pd/TiO_2	2(3:1)	83.6	1.03	0.41
8- 2wtPd%/TiO_2	2(0:2)	---	0	1.0

Table 3.2 XPS analysis results of some of the catalysts.

Table 3.2 and **Figure 3.10** give more details of XPS results. By comparing catalysts 2, 3 and 8 in **Table 3.2**, it is seen that with increasing Pd concentration, the surface

Au/Pd ratio is decreased, which is accompanied by an increase in surface Pd^{2+} concentration. These observations indicate that, besides alloying of Au with Pd which can modify the electronic properties of Au, the number of surface Au sites is also important for high catalytic activity.

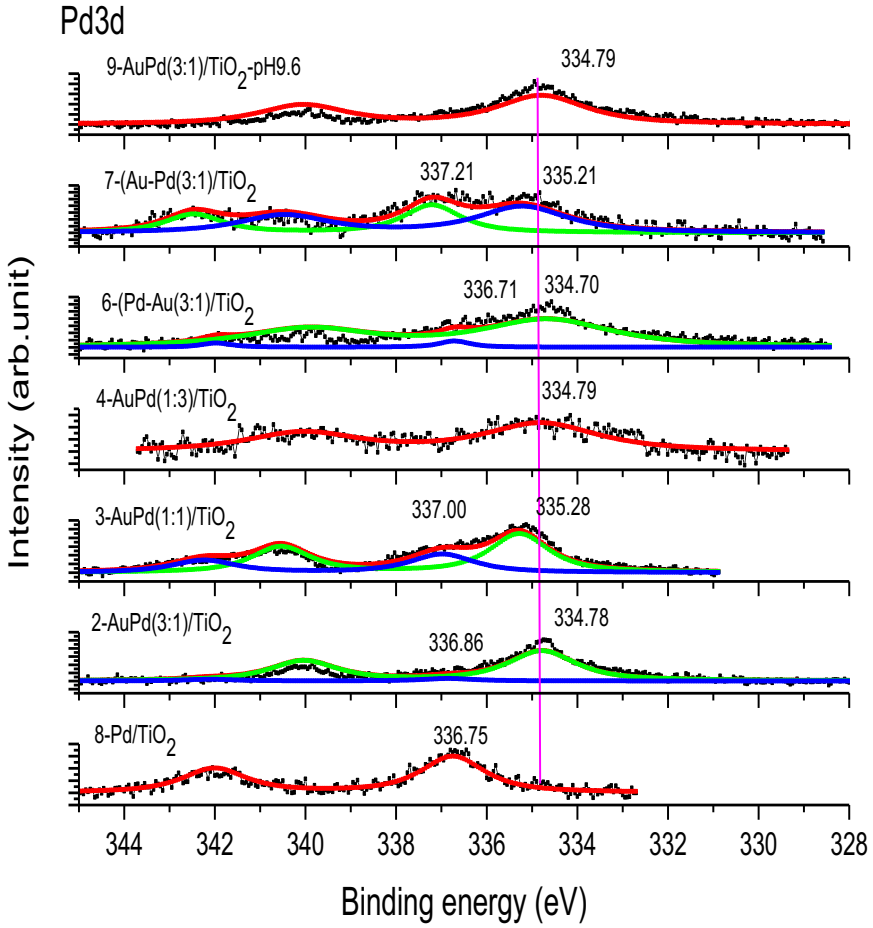

Figure 3.10. XPS analysis of the supported catalysts oxidized in air (before reaction).

When the Au/Pd ratio is below 3:1, more surface sites are occupied by Pd^{2+}, leading to decreased catalytic activity. More interesting information can be obtained by comparing catalyst 2 with catalyst 6 and 7. In catalyst 2, Au and Pd components are simultaneously reduced and deposited on the catalyst support, while in catalyst 6 and 7, Pd and Au are reduced and deposited in different sequences. In catalysts 6 and 7, both the surface Au and bulk Au concentrations (**Table 3.1**) are lower than those of catalyst 2. On the surface of the catalyst 7, there is a very high $Pd^{2+}/(Pd^{2+} + Pd^{0})$ ratio (0.41), because in this sample the Au was deposited first followed by Pd deposition.

Probably in this sample the surface of AuPd particles is PdO-rich, which could explain in possessing the lowest catalytic activity (only 9.8 % MO conversion after the 3 h reaction) amongst these three catalysts. For catalyst 8, the surface is completely covered by Pd^{2+}, indicating that Pd^{2+} is not active in this reaction. It can be further deduced that the alloying of Au-Pd can stabilize metallic Pd^{0} although probably there is a slight shift of the electron density from Pd to Au. The trace amount of surface PdO in catalyst 2 (**Table 3.2** and **Figure 3.10)** may contribute to the formation of the so-called "oxide-on-metal inverse catalysts" as reported by Bao et al. (116).

Actually, the Au-Pd particles supported on various catalyst supports have been widely investigated for different catalytic applications. Besides size or dispersion, there are various structural features for the Au-Pd particles that can impact upon their catalytic performance. They could form separate Au and Pd particles, alloy particles and core-shell structures.

For example, it was reported that the calcination of homogeneous Au/Pd alloys supported on Al_2O_3 resulted in progressive enrichment of Pd at the metal particle surface and a decrease in catalytic activity (38, 139). On the other hand, Au@Pd nanoparticles supported on silica were transformed into random alloy particles at 300 °C (140). Cybula et al. (133) found that for an AuPd/TiO_2 catalyst for phenol degradation under UV light, catalytic performance is highly dependent on the catalyst calcination temperature.

The catalysts calcined at 350 and 400 °C exhibited the highest photocatalytic activity while that calcined above 450 ^{o}C became poorer in catalytic performance. It was found that the higher calcination temperature caused segregation of the two metals and gold-enrichment in the shell region of Au/Pd bimetallic nanoparticles. Even in the alloyed particles, the distribution of Au and Pd was not homogeneous (133). This situation is quite similar to the cases presented within this chapter: Au-Pd alloy particles are formed and certain amount of Pd^{2+} is observed on the surface. Combining the literature with our results, it is proposed that the ideal catalyst should have a structure of alloyed Au-Pd with an Au/Pd atomic ratio around 3, and with a trace amount of PdO islands decorating the Au-Pd surface, as shown in **Figure 3.11** (next page).

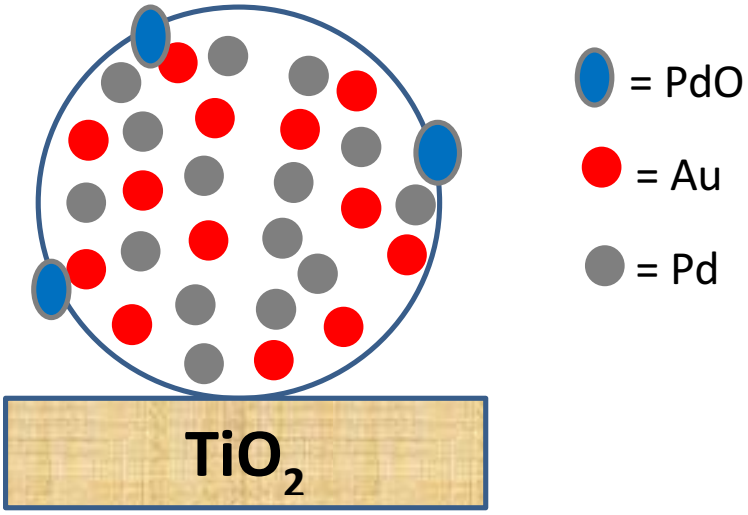

Figure 3.11. Ideal AuPd/TiO_2 catalyst for the MO degradation reaction.

3.3.3 Supported metal catalysts for PROX reaction

The catalysts prepared by the sonication-assisted method were tested for the low temperature preferential oxidation (PROX) reaction because it is an important industrial reaction used for purification of H_2 in hydrogen fuel cells (141, 142). Nowadays the majority of the world's hydrogen supply is produced by reforming hydrocarbons (129, 142-144). This 'reformate' hydrogen contains significant quantities of CO that poison current fuel cell devices. The PROX reaction removes CO through selective (preferential) oxidation of CO while avoiding oxidation of hydrogen in reformate.

For the PROX reaction, a series of metals were screened and it was found that Ru/TiO_2 (129), Au-Cu/SBA-15 and Pt/Al_2O_3 catalysts exhibited high catalytic activities. The Ru/TiO_2 and Au-Cu/SBA-15 catalysts were tested previously at high GHSVs close to 20000 h^{-1} and both of them were able to lower the CO concentration to several ppm (**Table 3.3**). At above 200 ^oC on the Ru/TiO_2 catalyst the methanation reaction was the dominant reaction rather than PROX reaction (129); while Au-Cu/SBA-15 catalyst

was extremely active even at room temperature. However the catalyst was not stable and was deactivated due to the reversible alloying of Au and Cu (142).

Catalyst	Reaction temperature (°C)	CO concentration (ppm)		Stability tested (h)
		Before reaction	After Reaction	
10 (2 wt% Pt/Al2O3)	150-20	10,000	2-5	100
11(2 wt% Ru/Al2O3)	200-270	10,000	5-10	20
12(2 wt% Cu–Au/SBA-15)	25	10,000	5-10	12

Table 3.3. Catalytic performances of several catalyst for PROX reaction.

The 2wt%Pt/γ-Al_2O_3 nanorod catalyst was prepared by the impregnation method and the sonication-assisted method in this work. As shown in **Figure 3.12**, the sonication method prepared 2wt%Pt/γ-Al_2O_3 was able to lower the CO concentration from 10000 ppm to ca. 51 ppm at ca. 160 °C, while the impregnation method prepared 2wt%Pt/γ-Al_2O_3 could only lower the CO concentration to ca. 1700 ppm at ca. 200 °C.

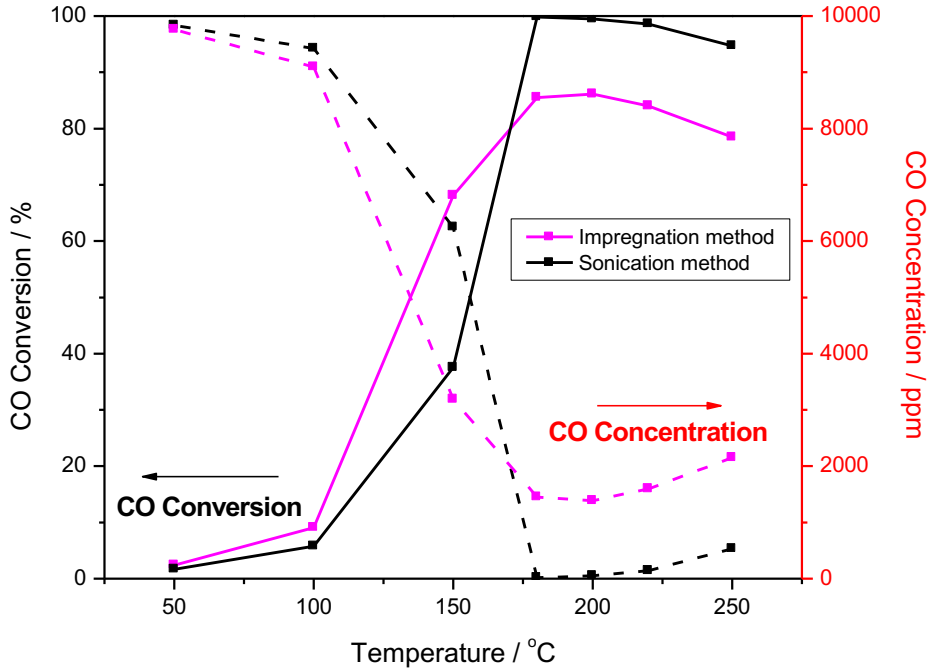

Figure 3.12. PROX reaction on Pt supported catalysts. The catalysts were reduced in 5 % H_2 at 300 °C for 40 minutes prior to the reaction. The catalytic reaction was carried out in the flow of 1 % CO, 1 % O_2, 78 % H_2, 20 % He at a GHSV of 5000 h^{-1}.

The sonication method prepared catalyst is very stable. Upon a 100 h on stream lifetime test, no deactivation was observed. We further increased the Pt loading to 3 wt. % and lowered the CO concentration to ca. 100 ppm in the feeding gas, and both the γ-Al_2O_3 nanorods and commercial γ-Al_2O_3 from SASOL were used as the support.

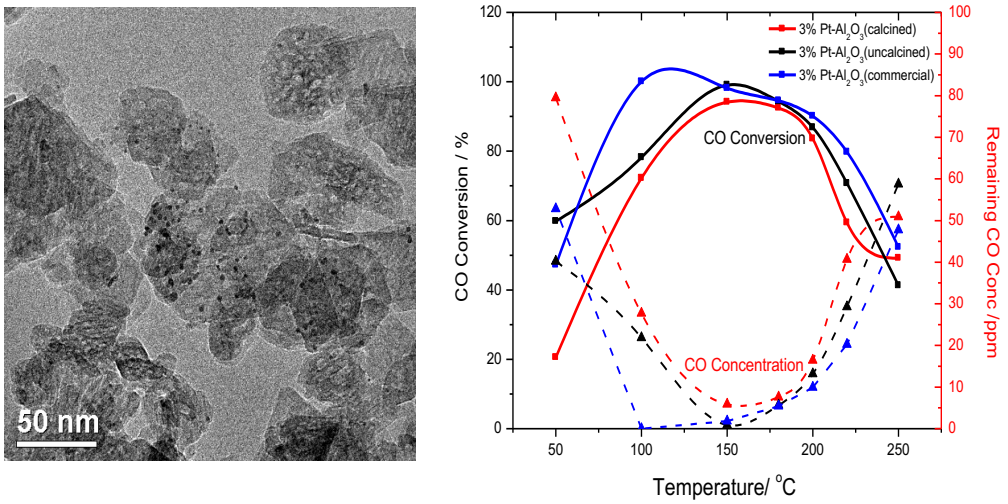

Figure 3.13. PROX reaction on Pt supported catalysts. (left) TEM image of the 3%Pt/Al_2O_3 (SASOL), and (right) the catalytic performances of the 3%Pt/Al_2O_3 catalysts. Two kinds of Al_2O_3 supports were used. One was Al_2O_3 nanorods with and without calcination, and the other was γ-Al_2O_3 from SASOL. The catalysts were reduced in 5 % H_2 at 300 ^oC for 40 minutes prior to the reaction. The catalytic reaction was carried out in the flow of 100 ppm CO, 100 ppm O_2, 99.78 % H_2, 0.20 % He at a GHSV of 50 h^{-1}.

It is observed in **Figure 3.12** and table 3 that the 3wt%Pt/γ-Al_2O_3 (SASOL) is able to lower the CO concentration to several ppm at a reaction temperature of ca. 100 ^oC, much lower than the 3wt%Pt/γ-Al_2O_3 nanorods, which show the highest CO removal at ca. 150 ^oC. The detailed reason for this catalytic performance is not yet clear. However, it is apparent that the sonication method prepared catalysts are promising for practical catalytic applications, particularly when a two-stage reaction

configuration is applied, in which the first stage reaction will remove most of CO while the second stage reaction will lower the CO concentration to several ppm.

3.4 Conclusion

In this work, the sonication-assisted precipitation-reduction has been extended to the preparation of various mono- and bi-metallic catalysts supported on various supports and applied for photocatalytic degradation of MO and also the PROX reaction. In general, there are three advantages for the sonication method as compared with the conventional methods, including the high dispersion of metal nanoparticles on the catalyst support, the much higher DE values compared to the DP and CP methods, and the very fast preparation procedure as the deposition only takes 10-20 seconds.

The photocatalytic degradation of MO over a series AuPd/TiO_2 showed that the AuPd(3:1)/TiO_2 catalyst is much more active than the other catalysts, mainly because of the high dispersion of the metal particles, the formation of Au-Pd alloy particles and the decoration with trace amounts of PdO on the surface of the Au-Pd alloy particles. It was found that, besides the solution pH value, the addition of the metal solution into the $NaBH_4$ solution in the preparation (the inverse sonication method) and the separate deposition of Au or Pd leads to phase separation of Au and Pd, which is not conducive to catalytic activity.

For the PROX reaction, the highly dispersed Ru/TiO_2, Au-Cu/SBA-15 and Pt/γ-Al_2O_3 catalysts prepared by the sonication method were found to be very active. The Pt/γ-Al_2O_3 catalyst was also quite stable. Moreover, it was found that the Pt/γ-Al_2O_3 (SASOL) catalyst was able to lower the CO concentration to several ppm at lower reaction temperature (100 ^{o}C), indicating promise for practical application.

Chapter 4

Gold Nanorods, Length, Pre- and Post- Immobilization and Structure-Conversion Symbiosis

4 Gold Nanorods (AuNRs): Length, Pre- and Post- Immobilization and Structure-Conversion Symbiosis.

4.1 Introduction

In order to grow, anisotropic nanoparticles like nanorods have to overcome a process that otherwise does not happen spontaneously. It is a relatively complex process and nanorods, unlike spheres, are a field still to be exploited although many studies have already been carried out (21, 26, 54, 96, 145-148).

Gold nanorods are anisotropic nanoparticles, being the most studied shape (54, 59, 96, 148-150). Even though several synthesis methods have been developed such as the template method (127, 151) where relatively small nanobars can be obtained or electrochemical methods (152-154), it is the seed-mediated method which has been highlighted (59, 155).

The seed-mediated method has been applied in the experiments as it has many advantages including the one that comes with the wet chemistry approach; no prefabricated templates are necessary. In addition, it has been shown to give a good yield of nearly mono-disperse nanoparticles (97).

In this chapter, the synthesis of colloidal gold nanorods using seed-mediated synthesis method (59) has been carried out and the resultant nanorods successfully supported on titania via sol-immobilization. We have also performed the photodegradation of methyl orange and selective oxidation of hydroxymethyl furfural in order to obtain an understanding of the performance of the catalyst prepared.

4.2 Experimental

In this chapter, gold nanorods AuNRs (59) with different aspect ratios (AR) have been synthesized and subsequently supported by sol-immobilisation (110). The support used was titania TiO_2 Degussa P25 which is a photocatalyst that is used widely due to

its stability, non-toxicity, low cost and relativity high levels of activity in many photocatalytic reaction systems (156). Obtaining adequate control over the morphology of the nanoparticle is essential and at this point, within the different synthesis techniques, the bottom-up synthesis methods offer better control of the shape and size using, for this purpose, stabilizing agents (83). The catalytic activity of the nanoparticles was tested by selective oxidation of hydroxymethyl furfural and photodegradation of the azo-dye methyl orange (MO).

4.2.1 Synthesis of Gold Nanorods (AuNRs)

A- Synthesis of colloidal Gold Nanorods:

Gold nanorods (AuNRs) with various aspect ratios (AR) were synthesized through the well-known method of El-Sayed (59) with modifications. Seed preparation was carried out by mixing $HAuCl_4 \cdot 3H_2O$ (5 ml, 1 mM) with CTAB (5 ml, 0.2 M) solution, followed by addition of freshly made, ice cold $NaBH_4$ (600 μl, 10 mM) under rapid stirring for 1 min. $NaBH_4$ is a strong reducing agent and its addition resulted in a brownish-yellow coloured solution. The mixture was then allowed to stand without disturbance at 28-30°C for at least 1 hour before use.

To make gold nanorods, the seeds were then added to a growth solution and incubated at 30°C overnight to allow complete rod growth. The growth solution was typically prepared as follows. The desired amount of gold solution ($HAuCl_4.3H_2O$ 1 mM), in order to achieve the wanted metal loading, was first mixed with CTAB solution (0.2 M). Then, it was acidified with HCl to reach a pH about 3. According to the rod dimension and longitudinal plasmon wavelength desired, an appropriate amount of $AgNO_3$ (1 mM) was added to the mixture, followed by the rapid addition of L-Ascorbic Acid (AA) solution (78.8 mM). The mixture turned colourless instantly and finally the rod growth process was initiated due to the addition of the seed solution as prepared above. The colour of the mixture would usually change within minutes, suggesting successful growth of seed particles. This method typically produces short nanorods (rods with an aspect ratio (AR) up to 4-5).

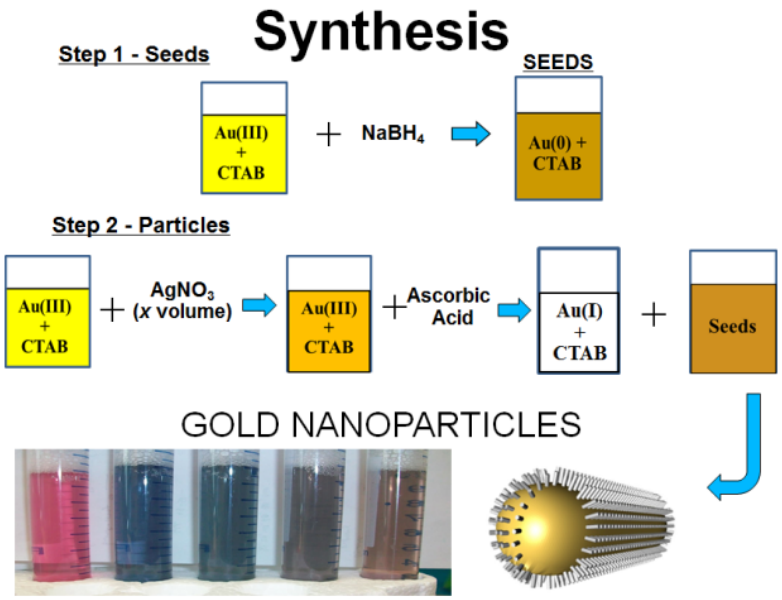

Figure 4.1. Seed-mediated growth in a typical synthesis of gold nanorods. Simply by varying the amount of silver added the aspect ratio (AR) can be tuned. Small amounts of silver produce spheres, and as the silver amount is increased, the length of rods increases as well.

B- Immobilization of Colloidal Gold Nanorods:

Before AuNR in colloidal solution can be immobilised, they must be purified by centrifugation in order to remove the excess of reagents, especially the surfactant CTAB. Typically, the solution was centrifuged at 14,500 rpm for 15 min to separate the gold nanorods. The colourless supernatant was very carefully discarded. The solid pellet was then re-dispersed in deionised (DI) water depending upon the quantity of the residue. The centrifugation was repeated 2-3 times and finally the solid residue was re-dispersed in DI water.

In the next step the colloidal suspension was transferred to a 250 ml round bottom flask followed by the procedure outlined above with modifications (110). 25 ml of titania water solution was acidified to pH 1 with sulfuric acid and was added to the colloidal nanoparticle solution (and 25 ml more used to wash down the glassware) and it was left for 2 hours under vigorous stirring and then filtered and washed with distilled water until a neutral pH value was obtained. The solid was dried overnight in the vacuum oven at 60 °C and finally grinded. No further treatments were performed.

4.2.2 Photodegradation of Methyl Orange (MO)

In a typical reaction, 10 ml of MO solution (40 mg/l) and 20 mg of solid catalyst were mixed in a 12 ml vial with a magnetic stirrer. The mixture was stirred overnight in the dark (after dark reaction, one sample of 2 ml was taken and kept in the dark for subsequent analysis) and then irradiated under visible light (400-800 nm) for 3 hours in a photoreactor LuzChem ICH2 (shown Chapter 2) at constant temperature of 30 °C and under vigorous stirring (1000 rpm). Then, the sample was taken from the mixture and the UV-Visible spectrum of the MO solution was measured with a UV-Visible spectrophotometer.

4.2.3 Selective Oxidation of 5-Hydroxymethyl-2-furfural (HMF)

The oxidation of 5-hydroxymethyl-2-furfural (HMF) was carried out using an autoclave (Parr Instruments) reactor of 100mL capacity. This reactor was equipped with a magnetic stirrer (0-1500 rpm), specifically a cross-magnetic stirrer bar, to achieve homogeneous mixing of oxygen gas into the solution. It was also equipped with temperature and pressure measurement and control equipment.

The reactor was charged with an aqueous solution (10 mL water) containing the appropriate amount of HMF, metal catalyst and base (NaOH) (molar ratio [1:0.01:4]). The temperature was increased to 60 °C and the reaction mixture was stirred at ca. 1500 rpm for 4 h. The autoclave was purged 3 times with O_2 (5 bar) and then pressurized at 20 bar. At the end of the reaction, the reactor was cooled on ice and the solution was filtered under vacuum using 0.2 μm PTPE filter paper.

Then, the solution was diluted before analysis with a HPLC using a 0.01M H_2SO_4 solution as the mobile phase. The identification and quantification of compounds was archived by calibration using commercial samples. This reaction was conducted in collaboration with a visiting researcher and Erasmus practice student resident in the group, Susana Guadix Montero.

4.3 Results and discussion

Gold nanorods in colloidal state and supported on titania and their catalytic activity was characterised using techniques such as UV-Vis-NIR Spectrophotometry, Coupled Plasma-Optical Emission Spectroscopy (ICP-OES), X-ray Powder Diffraction (XRD), Transmission Electron Microscopy (TEM), High-Performance Liquid Chromatography (HPLC) and Scanning Electron Microscopy (SEM).

4.3.1 Colloidal Gold Nanorods (AuNRs)

UV-Vis absorption spectra for two different seeds made with different concentrations of CTAB can be seen in **Figure 4.2**. When the synthesis was carried out with a lower concentration of CTAB than that established by the method of Nikoobakht and El-Sayed (59) larger nanoparticles are obtained. Seeds 1 represented in blue were prepared with a molar ratio (CTAB:Au=200) which leads to bigger seeds and it can be seen by the higher intensity of the UV-Vis absorption spectra. These seeds lead to the creation of spherical nanoparticles as the blue dotted line plot shows, whereas smaller seeds (Seeds 2, represented by “red” colour lines) were made at a higher molar ratio (CTAB:Au=400) leading successfully to the creation of the desired morphology (nanorods).

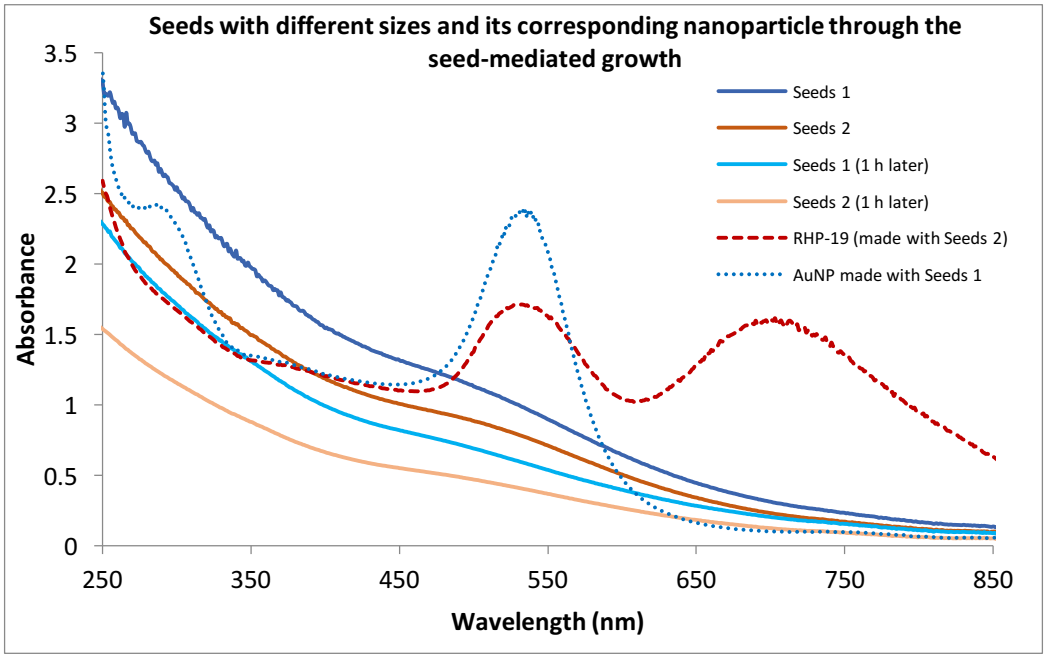

Figure 4.2 UV-Vis absorption spectra of gold seeds for the synthesis of AuNR made with two different concentrations of CTAB (0.1 and 0.066 M) and measured just after synthesis and 1 hour later.

In the seed-mediated technique, the growth solution consisted of an aqueous solution of the surfactant cetyltrimethylammonium bromide (CTAB) and gold in 3+ oxidation state (Au^{3+}) that is selectively reduced from Au^{3+} to Au^{+} by a mild reducing agent, ascorbic acid. This is followed by the addition of the gold seed solution which catalyse the reduction of Au^{+} on the seed surface. It has been proposed that isotropic morphology breaking of the seeds by crystal twinning results in formation of penta-tetrahedral structures with different facets and the selective interaction of CTAB with some specific facets of gold seed result into anisotropic growth and thus formation of nanorods (17). However, the microscopic mechanism of anisotropic growth is still not well understood.

Figures 4.3 and **4.4**, below, show three different nanorods with different aspect ratios in colloidal suspension for two sets of experiments. The synthesis method is exactly the same for each set of syntheses and nanorod elongation is achieved by simply adding different amounts of silver that acts as a point of growth. Without proper and accurate synthesis conditions, especially temperature control, results obtained for the same reaction are very changeable, even when performed by the same person and in

the same laboratory. More studies have to be undertaken in order to obtain accurate control of nanorod synthesis.

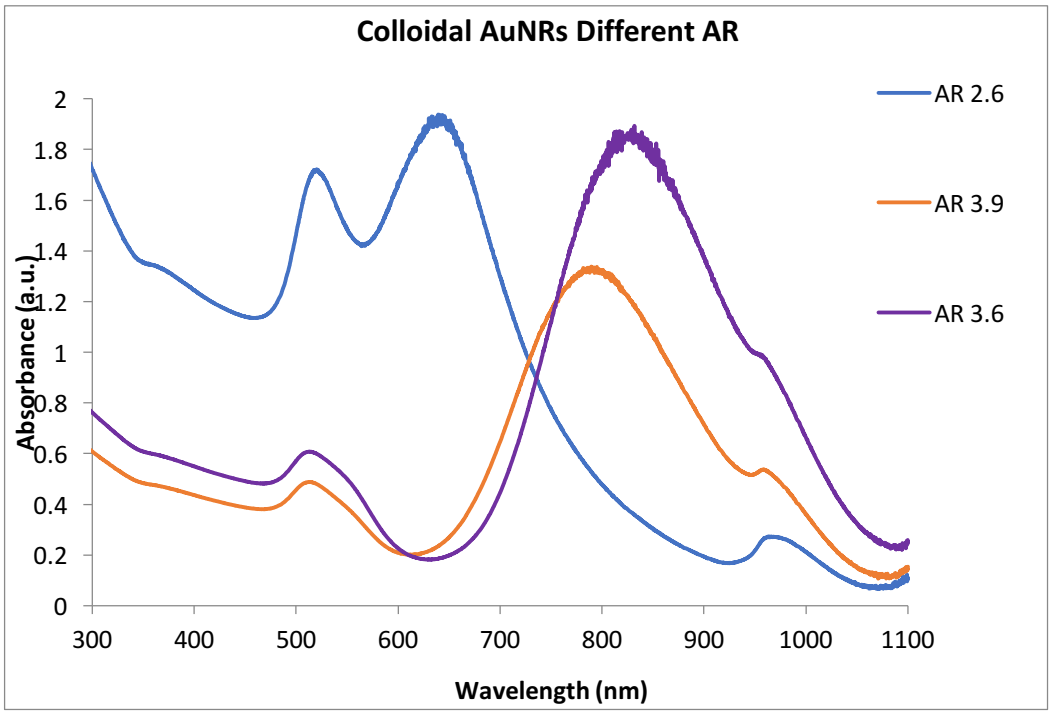

Figure 4.3. UV-Vis absorption spectra of AuNR colloidal suspensions of different aspect ratios. Catalysts RHP-14, 15 and 16.

For the rods shown in **Figure 4.3** aspect ratios (AR) have been determined from TEM measurement of images of the supported gold nanorods. Below, in the supported nanoparticle section, **Figures 4.7 and 4.8** show comparative UV-Vis solid diffuse reflectance spectra of both sets of synthesis, respectively. Significant differences especially for the gold nanorods in **Figure 4.4** were found.

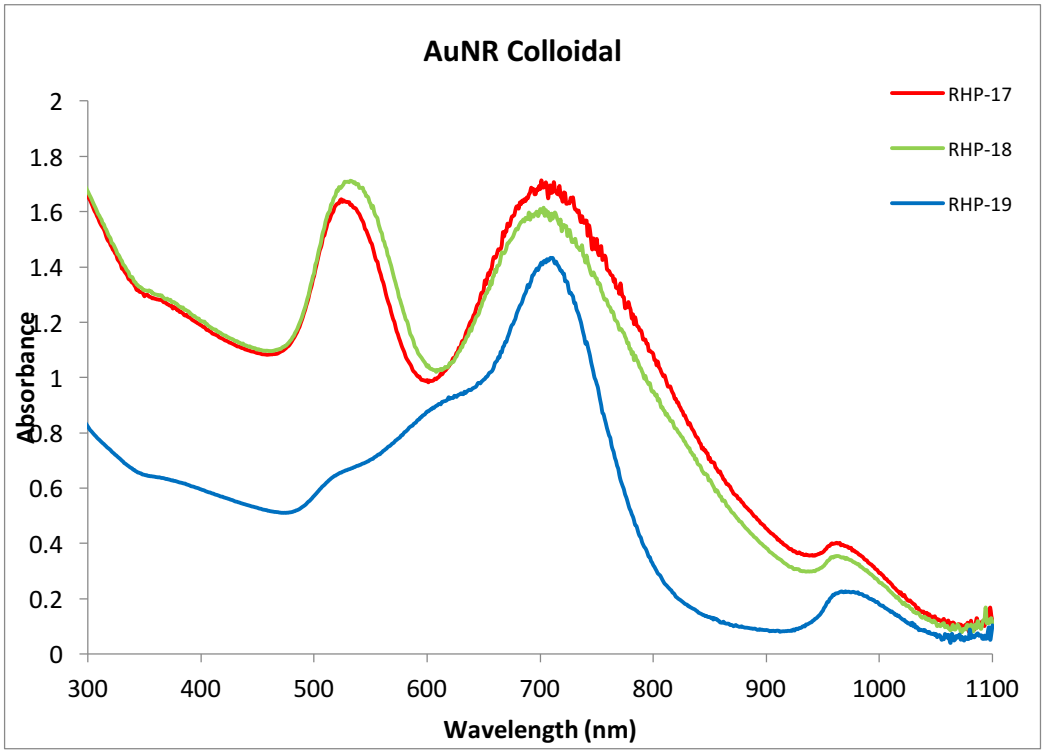

Figure 4.4. UV-Vis absorption spectra of AuNR with different aspect ratios in colloidal suspension

Figures 4.5 and **4.6** (next page), present representative images at different magnification for two nanorods with different aspect ratios, respectively. In both cases, the diameter is quite similar with variation in the length occurring, and which is achieved by modifying the amount of silver employed in the synthesis. Given that the aspect ratio (AR) is the the length divided by the diameter, for the same diameter, longer rods result in higher aspect ratios.

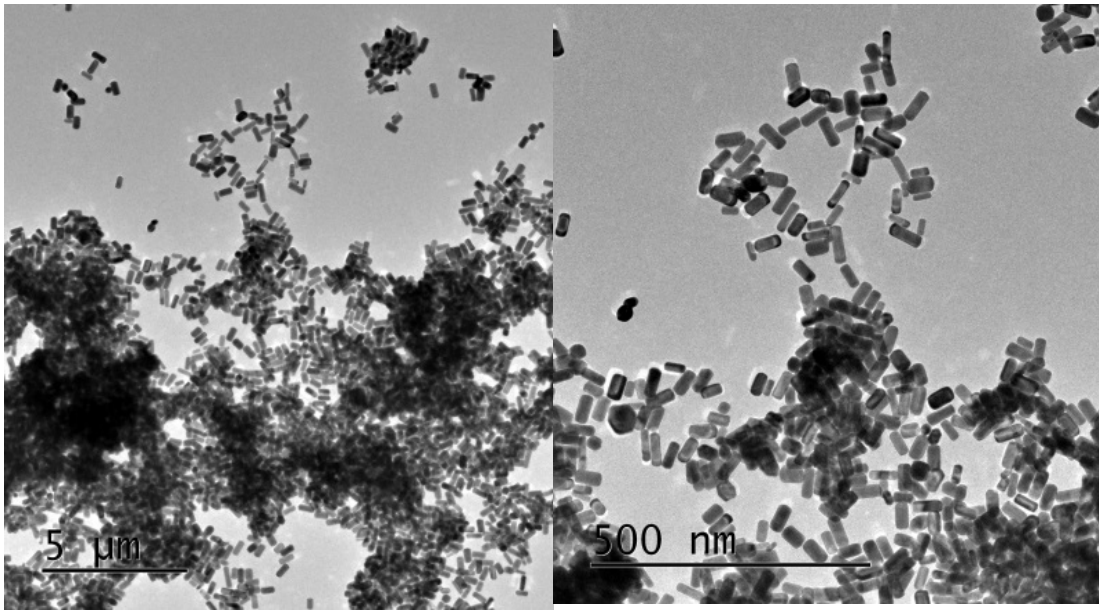

(a) **(b)**

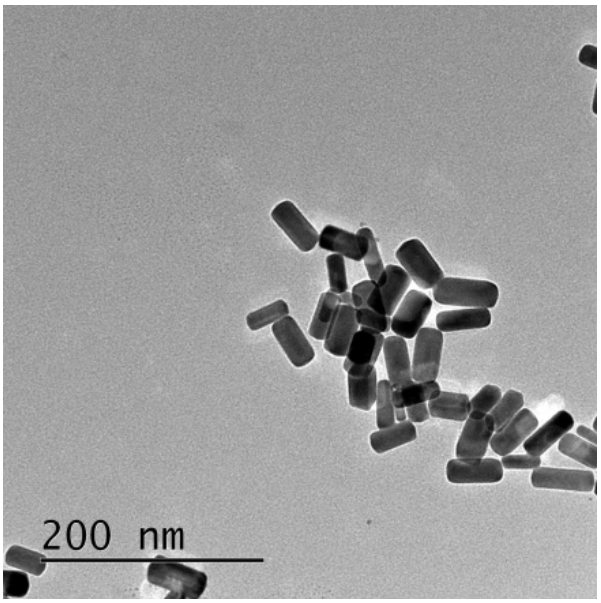

(C)

Figure 4.5 TEM images (a) (b) and (c) of short AuNRs. Rods in colloidal suspension of catalyst RHP-20 prior to immobilization.

The images show a homogeneous nanoparticle size distribution. Scaling up of the synthesis results in problems to overcome to obtain a homogeneous nanoparticle size distribution because of the influence of different variables.

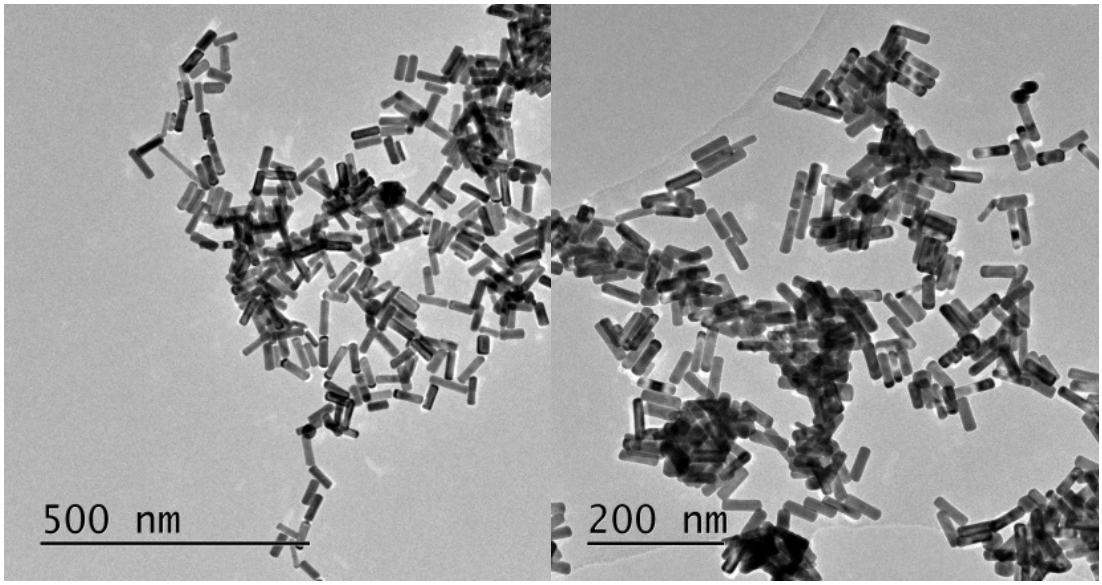

(a) **(b)**

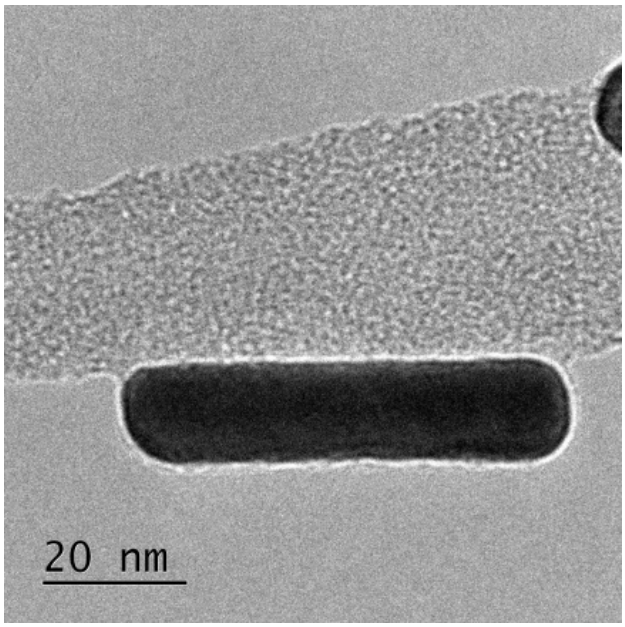

(C)

Figure 4.6 TEM images (a) (b) and (c) of longer AuNRs (higher Aspect Ratio AR). Rods in colloidal suspension of catalyst RHP-21 prior to immobilization.

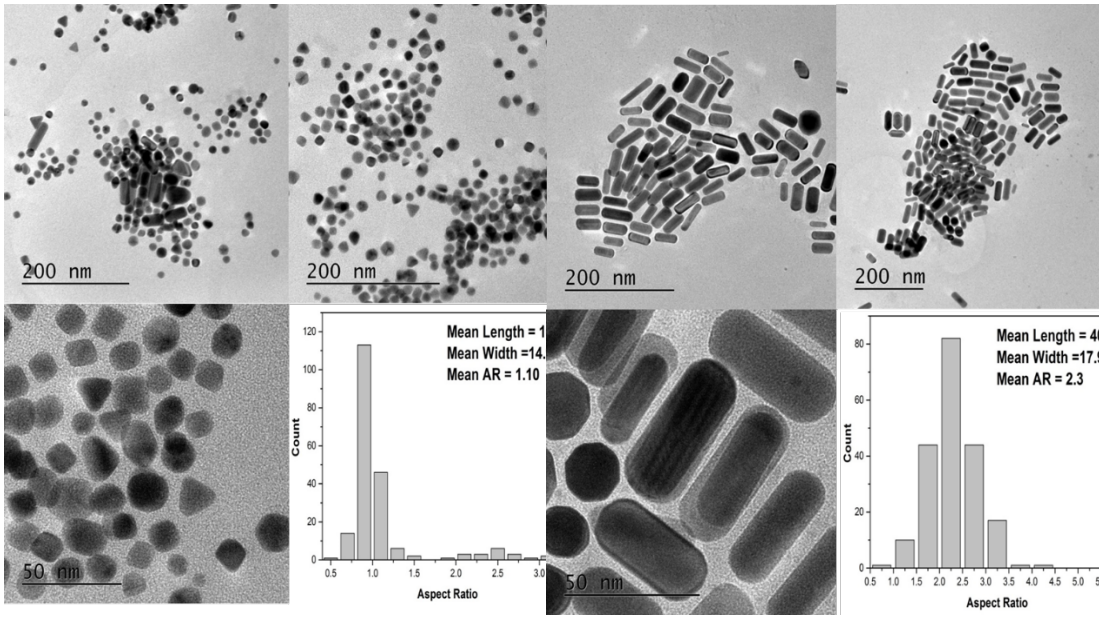

(a) RHP-49 **(b) RHP-50**

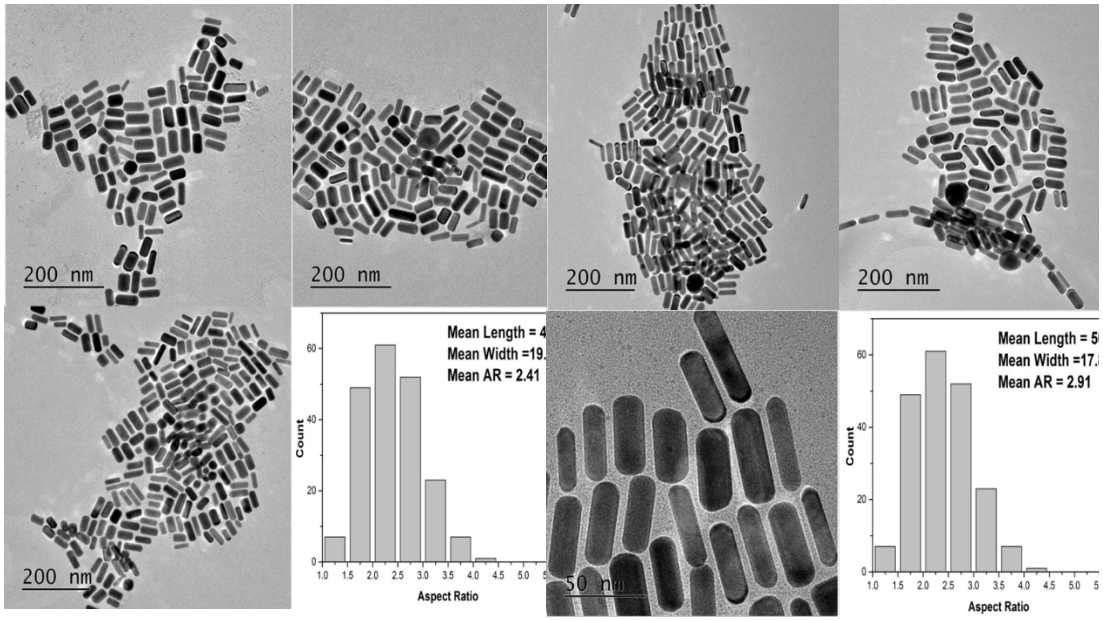

(c) RHP-51 **(d) RHP-52**

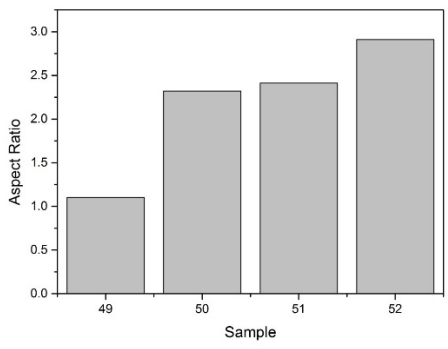

(e)

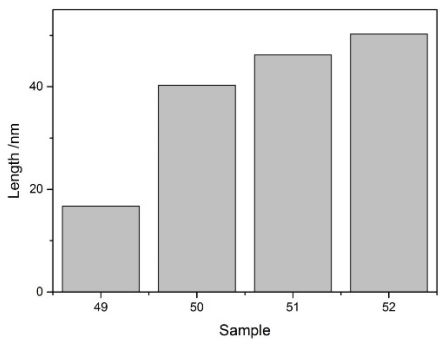

(f)

Figure 4.6 (Previous page) TEM images of colloidal nanorods (a), (b), (c) and (d) with calculated aspect ratios (AR) corresponding to catalyst RHP-49, 50, 51 and 52. Charts (e) and (f) correspond to the aspect ratios and length of the samples measured.

4.3.2 Supported Gold Nanorods (AuNR/TiO_2)

In order to obtain stable and durable catalyst materials, the metal used in this approach should be chemically inert, especially towards (photo) oxidation. For this reason, noble metals are most suited for this purpose (157). The photocatalytic activity of platinum deposited on TiO_2 has been more extensively studied, however gold supported on TiO_2 (Au/TiO2) has attracted increasing attention in recent years (157). The reason for this interest on Au/TiO_2 comes primarily from the field of heterogeneous catalytic oxidation and use of Au/TiO_2 catalysts is well established in catalysis.

Table 4.1 details the loading of gold and silver in some of the nanorods synthesised. The digestion was conducted with aqua regia which is able to dissolve the noble metals. The initial theoretical metal loading was 1 wt. % for all cases but the amounts obtained were highly variable. The reason for this is that in the different steps of the synthesis, especially in the centrifugation, aggregation and re-dispersion of metal occurs, resulting in a considerable loss of metal. RHP-49 are spherical NP prepared in the same way as nanorod NR. TEM images showed a mixture of different shapes, that could be unreacted seeds particles and NR width-sized NPs. RHP-50 to -52 showed unreacted seeds-sized particles and transverse and longitudinal band, which however do not vary significantly and exhibit quite broad distribution. The decrease of intensity (if real) could be associated with loss of gold (not found by ICP).

Catalysts Code	Au Metal Loading %	Ag Metal Loading %	LSPR (nm)
RHP-14	0.193	0.004	*680*
RHP-15	0.675	0.021	*790*
RHP-16	0.294	0.010	*830*
RHP-17	0.576	0.008	*610*
RHP-18	0.729	0.013	*700*
RHP-19	0.628	0.011	*710*
RHP-20	0.420	0.008	*650*
RHP-21	0.317	0.006	*750*
RHP-22	0.256	0.006	*750*
RHP-49	0.51	0.025	*540*
RHP-50	0.64	0.028	*675*
RHP-51	0.67	0.031	*660*
RHP-52	0.63	0.03	*730*

Table 4.1 ICP-OES analysis results and list of the most important gold nanorods catalyst supported on titania (AuNR/TiO_2) synthesised, with different longitudinal surface plasmon resonance maxima (LSPR). Note: RHP-49 are spheres made emploting CTAB as capping agent.

In **Figure 4.7** the normalized UV-Vis diffuse reflectance spectra are shown for nanorods supported on titania and were previously represented in the **Figure 4.3** in colloidal suspension (unsupported). Again, the two characteristic peaks due to the transverse and longitudinal surface plasmon resonance (SPR) can be observed. In this case, as illustrated below in **Table 4.2**, the values of both the transverse and longitudinal SPR are shifted to longer wavelength when the nanorods are supported. This may be due to the interaction of nanoparticles with titania.

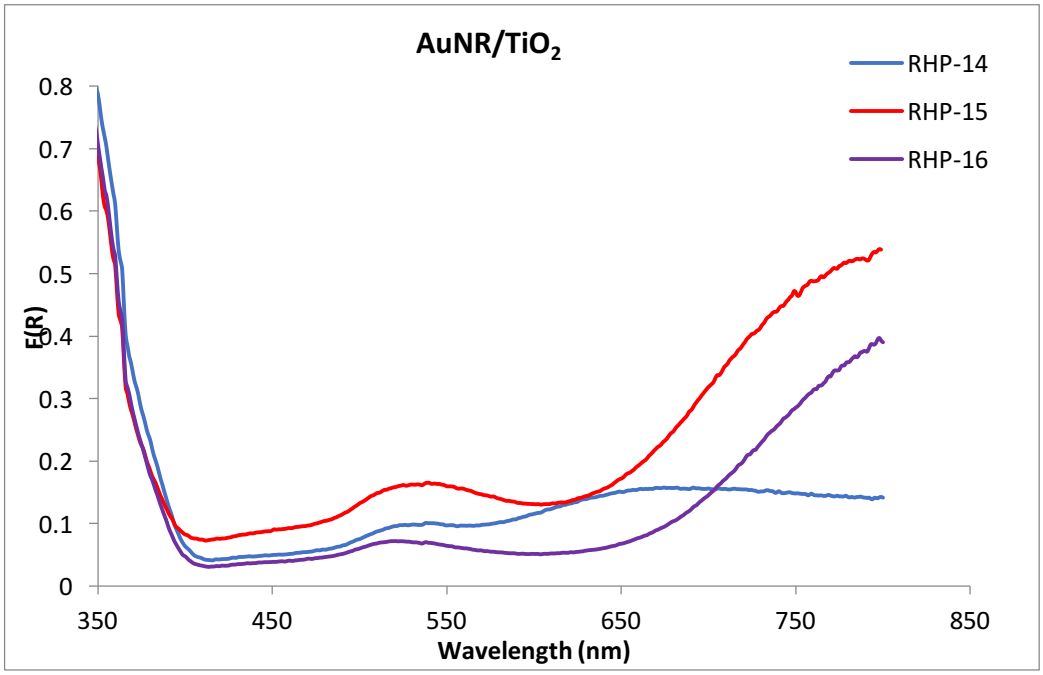

Figure 4.7 Normalized UV-Vis diffuse reflectance spectra of AuNR/TiO_2 with different aspect ratios.

It should be noted that the spectrophotometer used for solid catalyst characterisation can only make measurements up to 800 nanometres so nanorods and nanoparticles with surface plasmon resonances above 800 nm or near this value cannot be measured/evaluated properly, although the measurements can still provide a hint on the position of the plasmon band.

Table 4.2 Wavelength peak values belonging to the transverse and longitudinal surface plasmon resonance for the same nanoparticles before and after they are supported on titania.

	Peak [Wavelength (nm)]			
	Transverse SPR		Longitudinal SPR	
	Colloidal	*Supported*	*Colloidal*	*Supported*
RHP-14	520.2	538	649.4	682
RHP-15	513	539	789.4	**798**
RHP-16	514	520	831.8	**798**

In **Figures 4.4** (in the previous section for colloidal nanoparticles) and **4.8** the UV-Vis spectrum is shown for colloidal suspension and solid diffuse reflectance for the same three nanorods before and after being immobilized, respectively. In this case, note the relatively large change that occurs for the RHP-17 catalyst represented by the blue line. The change of its profile may give the impression that its morphology is not fully defined and that probably during the drying process the morphology changed with a consequent change in its profile and surface plasmon resonance absorption.

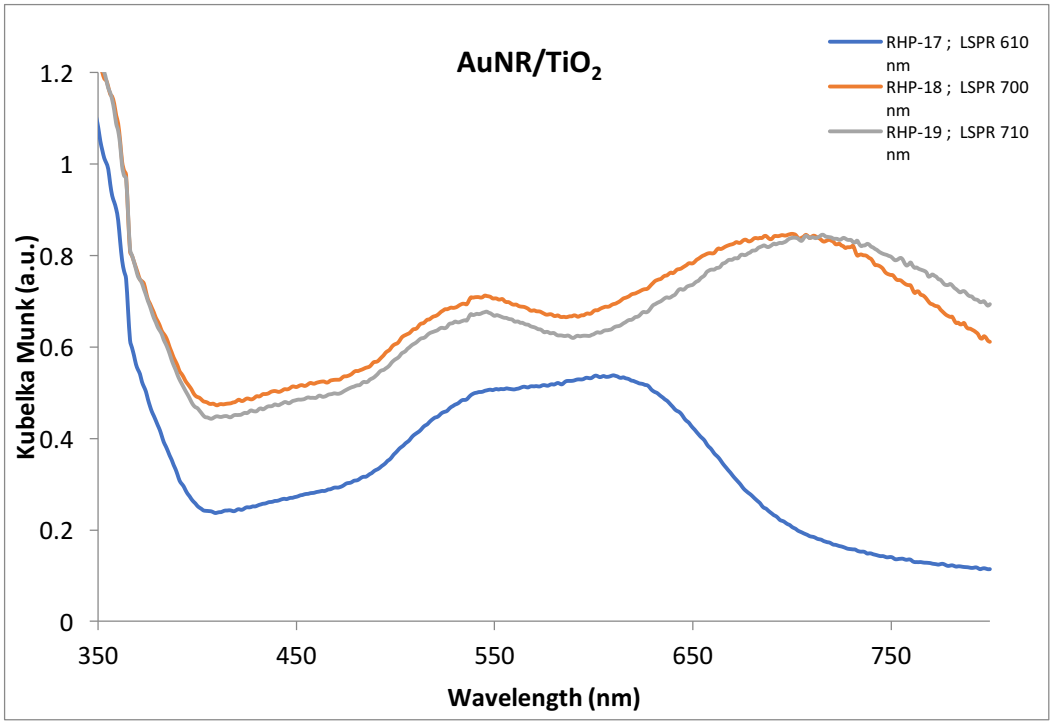

Figure 4.8 Normalized UV-Vis diffusion reflectance spectra of AuNR/TiO_2 with different LSPR.

Represented in **Figure 4.9** the change in intensity for the same catalyst employing different drying conditions can be observed. The difference may simply be due to the amount of water that could still be in the one dried at room temperature, as it shows a higher intensity.

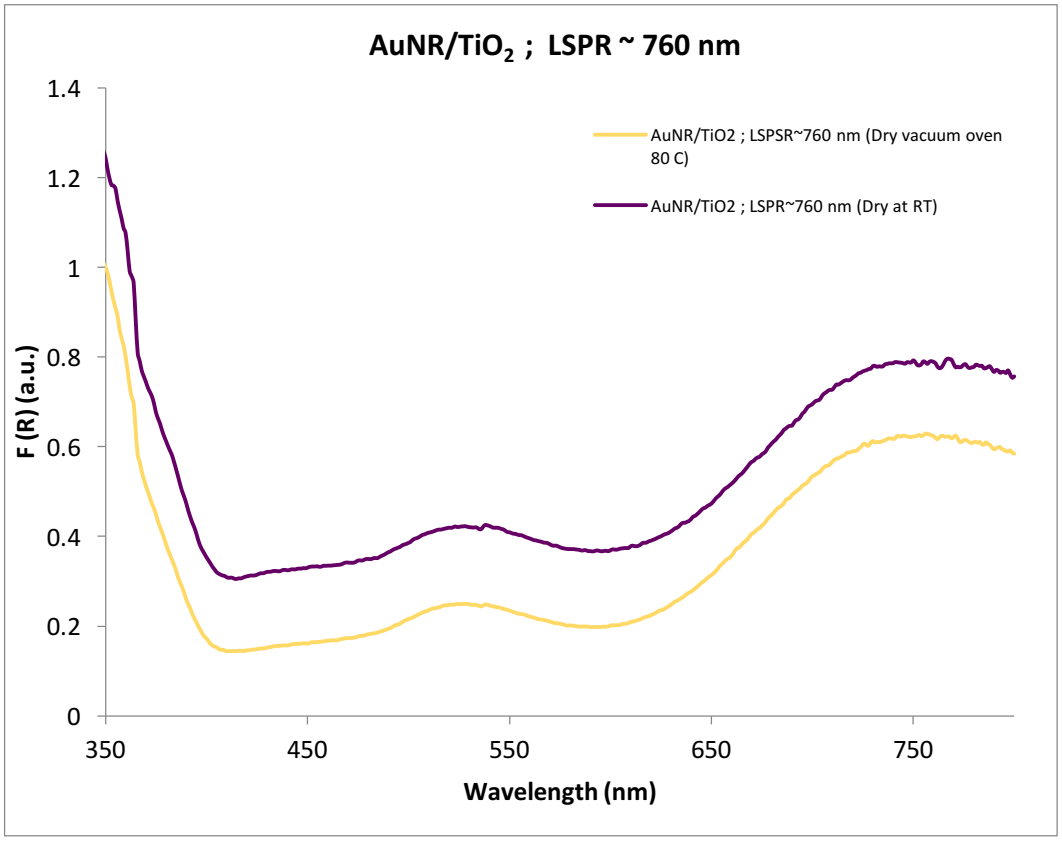

Figure 4.9 Normalized UV-Vis diffusion reflectance spectra of AuNR/TiO_2 of the same catalyst dried under different conditions.

Gold nanorods have been immobilized as shown in the TEM images of **Figure 4.10**. The solid catalysts (titania + rods) have kept the characteristic colour of rods, and this is the first evidence that they have been successfully immobilized. The rods supported on titania and measured through TEM include two aspects as follows.

On one hand, observation or measurement of anisotropic nanoparticles is somewhat difficult as they might not be completely perpendicularly positioned against the TEM beam. This tilt could induce an error in the measurement and subsequent quantification of an average size of these nanoparticles.

On the other hand, despite the apparently weak bond that holds the rods on the titania, this bond is relatively strong. As proof of this, note that the different rods were used in the selective oxidation of hydroxymethylfurfural in an alkaline water solution at 60 C, 20 bar pressure of O_2 for 4 hours under vigorous stirring. During the filtration of spent catalyst, it was observed that the colour of the catalyst hadn't changed and ICP analysis of the reaction mixture showed the absence of dissolved metal.

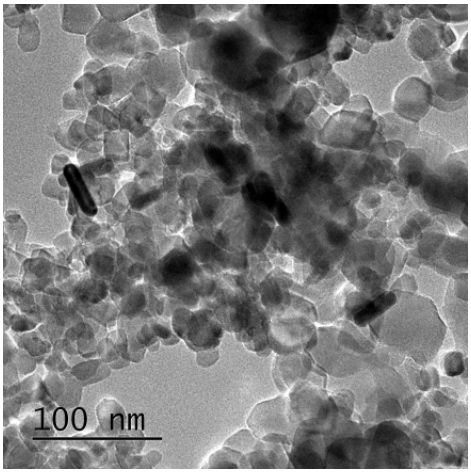

(a)

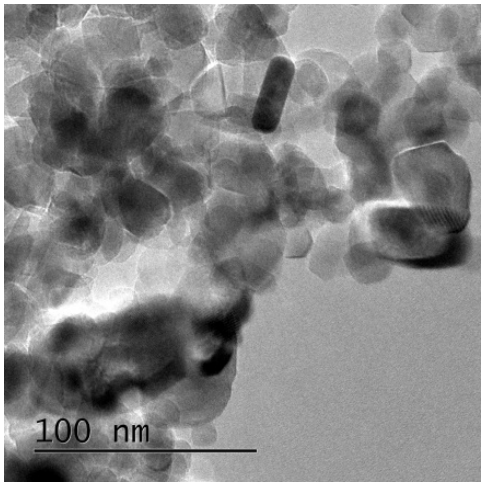

(b)

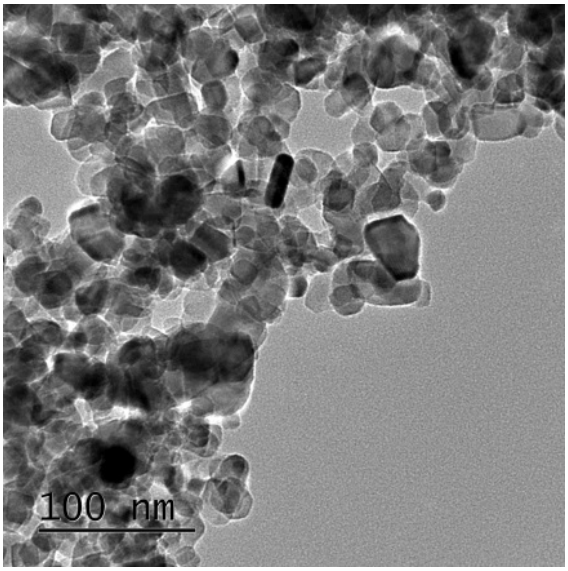

(C)

Figure 4.10 TEM images (a) (b) and (c) of supported AuNRs/TiO_2.

Image	*Length(nm)*	*Width (nm)*	*Aspect Ratio*
1	33.2	12.1	2.7
2	34.8	13.4	2.6
3	34.5	13.4	2.6
Average	**34.2**	**13**	**2.6**

Image	*Length (nm)*	*Width (nm)*	*Aspect Ratio*
1	31.4	9.7	3.2
2	53.8	11.4	4.7
3	43.7	12.2	3.6
4	44.1	11.2	3.9
5	49.3	11.4	4.3
6	49.4	12.0	4.1
7	48.1	11.9	4.0
8	39.6	11.2	3.5
9	42.9	10.6	4.1
Average	**44.7**	**11.3**	**3.9**

Image	*Length (nm)*	*Width (nm)*	*Aspect Ratio*
1	39.5	12.9	3.1
2	42.1	14.2	3.0
3	42.4	12.3	3.4
4	48.3	12.7	3.8
5	28.0	10.2	2.8
6	41.4	13.1	3.2
7	51.9	10.6	4.9
8	30.2	10.0	3.0
9	51.7	10.4	5.0
10	39.2	12.3	3.2
11	53.6	10.9	4.9
Average	**42.6**	**11.8**	**3.6**

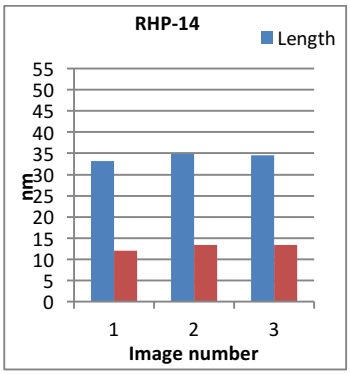

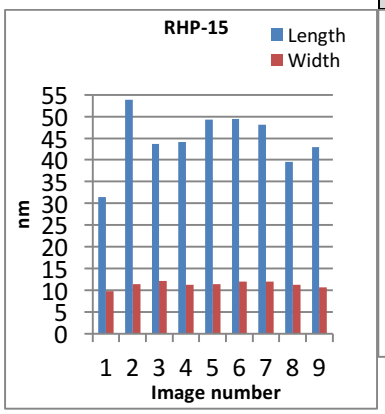

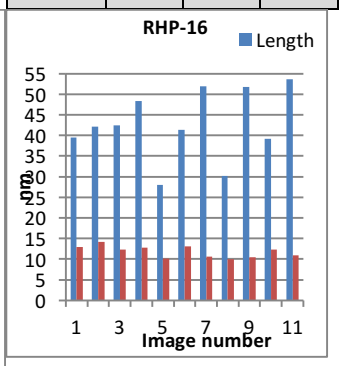

Figure 4.11 Comparison of supported gold nanorod dimensions (TEM analysis) of catalysts RHP-14, 15 and 16. In both, tables at the top and the bottom charts are shown the values of length and width for the gold nanorods found in the different TEM images. Tables above also illustrated the average values of Aspect Ratio (AR = L / w) for each AuNR/TiO_2 catalysts.

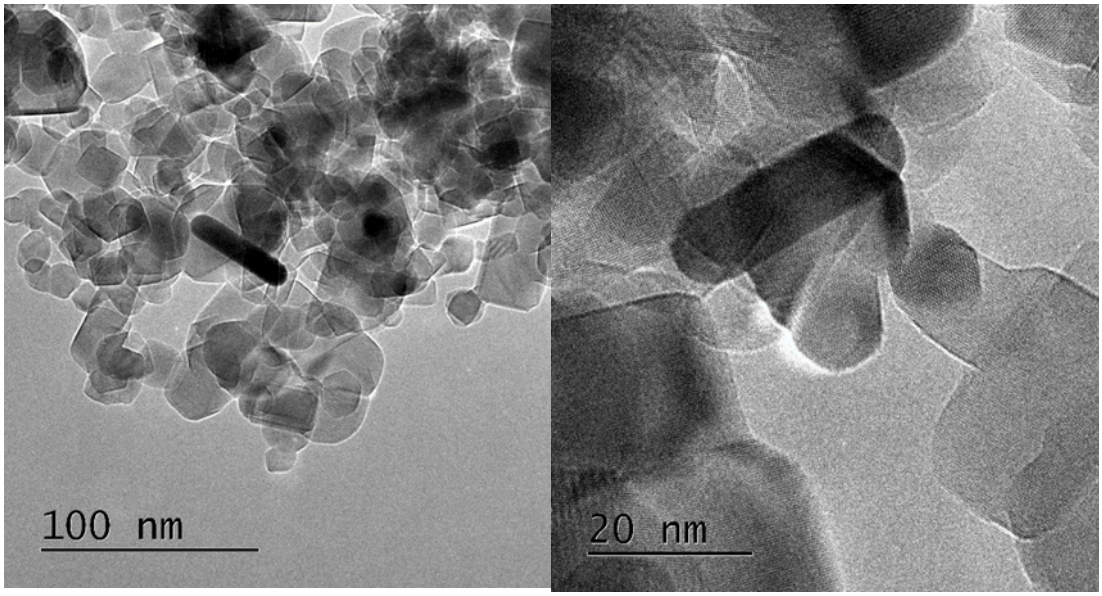

a b

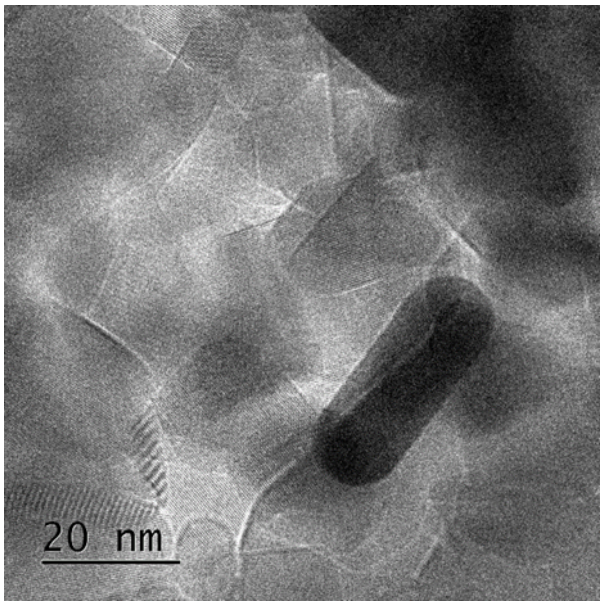

c

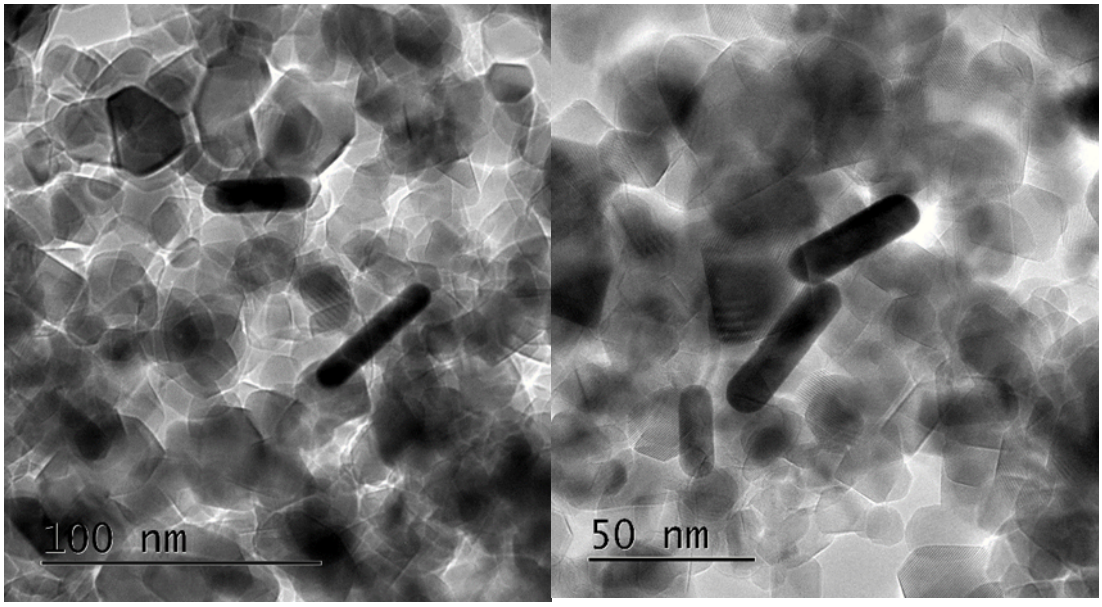

d e

Figure 4.12. TEM images for RHP-14 (c), RHP-15 (a and b) and RHP-16 (d and e), which can be characterised by increasing the length of the rods as determined from UV-vis diffuse reflectance measurements.

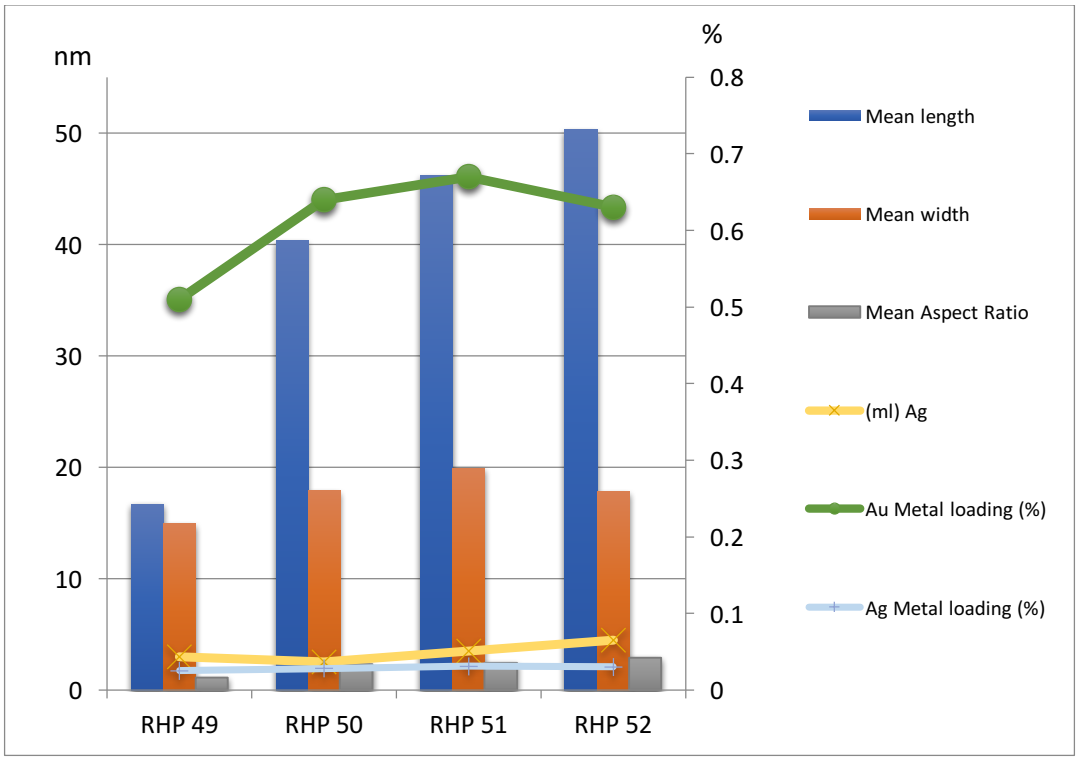

Figure 4.12. TEM analysis of catalysts compared with the metal loading.

When the amount of silver was increased in the growth solution (2.5; 3.5; 4.5ml) made longer rods and higher aspect ratios resulted, but the widths were not affected. RHP-49 was made with silver when they should have been spherical nanoparticles. But when seeds (pentagonal shaped particles) were left to grow a little bit (a few hours after their preparation), they became little spherical nanoparticles and then, when added to the growth solution, they should only grow to be spherical nanoparticles. In this case the silver should not play the same role as with nanorods, but in the TEM results it can be seen that there were some rods and different shapes also in the RHP-49 case. 99 % of the silver used to make the rods was lost in the process. The question remains as to whether the residual silver that can be seen to be present in the supported catalysts was attached to the Au nanoparticles or was in the solution/attached on the CTAB/NO_3^- structures and was deposited on the support.

Figure 4.13 (next page) shows TEM images of three nanorod catalysts. These can be characterised by increasing the length of the rods as determined from UV-vis diffuse reflectance measurements. However, TEM analysis was inconclusive as very few of the rods could be actually found to make counting and measurements statistically representative. Aspect ratios were calculated previously and showed in **Figure 4.11**being 2.6 for RHP-14, 3.9 for RHP-15 and 3.6 for RHP-16.

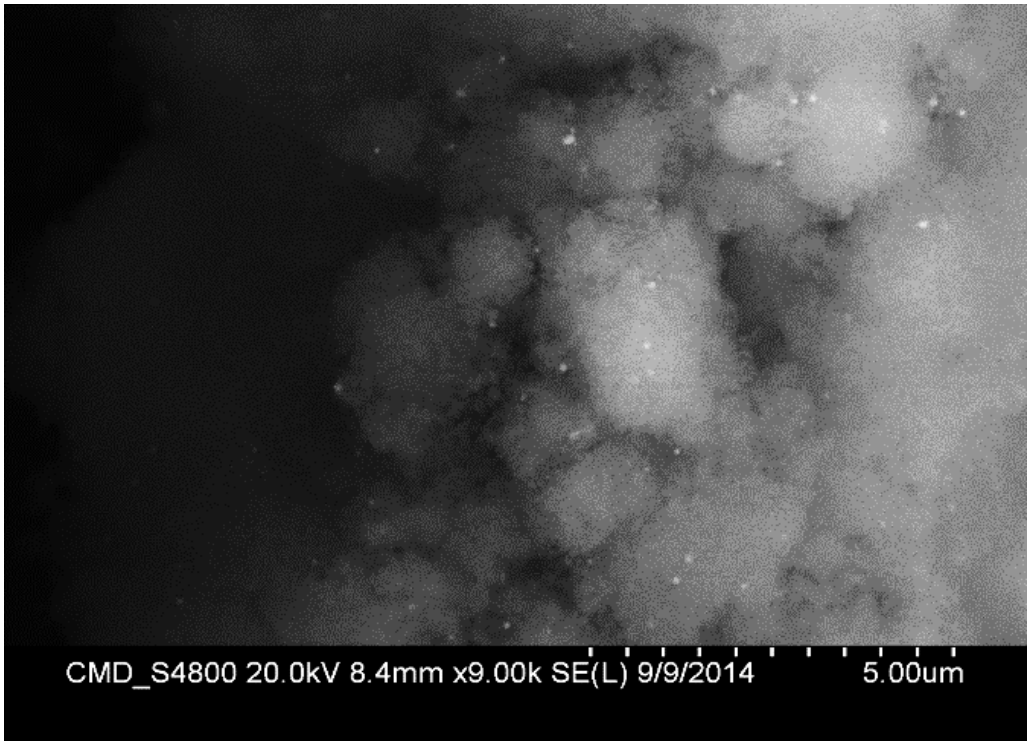

Figure 4.13 An SEM image of back-scattered electrons for supported AuNRs/TiO_2 (RHP-15). The bright points correspond to gold nanorods.

Due to the low resolution of the employed SEM instrument it was not possible to obtain detailed information on the immobilized nanorods on titania. However, it could be observed that the dispersion of the nanoparticles on the support was fairly homogeneous.

Figure 4.14 shows the XRD patterns of AuNR/TiO_2 (Titania Deggusa P25 anatase-rutile). All the reflections observed correspond to the anatase and rutile phases. No reflections for gold nanoparticles could be observed, which could be a result of the very low Au loading of nanoparticles (< 0.73 wt. %, **Table 4.1**). However, SEM observation indicated homogeneous distribution of the nanoparticles (**Figure 4.12)** and confirmed retention of the TiO_2 morphology.

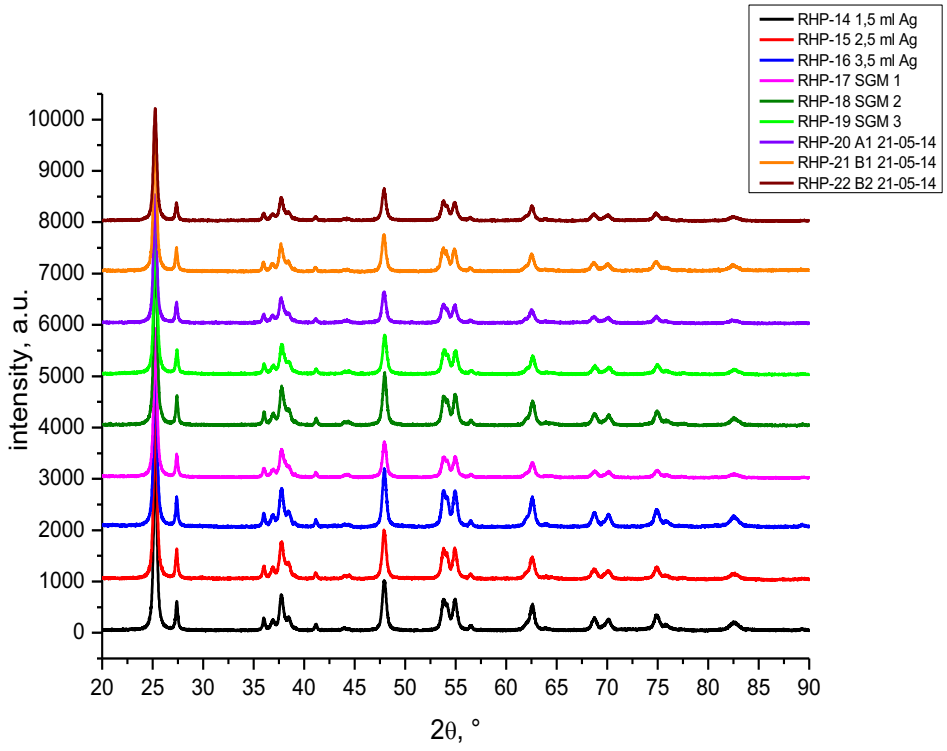

Figure 4.14 XRD analysis of the most important gold nanorod supported on titania materials listed in **Table 4.1**.

Colloidal synthetic methods have proved a great success in nanoparticle creation since stabilizing agents (surfactant or polymer) have given better size and shape control of nanoparticles with a narrow size distribution. For the immobilization of the spherical nanoparticles synthesized by the above procedure, the sol-immobilization method (108, 110) was used. During initial synthesis, that served as training, with spherical nanoparticles it was found that this method provided a good dispersion of the nanoparticles on the substrate metal oxide support once they were immobilized. Due to this success, sol-immobilization method motivated application in the immobilization of the different morphologies in a novel way not previously reported.

In order to get a better understanding of the possibility of a size-shape-catalytic activity relationship, two different types of reaction were carried out for this purpose. In the first reaction, we tested the performance of catalysts for methyl orange (MO) photodegradation under visible light. Azo dyes such as methyl orange (MO) absorb in the visible spectrum and their degradation leads to a decrease in their absorbance. This is very fast and easy way to analyse the degradation by UV-VIS spectroscopy. In short,

it is a quick and easy way to measure the photocatalytic activity of the catalysts prepared. In the second approach, selective oxidation of HMF was performed in order to measure size effects on catalytic activity.

4.3.3 Methyl Orange (MO) Photodegradation

Figure 4.15 shows representative UV-Vis spectra of MO before and after photodegradation test (RHP-16, rods supported on titania).

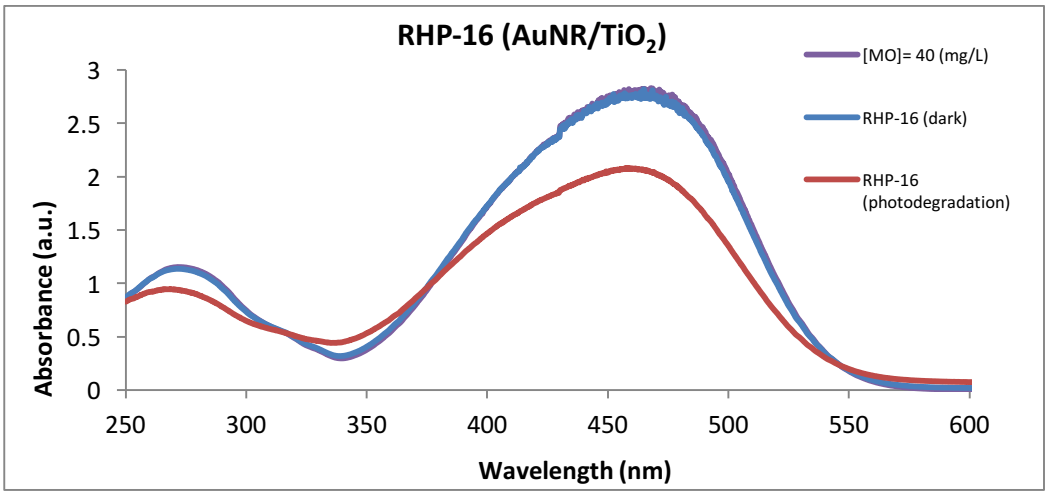

Figure 4.15. UV-Vis absorption spectra representative of Methyl Orange before and after 3h of photoreaction and dark reaction. The vials were prepared with 10 ml of [MO] = 40 mg/L and 20 mg of catalyst.

Table 4.3 shows the conversion values for the supported nanorod catalysts and TiO_2. Reproducibility tests showed that the experimental error was higher than the differences shown (around 10%) which prevents clear conclusions being drwn. As is observed, the conversion obtained in all the cases is similar to the conversion with TiO_2, so it might seem there is no promotion by the nanorods in the photodegradation of Methyl Orange as had been expected. Therefore, further tests are needed to confirm this hypothesis. Alternatively, a more suitable and established probe reaction might be required, such as benzyl alcohol oxidation (108). This reaction has been studied extensively in the literature and it can be performed by both thermo- (158, 159) and photocatalytic routes (160). Also, it allows one to follow not only conversion of the

benzyl alcohol, but also selectivity to different products corresponding to various reaction pathways.

Table 4.3 Summary table of conversion values for the nanorods tested in the photodegradation of MO under visible light during 3 hours in the LuzChem ICH2, at 30℃.

Catalysts Code	Au Metal Loading %	Ag Metal Loading %	LSPR (nm)	% Conversion
RHP-14	**0.193**	**0.004**	**680**	**18.9**
RHP-15	**0.675**	**0.021**	**790**	**20.2**
RHP-16	**0.294**	**0.01**	**830**	**19.6**
RHP-17	**0.576**	**0.008**	**610**	**19.9**
RHP-18	**0.729**	**0.013**	**700**	**17.6**
RHP-19	**0.628**	**0.011**	**710**	**26.3**
RHP-20	**0.42**	**0.008**	**650**	**11.0**
RHP-21	**0.317**	**0.006**	**750**	**15.2**
RHP-22	**0.256**	**0.006**	**750**	**24.9**
TiO_2	**…**	**…**	**…**	**20.9**

4.3.4 Selective Oxidation of 5-hydroxymethyl-2-furfural (HMF)

Selective oxidation of hydroxymethylfurfural to furandicarboxylic acid (FDCA) is an attractive reaction that can be used to produce FDCA as an alternative to terephthalic acid for production of plastics (161, 162). This reaction was conducted in collaboration with a visiting researcher and Erasmus practice student resident in the group, Susana Guadix Montero. It was found that gold nanorods were not only active, showing higher conversion of HMF than pure titania support, but also increased selectivities to 5-hydroxymethyl-2-furancarboxylic acid (HMFCA), FDCA and so far, further unidentified products (**Table 4.4**). Although these catalysts provide high amounts of yet unidentified degradation products, further experiments are being carried out to increase the impact of supported nanorods and also to identify all products. More

specific conclusions as to how precisely the morphology of the nanorods affects the product selectivity could not be drawn.

Table 4.4 Data of conversion and selectivity of the most important rods studied above. The reaction was carried out in an autoclave at 60 °C, 20 bar O_2 under vigorous stirring (1500 rpm).

Cat. Ref.	X (%) HMF	S (%) FDCA	S (%) HMFCA
TiO_2	56.3	1.6	7.8
RHP-14	62.6	0.0	11.0
RHP-15	63.0	1.9	52.3
RHP-16	67.9	1.5	17.4
RHP-17	99.0	1.4	15.8
RHP-18	98.4	2.0	32.6
RHP-19	98.9	1.5	19.9
RHP-20	63.4	1.6	19.0
RHP-21	72.4	1.5	13.3
RHP-22	75.4	1.4	16.6
RHP-49	100	48.1	41.6
RHP-50	100	0.0	77.8
RHP-51	92.8	0.0	40.5
RHP-52	95.8	0.0	37.2
RHP-57	100	50.1	43.6
TD-WI	100	11.7	80.7

The activity of this catalyst was compared under the same conditions with another spherical nanoparticle, like RHP-57 (Standard AuNPs, deposition precipitation) and TD-WI (AuNPs made by wetness impregnation). After 19h of reaction, conversion of HMF is complete or close to completion (conversions lower than 80 % can be obtained in under 2h reaction time), but we don't obtain complete FDCA selectivity yet.

RHP-49 gave us a similar activity than the standard catalyst made by deposition method RHP-57. Between the rods, we can say that the HMFCA selectivity decreases as long the rods have a longer length and they did not convert HMFCA into FDCA, as is showed in the **Figure 4.16**.

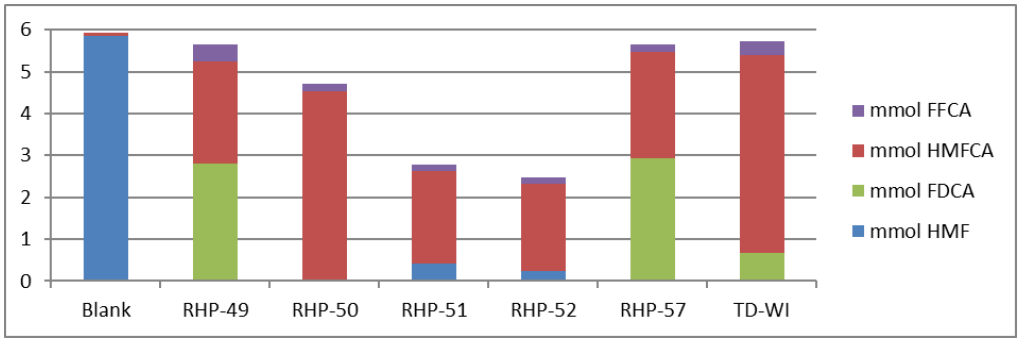

Figure 4.16. Comparison of the final concentration of the products reaction using different catalysts.

We can see an important difference in the carbon mass balance between the spherical nanoparticles and the nanorods, being close to 100% for the spherical and significantly lower for the rods can be seen. The longest rods, RHP-51 and RHP-52, showed a carbon mass balance even lower than 50%. They did not achieve the 100% of HMF conversion and even the colour of these two solutions was darker at the end of the reaction.

Figures 4.17 and 4.**18** show the dependence of the Ag loading on Au loading and dependence of the HMFCA selectivity on Au loading (a) and on Ag loading (b) in the gold nanorod catalysts (RHP-14 to RHP-20). It seems like the higher the amount of gold and silver, the higher the selectivity towards HMFCA.

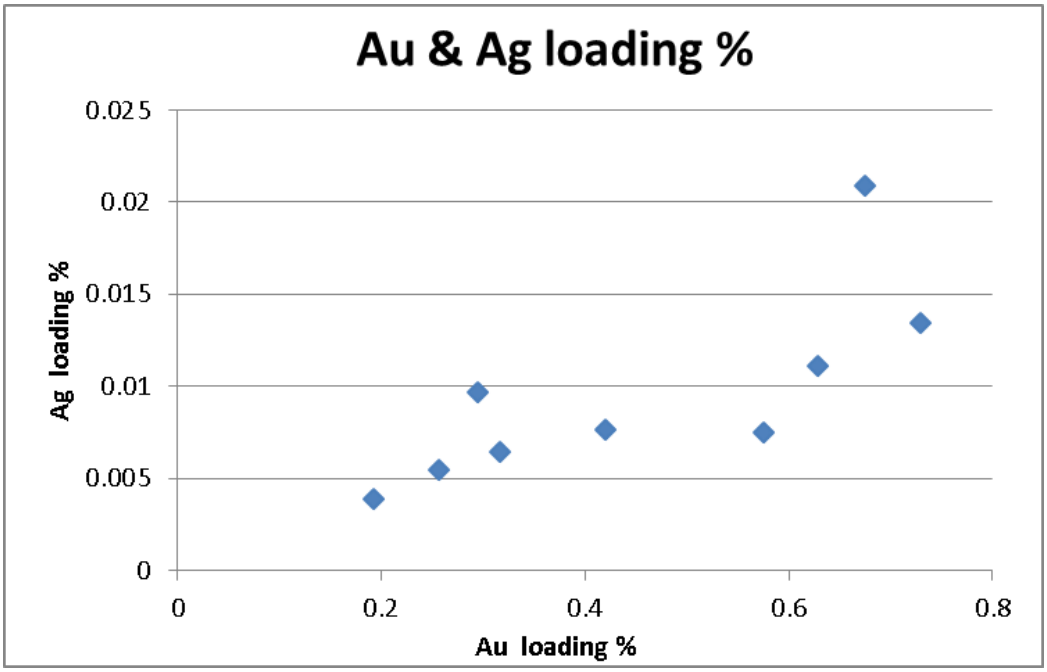

Figure 4.17 Dependence of the Ag loading on Au loading in the gold nanorods catalysts (RHP-14 to RHP-20) obtained from ICP analysis from digestion of the catalysts in aqua regia.

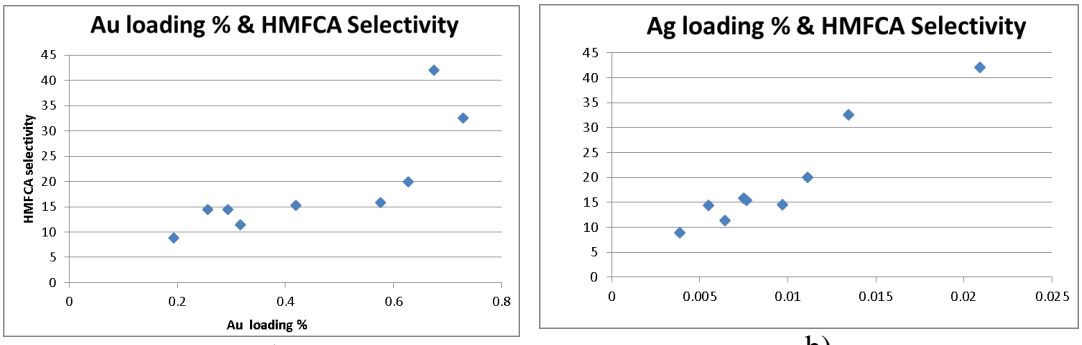

a) b)

Figure 4.18 Dependence of the HMFCA selectivity on Au loading (a) and on Ag loading (b) in the gold nanorods catalysts (RHP-14 to RHP-20). Au and Ag loadings obtained from ICP analysis from digestion of catalyst in aqua regia.

These preliminary results corroborate the fact that other morphologies (in addition to spheres) are active, and this sets the basis for future experiments to discern different catalytic performances.

4.4 Conclusions

In this thesis, on the knowledge and skills necessary to have a better control of the morphology of the nanoparticles have been the subject of attention with successful results and immobilization on titania in a "novel way". This chapter demonstrates that the synthesis of variable shape and size nanoparticles can be carried out precisely and also with subsequent immobilization.

The first clue that indicated success in the immobilization of different morphologies iwas the catalyst's colour because after the nanoparticle immobilization on titania the initial colloidal nanoparticles colour was preserved. The preservation of the structure was also confirmed by UV-Vis diffuse reflectance spectra and TEM images of supported nanoparticles. Thus, we managed to perform for the first time, the immobilization method of supported nanoparticles of variable anisotropic morphologies such as rods or stars (next chapter) on titania was performed.

It is noteworthy that the nanorods were active in both methyl orange photodegradation although there was no clear picture of size-shape dependency and also in the selective oxidation of HMF, which has been deeply studied. More research is necessary in this field to achieve a clear outcome, although compared with spherical nanoparticles it seems very obvious that gold nanorods have much lower activity.

For wider knowledge of the control in the synthesis of the nanoparticles in relation to both size and shape, more experiments must be done employing modification of different variables involved in the synthesis of noble metal nanoparticles.

Chapter 5

Gold NanoStars, Pre- and Post-Immobilization, Structure-Conversion Symbiosis

5 Gold NanoStars (AuNSs), Pre- and Post-Immobilization, Structure-Conversion Symbiosis

5.1 Introduction

Gold nanostars (AuNSs) or gold branched nanoparticles are one the most explored anisotropic gold nanostructures after gold nanorods (101, 148, 163, 164) specially due to their enhanced interaction with light (165).

Several methods have been reported for gold nanostar synthesis and although most of them require a capping agent such as poly-(vinylpyrrolidone) PVP (101) or cetyltrimethylammonium bromide CTAB (34, 112) which are the most extensive and well-known capping agents used, there is also a surfactant-free method (112) that could have interesting applications in catalysis due to the lack of polymer that affects the nanoparticle catalytic activity.

A novel surfactant-free synthesis method was reported by Tuan-Vo-Dinh's group (102) for the first time, leading to plasmon tunable AuNSs. The synthesis is very quick, and does not require a capping agent. Plasmon peaks shift to the near infrared region (NIR) and the number of branches increase as the aspect ratio increases, playing a crucial role in defining the optical properties of the AuNSs.

Optimization of the synthesis of gold nanostars (AuNS) is essential in order to control and apply their interesting plasmonic properties. The influence of different parameters such as shape, size or dispersity of AuNS has to be determined.

In this chapter, although several AuNSs synthesis methods were considered and applied, the focus has been upon investigating surfactant-free AuNSs (102) applications in heterogeneous catalysis which are potentially interesting due to absence of the polymer/surfactant component which could strongly affect catalytic activity. Surfactant-free AuNSs were fabricated and successfully supported for the first time via the sol-immobilization method onto titania TiO_2, and applied for Methyl Orange (MO) photodegradation. The reduction of 4-nitrophenol (4-NP) to 4-aminophenol (4-AP) with $NaBH_4$ was investigated for both colloidal and supported nanostars on titania.

5.2 Experimental

Synthesis of colloidal gold nanostars (AuNSs) of similar size was carried out by three different methods. It was mainly investigated for surfactant-free AuNSs due to its higher catalytic activity of such colloidal nanoparticles in both Methyl Orange photodegradation and 4-nitrophenol reduction.

5.2.1 Synthesis of seed-mediated multipod Au nanoparticles (DMF/PVP)

In this first method, gold nanostars were synthesized using the method reported in reference (101) where, in a typical synthesis procedure, an aqueous solution of chloroauric acid was mixed with different concentrations of PVP (average MW = 10 000) solution in *N*,*N*-dimethylformamide (DMF), followed by the rapid addition of PVP-coated Au seeds in ethanol (111) under stirring. Within 15 minutes, the colour of the solution changed from pink to colourless and finally turned blue indicating the formation of gold nanostars in solution.

These nanoparticles were not supported due to difficulties removing the polymers and also due to their lower catalytic activity compared to surfactant-free AuNSs.

5.2.2 Synthesis of CTAB-coated AuNSs

CTAB-coated AuNSs were synthesised using a modified procedure (112, 113) . In a typical synthesis, Au seeds were first prepared by mixing a solution of chloroauric acid 0.25 mM with trisodium citrate 0.1 M in 20 mL of Millipore water, following which 60 μL of freshly prepared ice-cold sodium borohydride 0.1 M was quickly added under moderate stirring. Immediately, the solution turned brown-pink and slowly developed into its final red colour due to the formation of spherical gold nanoparticles approximately 4–5 nm in diameter. The sample was stored overnight in the dark under ambient conditions.

AuNSs samples were synthesized using CTAB as a template. A solution of 5 mM CTAB was mixed with solutions of 10 mM chloroauric acid and 0.01 M silver nitrate under vigorous stirring for 1 minute. Then, 0.1 mL of L-ascorbic acid 0.1 M was added dropwise. Upon addition of the last drop of L-ascorbic acid, the solution turned clear, and the

appropriate volume of gold nanoseed was immediately added. Samples were left in the dark under ambient conditions until use.

5.2.3 Synthesis of Surfactant-Free AuNSs

Finally, free-surfactant method (102), gold nanostars (AuNSs) were prepared by a seed-mediated growth method. The seed preparation consists of the addition of 15 ml of 1 % citrate solution to 100 ml of boiling 1 mM $HAuCl_4$ solution under vigorous stirring. After 15 min of boiling while keeping the solution volume stable, the solution was cooled and filtered through a 0.22 µm nitrocellulose membrane, and then kept at 4 °C for long-term storage. For nanostar synthesis, 956 µl of the above citrate-stabilized seed solution was added to 96 ml of 0.25 mM gold chloride ($HAuCl_4$) solution (with 96 µl of 1 M HCl) in a 250 ml round bottom flask at room temperature under moderate stirring (700 rpm). Quickly, 956 µl of silver nitrate ($AgNO_3$) of different concentrations (1–2 mM) and 480 µl of ascorbic acid (AA; 100 mM) were added simultaneously. The solution was stirred for 30 s as its colour rapidly turned from light red to blue or greenish-black.

5.2.4 Surfactant-Free AuNSs Immobilization

Immediately after synthesis, surfactant-free AuNSs were immobilized onto TiO_2 using two different approaches. The procedure was exactly the same as the one described previously for gold nanorods in Chapter 4; the colloidal suspension was transferred to a 250 ml round bottom flask followed by the procedure outlined previously with modifications (110). 25 ml of titania water solution was acidified to pH 1 with sulfuric acid and was added to the colloidal nanoparticle solution (and 25 ml more used to wash down the glassware). It was left for 2 hours under vigorous stirring and then filtered and washed with distilled water until a neutral pH value was obtained. The solid was dried overnight in a vacuum oven at 60 °C and finally ground. No further treatments were performed.

5.2.5 Catalytic testing

Reduction of 4-nitrophenol and photodegradation of Methyl Orange were carried out to test the catalytic activity of the gold nanostars. Conversion was calculated based on the following equation:

$$\boldsymbol{Conversion}_{x}(\%) = \frac{[X]_{initial} - [X]_{end}}{[X]_{initial}} x100$$

Equation 5.1. Equation used to determine conversion.

5.2.5.1 4-Nitrophenol Reduction

The catalytic properties of AuNSs both in colloidal suspension and as immobilized nanoparticles were examined via reduction of 4-nitrophenol to 4-aminophenol reaction in the presence of $NaBH_4$ in excess. The reaction conditions reported by Ye et al (114) were adopted as we will be indicated later on. 4-nitrophenol [4-NP] reduction was carried out in situ at room temperature in a standard quartz cell with a path length of 1 cm.

C- *Colloidal:* The aqueous solution of sodium borohydride ($NaBH_4$) 0.1 M was freshly prepared (and kept ice-cold). First, 0.3 ml of a $NaBH_4$ solution was mixed with 3 ml of 0.1 mM [4-NP]. Then, a volume of 25 µl gold nanoparticles was immediately injected.

D- *Solid:* samples (10 mg) were added in the cuvette. Immediately after that, the same volume of [4-NP] was introduced and finally the $NaBH_4$.

UV–vis absorption spectra were immediately recorded after last step in both cases with a certain time interval at a scanning range of 220–520 nm at room temperature.

The following **Figure 5.1** shows the scheme for the catalytic reduction of 4-nitrophenol to 4-aminophenol.

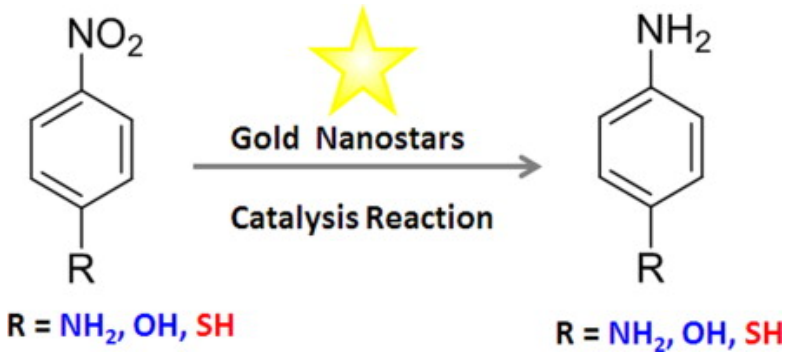

Figure 5.1. Scheme for catalytic reduction of 4-nitrophenol to 4-aminophenol by gold nanoparticles (166), reproduced with permission of Elsevier.

5.2.5.2 Methyl Orange (MO) Photodegradation

In a typical reaction, 10 ml of MO solution (40 mg/L) and 20 mg of solid catalyst were mixed in a 12 ml vial with a magnetic stirrer. The mixture was stirred overnight in the dark (after the dark reaction, one sample of 2 ml was taken and kept in the dark for subsequent analysis) and then irradiated under visible light (400-800 nm) for 3 hours in a LuzChem ICH2 photoreactor (Chapter 2) at a constant temperature of 30 °C and under vigorous stirring (1000 rpm). Then, a sample was taken from the mixture and the UV-vis spectrum of the MO solution was measured with a UV-Vis spectrophotometer.

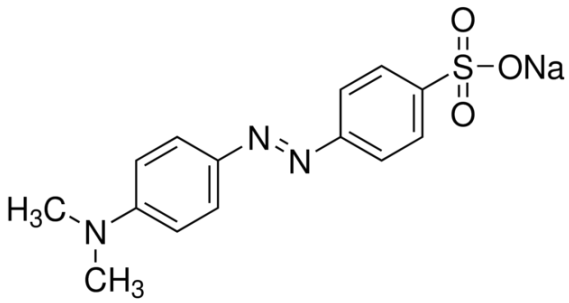

Figure 5.2. Methyl Orange (MO) chemical structure

5.3 Results and Discussion

In this chapter, characterization and catalytic activity of colloidal and supported gold nanostars (AuNSs) will be discussed. And first time prepared AuNSs supported on titania immobilized via sol-immobilization method will also be analysed in depth.

5.3.1 Characterization of AuNSs

The prepared anisotropic nanoparticles via surfactant-free, CTAB-coated and PVP/DMF methods commented previously, and the subsequent solid catalyst where AuNSs were immobilized on titania, were characterised using the following techniques such as UV-Vis-NIR Spectrophotometry, Coupled Plasma- Optical Emission Spectroscopy (ICP-OES) and Transmission Electron Microscopy (TEM).

5.3.2 Colloidal Gold NanoStars (AuNSs)

Gold nanostars have been synthetized using three different methods in which two very well-known and most used polymers PVP (101) and CTAB (112) have been compared with the surfactant-free method (102). Anisotropic gold nanoparticles (AuNSs) of different size and concentration were made in order to be contrasted.

In **Figure 5.3** (next page) the UV-Vis absorption spectra of gold nanostars synthesised by the three different methods in colloidal suspension are shown. Despite the effort tapplied o make particles of similar size via every method (about 50 nm), particles smaller than 100 nm could not been made by the PVP/DMF seed-mediated method.

Although the purple or blueish colours of the resultant solution after synthesis is an indication that AuNSs have been formed, further confirmation could be provided with UV-Vis spectral analysis. Plasmon resonance peaks of AuNSs can be observed at 710 nm for CTAB-coated method, 720 nm for surfactant-free and 830 nm for PVP/DMF. These results match with the literature followed.

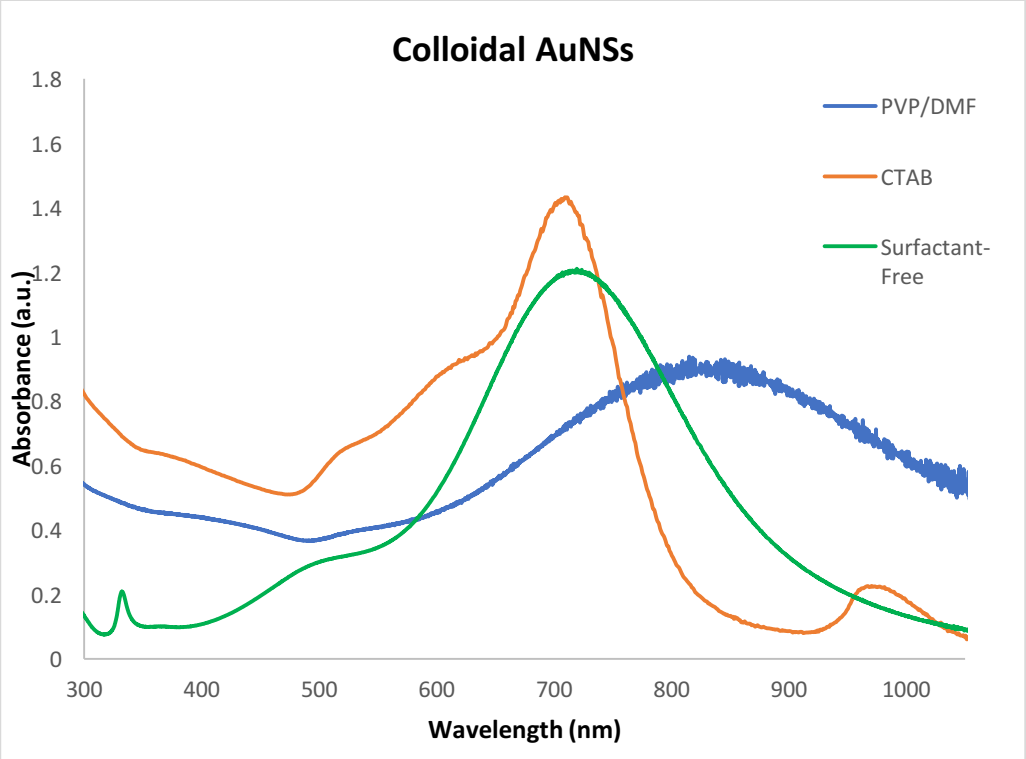

Figure 5.3. UV-Vis absorption spectra of AuNSs for PVP (blue), CTAB (orange) and surfactant-free (green) methods.

Due to higher catalytic activity of surfactant-free nanostars in the reduction of 4-nitrophenol, as will be shown in the catalytic reaction section, further synthesis and analysis of AuNSs made using this method have been produced.

In **Figure 5.4** the UV-Vis absorption spectra for three different nanostar systems in colloidal suspension prior to their immobilization on titania are shown. Surfactant-free methodology was carried out for their synthesis. From an initial comparison, it can be seen that for the same synthesis, in which an increase of silver was applied, plasmon band tunability was achieved and bigger nanoparticles with more branches were obtained as the amount of silver increased (102). The surface plasmon resonance band (SPR) peak is red-shifted for nanoparticles when adding more silver.

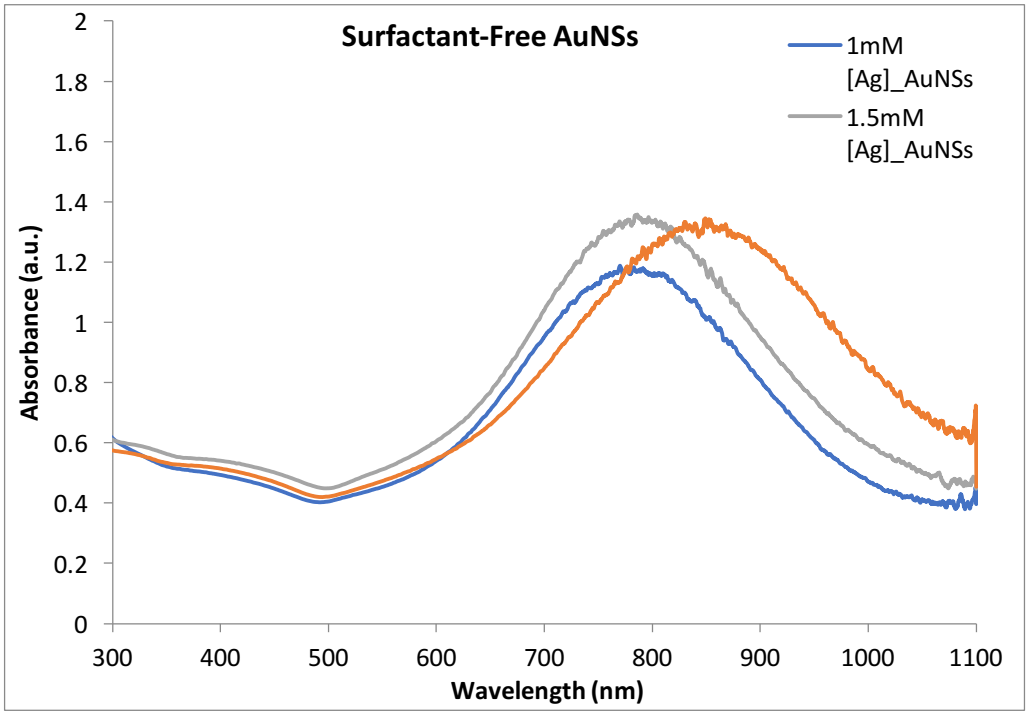

Figure 5.4. UV-Vis absorption spectra of AuNS with different sizes, where plasmon tunability was achieved by adjusting the amount of silver concentration from 1 (blue line) to 2 mM (orange line).

Plasmon bands of AuNSs in **Figure 5.4** are found at 770 nm for nanoparticles made with 1mM [Ag], 780 nm for 1.5 mM [Ag] and 850 nm for 2 mM [Ag].

In order to compare size effects on catalytic activity, gold nanostars were synthesised. **Figure 5.5** shows a colloidal solution for the three different nanoparticle systems synthesised that were subsequently immobilized on titania.

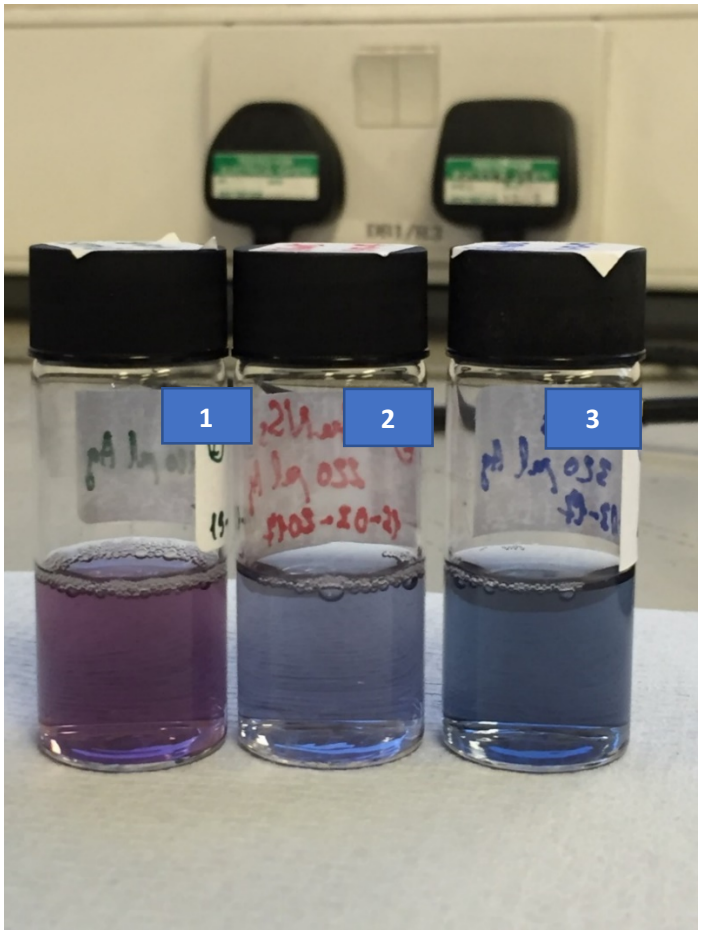

Figure 5.5. Colloidal AuNSs 1, 2 and 3 synthesised via surfactant-free from smallest to biggest due to increasing of Ag^{+} concentration (1, 1.5 and 2 mM respectively).

The UV-Vis spectrum of gold nanostars made by the surfactant-free method is shown in **Figure 5.6**. A drastic decrease in the absorption is observed once the nanoparticles are filtered through a nitrocellulose membrane in order to stabilize gold nanostars after synthesis to avoid agglomeration as has been reported elsewhere (102). Partial retention of gold nanostars was observed by the characteristic blue colour on this filter.

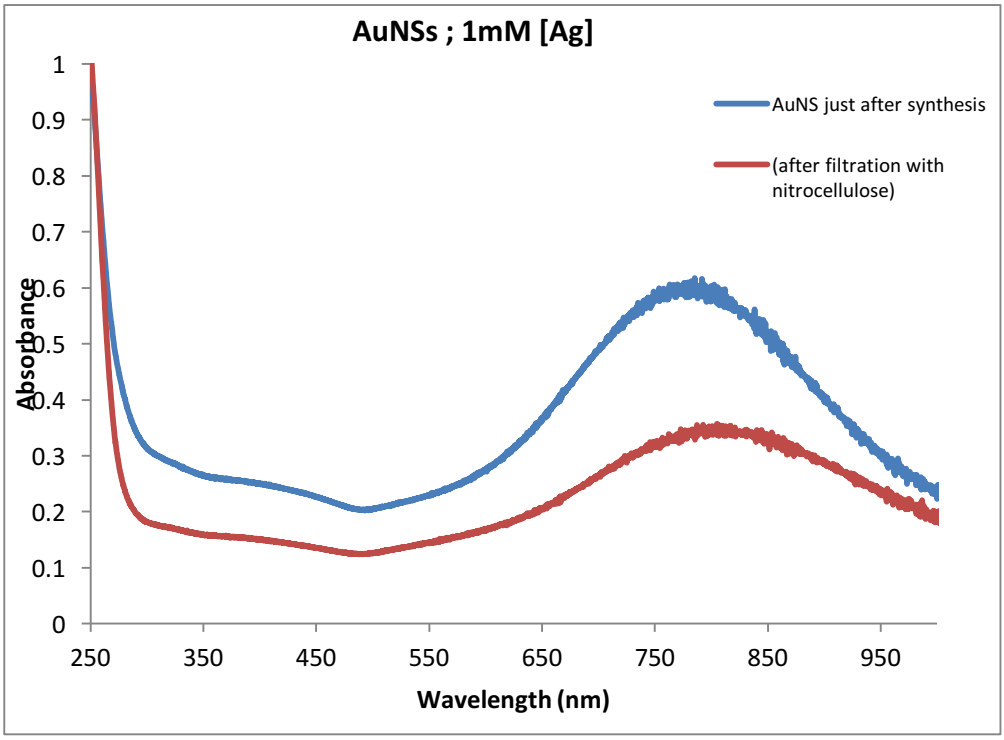

Figure 5.6. UV-Vis absorption spectra of AuNS before and after filtering through the nitrocellulose membrane.

For that reason, instead of stabilizing the nanoparticles by filtering through nitrocellulose or using a capping agent such as PVP prior to immobilization, it was decided decided to immobilize them directly onto titania already acidified in solution by adding the colloidal suspension to avoid the filtering and addition of the ligand steps. As reported in the supported AuNSs section, gold nanostars were successfully immobilized onto titania and further analysis has demonstrated their stability over time.

5.3.3 Transmission Electron Microscopy, TEM

TEM was performed to see the morphology and estimate the particle size of the nanoparticles. **Figure 5.7** shows the TEM images of gold nanostars made through reduction of Au^{3+} in a by PVP/DMF solution. The average gold nanoparticles size was 120 nm.

TEM observations, show that stars where created and no other shapes were found in any of the analysed samples.

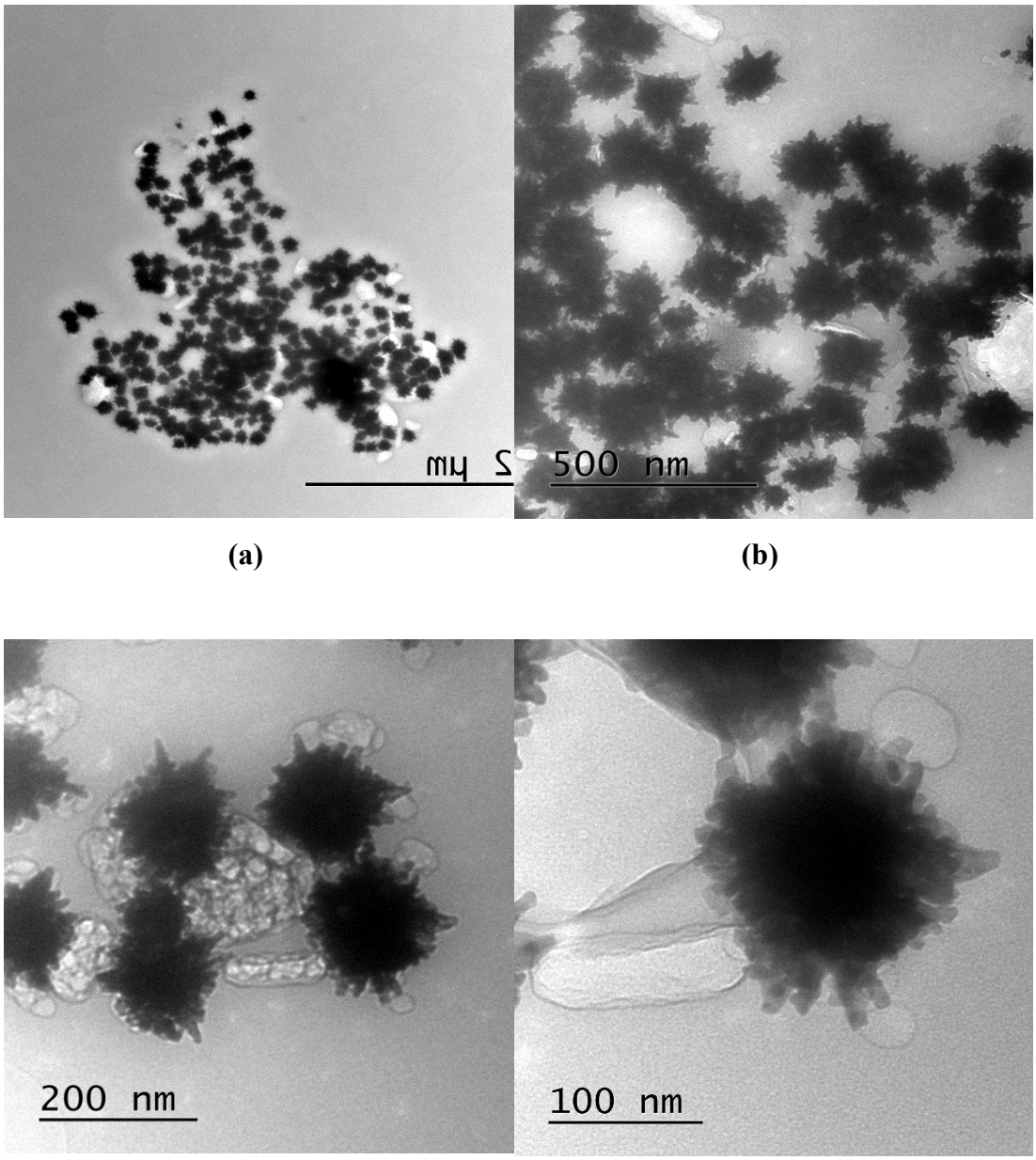

(a) **(b)**

(c) **(d)**

Figure 5.7. TEM images (a), (b), (c) and (d) of gold nanostars made by the method reported by Liz-Marzan (101).

With the PVP/DMF method, an optimum control of morphology is achieved but on the contrary, large nanoparticles are obtained. In addition, these nanoparticles have the drawback that the presence of a polymer could affect their catalytic activity.

Figure 5.8 shows nanostars in colloidal suspension made by the surfactant-free method. The average gold nanoparticle size spanned 50 nm to 80 nm depending on the amount of Ag^+ used. The yield of branched particles was high; however, particle shape distribution was wide.

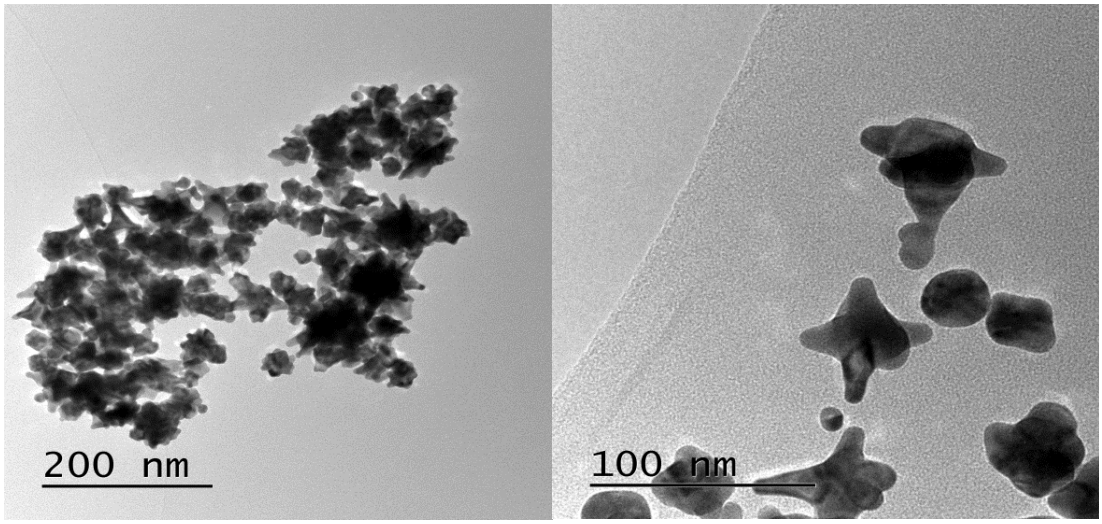

(a) **(b)**

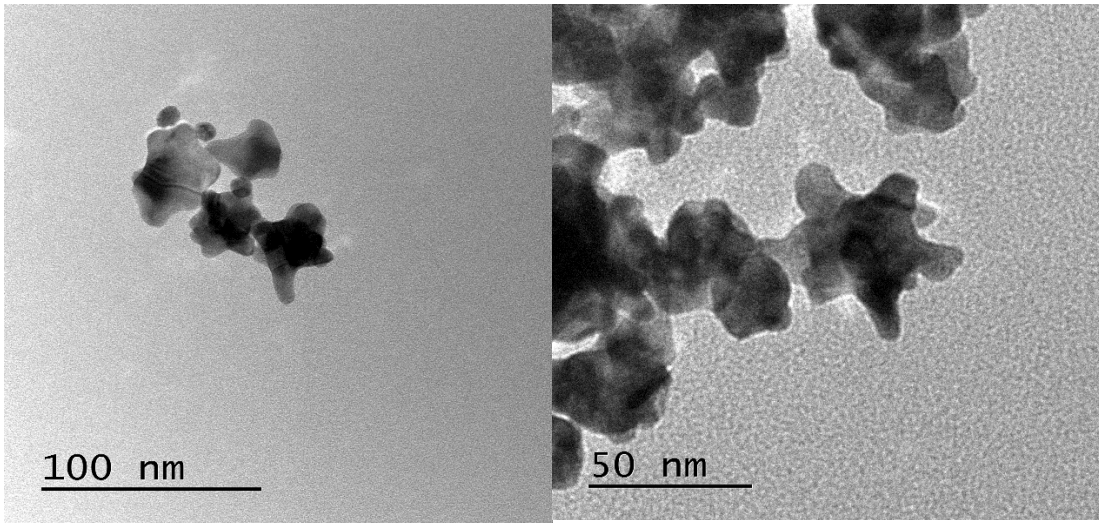

(c) **(d)**

Figure 5.8. TEM images (a), (b), (c) and (d) of colloidal AuNSs made through the surfactant-free method with 1mM [Ag] (102).

The advantage of this method also results in inconvenience. Besides being a fast and simple synthesis method, the advantage of using no stabilizing agent is that it is unnecessary to remove it in subsequent steps prior immobilization, as this may affect the catalytic activity. However, it has the disadvantage of lacking good morphology control and the resultant nanoparticles are not well defined.

5.3.4 Reduction of 4-nitrophenol

The 4-nitrophenol reduction to 4-amoniphenol by the presence of a strong reducing agent in excess like $NaBH_4$ is thermodynamically favourable because the difference of their standard electrode potentials is greater than zero. On the other hand, the reaction is kinetically restricted in the absence of an efficient catalyst. By adding $NaBH_4$ into a 4-NP solution, the solution changed from light yellow to bright yellow, caused by the formation of 4-nitrophenolate ions under highly basic conditions. As is shown in **Figure 5.9**, the original absorption peak also shifted from 317 nm to 400 nm. A control experiment first performed using just $NaBH_4$ as the reducing agent showed little or no decrease in the absorption peak at 400 nm with reaction time. Additionally, the peak at 300 nm corresponding to the production of 4-aminophenol (4-AP) was not observed. This indicates that the formation of 4-aminophenol product results from the catalysis by the NPs rather than from $NaBH_4$ alone. This is in agreement with what has been reported in the literature.

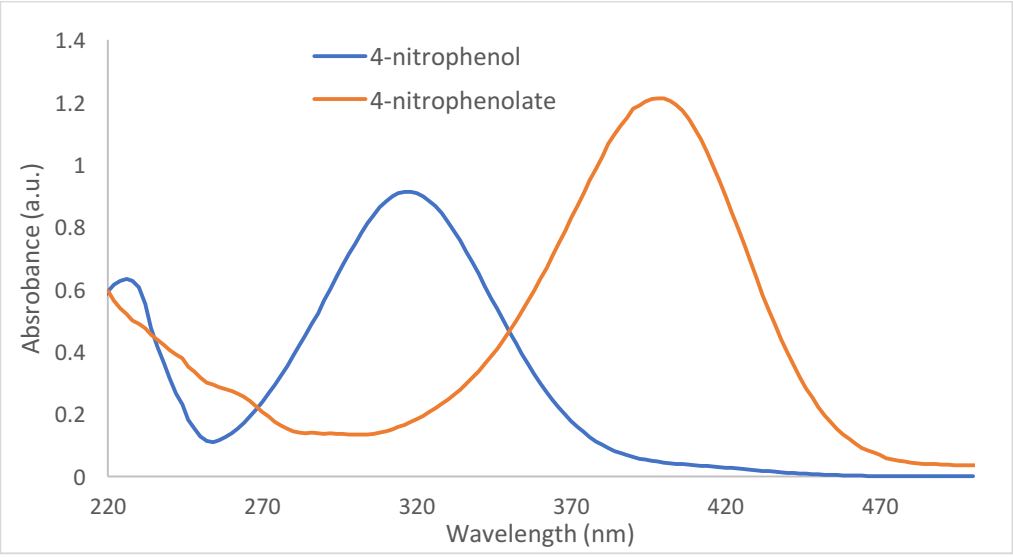

Figure 5.9. UV-vis absorption spectra of 4-nitrophenol and 4-nitrophenolate, (mixture of 4-nitrophenolate and $NaBH_4$)

A UV-Vis calibration curve to determine the concentration of 4-nitrophenolate was determined prior to conducting the reactions using the maximum absorbance value (~400 nm) of 10 dilutions of the original 4-NP solution within the concentration range of 0.10 mM to 0.005 mM, each containing 0.10 M $NaBH_4$. A linear equation was obtained from the plots of these concentrations as a function of time. The Beer's law was used in obtaining the subsequent concentration from the reaction.

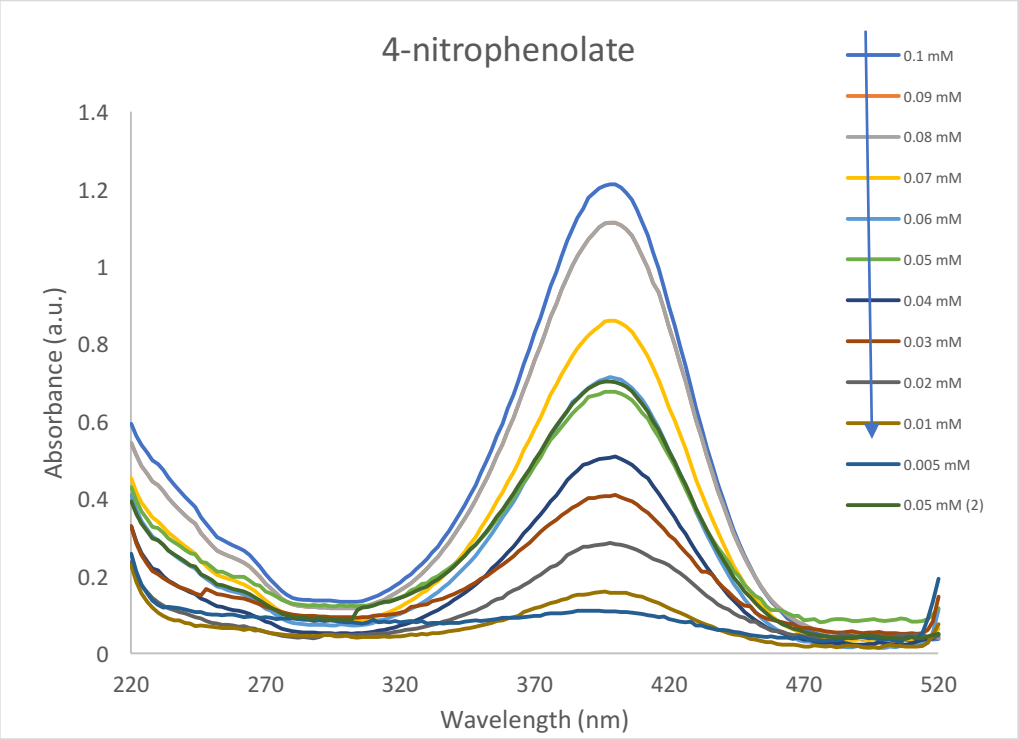

Figure 5.10. UV-vis absorption spectra of 4-nitrophenolate (mixture of 0.1 mM 4-NP and 0.1 M $NaNH_4$) for different concentrations used in the calibration curve.

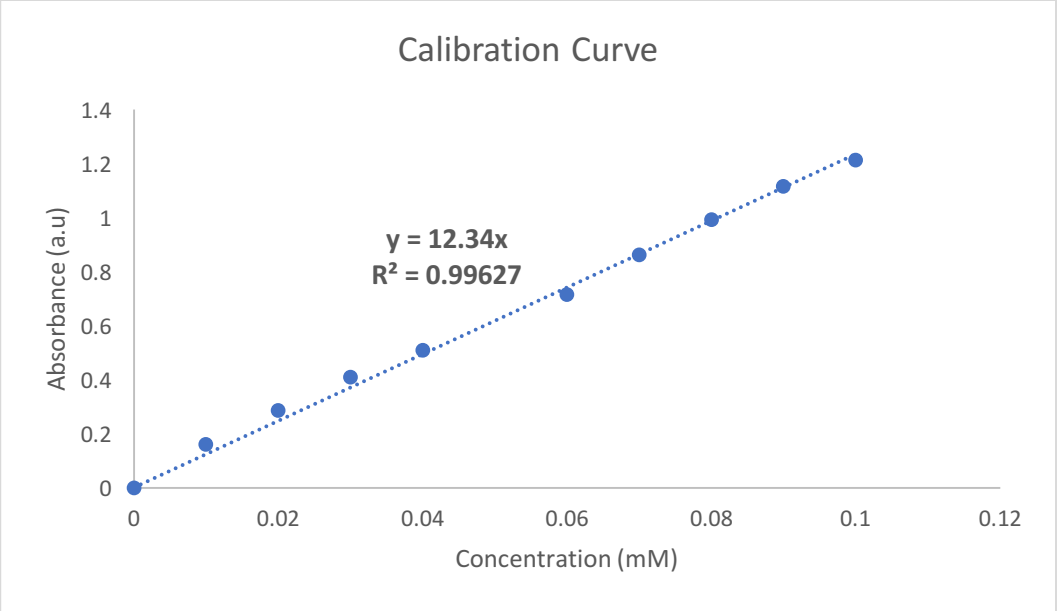

Figure 5.11. Calibration plot of 4-NP (0.1 mM to 0.01 mM) + $NaBH_4$ (0.1M) versus absorbance.

The peak intensity of the absorption peak at 400 nm decreased while increasing reaction time for all the catalysts, at the same time a new absorption peak corresponding to 4-aminophenol appeared at 300 nm as shown below in **Figure 5.12**. This is an example of the multiple reactions ocurring, in this case AuNSs surfactant-free 1 mM [Ag] was used as the catalyst.

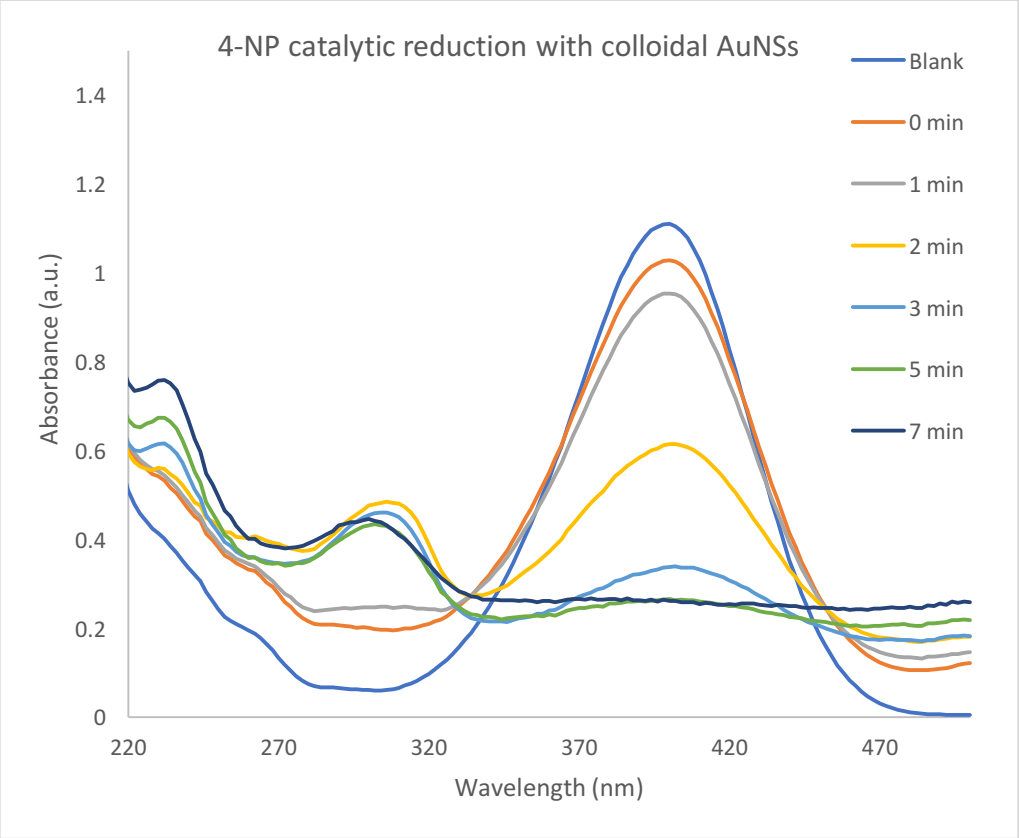

Figure 5.12. UV-Vis absorption spectra of 4-NP reduction with colloidal gold nanostars 1 mM [Ag] made via the surfactant-free method.

Full conversion was obtained with all the nanoparticles tested. In order to slow down the reaction since immediately after adding the catalyst, conversion is observed (**Figure 5.12**), small amounts of catalyst were used.

Catalytic efficiencies of all the catalysts was obtained by calculating the apparent rate constants (kapp). All catalysts showed a good linear relationship of $-\ln (C_t/C_0)$ versus reaction time (t) (**Figure 5.13** below) confirming pseudo-first-order kinetics as is well-known for this reaction.

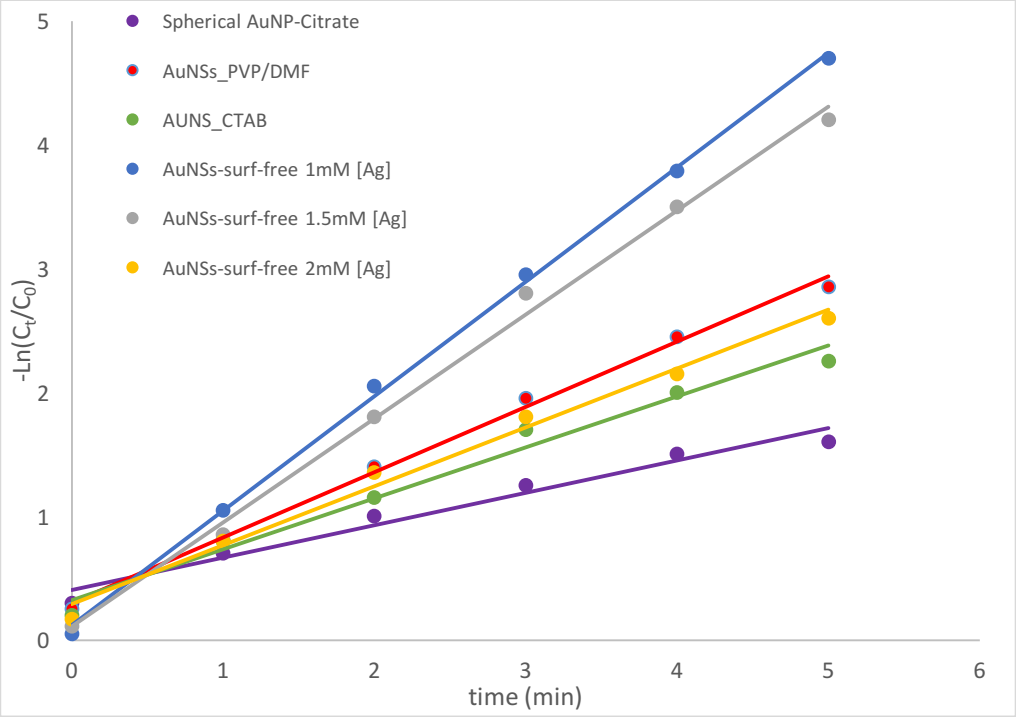

Figure 5.13. Plots of the natural logarithm of concentrations at 400 nm vs. the reduction time using different colloidal gold nanoparticles with the same molar ratio.

Table 5.1 below gives the apparent rate constant k_{app} values of the various reactions demonstrating the catalytic activity of the colloidal Au catalysts. Oddly, the smaller AuNSs made via surfactant-free synthesis gave the highest apparent rate constant values suggesting higher activity while the spherical AuNPs gave the lowest values, proving that AuNSs nanoparticles have potential catalytic activities of interest.

Catalyst	**Particle Size (nm)**	**Au/4-NP (molar ratio)**	**k_{app} (min^{-1})**
Spherical Citrate Seeds	15	1/1.5	0.26
PVP/DMF	120	1/1.5	0.52
CTAB	(unknown)	1/1.5	0.41
1 mM [Ag] _ Surfactant-free	60	1/1.5	0.92
1.5 mM [Ag] _ Surfactant-free	(unknow)	1/1.5	0.84
2 mM [Ag] _ Surfactant-free	(unknow)	1/1.5	0.47

Table 5.1 (previous page). Comparison of the apparent rate constants (k_{app}) for different colloidal gold nanostars and spherical nanoparticles for the reduction of 4-NP with $NaBH_4$.

As AuNSs made via the surfactant-free method showed better catalytic activity, it was decided to support them onto titania in order to see, first, if it is possible and then test their catalytic activity for both methyl orange photodegradation and 4-nitrophenol reduction.

5.3.5 Supported Gold NanoStars (AuNSs/TiO_2)

In **Figure 5.14** the UV-Vis diffuse reflectance spectrum of immobilized Au nanostars from the surfactant-free method 1 mM [Ag] is presented. The spectrum of the colloidal suspension was shown earlier in **Figure 5.4** where its plasmon band peak was at 770 nm. Although there was an instrumentation limitation, since wavelengths longer than 800 nm could not be recorded, the plasmon band resonance seems to be around the same wavelength supporting the idea that AuNSs have been immobilised.

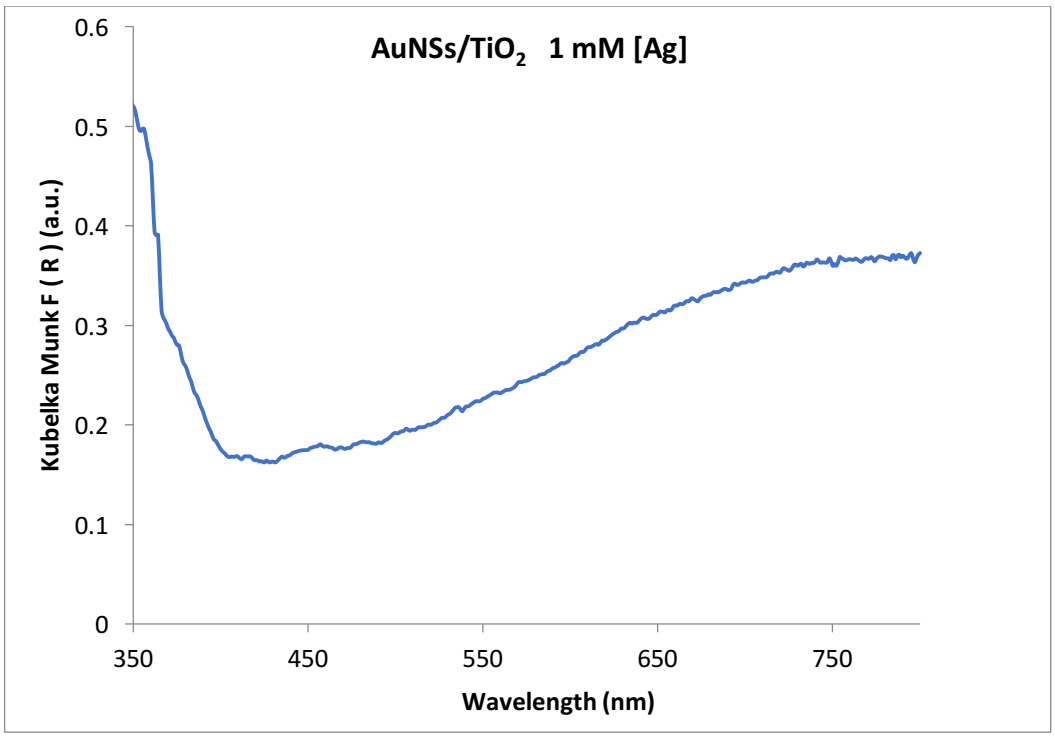

Figure 5.14. Normalized UV-Vis diffusion reflectance spectra of AuNSs/TiO_2 for AuNS (1 mM [Ag]).

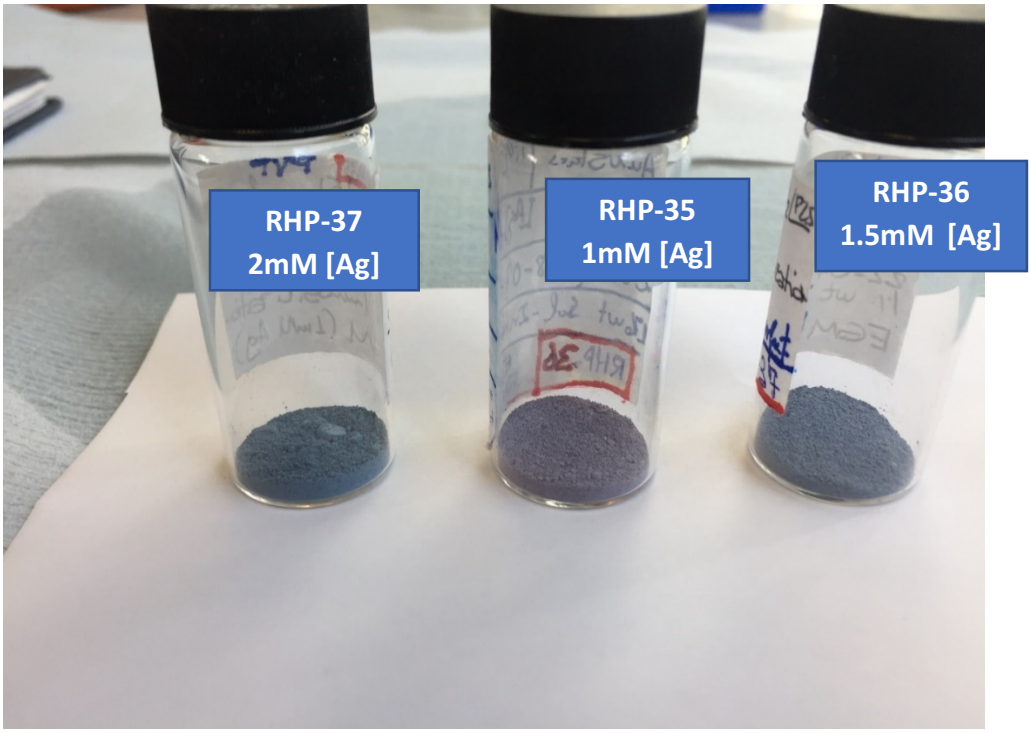

Figure 5.15. Image supported AuNSs on titania catalysts. The nanoparticles were made by the surfactant-free method with varying Ag^{+} concentration.

Although the solid catalyst possesses the characteristic purple/blue colour of nanostars in colloidal solution as shown in **Figure 5.15**, it was difficult to discern the morphology of nanostars once they were supported from the diffuse reflectance UV-Vis spectra obtained. However, the preservation of the shape in the supported catalyst was confirmed by TEM as shown below (**Figure 5.16**).

5.3.6 Transmission Electron Microscopy, TEM

TEM was performed to examine the presence of AuNSs, nanoparticle morphology and also estimate the particle size of the prepared AuNSs/TiO_2. It can be seen that gold nanostars have successfully been supported on titania as is shown in **Figure 5.15** (next page).

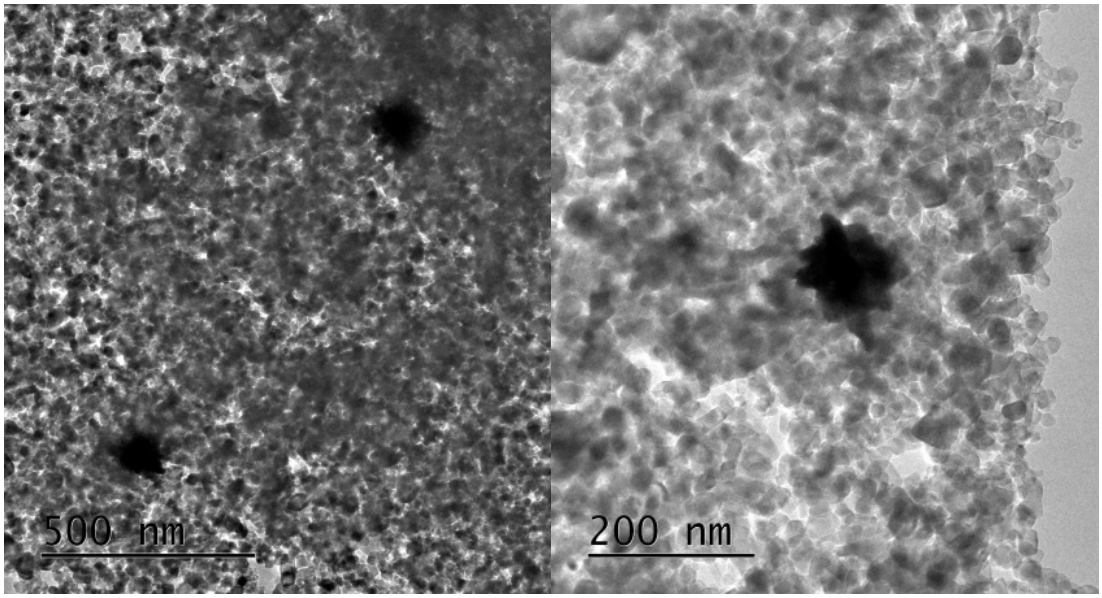

(a) **(b)**

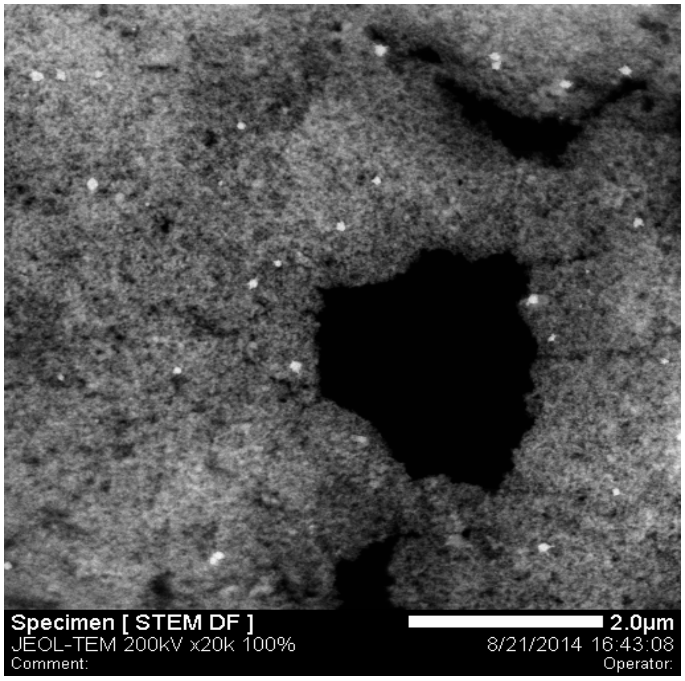

©

Figure 5.15. TEM images (a) and (b) and STEM image (c) of supported gold nanostars AuNSs/TiO_2 made through free-surfactant method 2 mM [Ag]. In the case of TEM images (a), (b) the dark shapes represent Au nanostars. In the STEM analysis (c) the bright spots represent Au nanostars and dark spots areas without sample (carbon film).

AuNSs of size 100 nm ± 10 nm were found. This corresponded to nanoparticle synthesis using 2 mM [Ag] which is the highest amount of silver used and therefore the biggest nanoparticles made applying the surfactant-free method.

5.3.7 Inductively Coupled Plasma-Optical Emission Spectroscopy, ICP-OES

Inductive Coupled Plasma-Optical Emission Spectroscopy, ICP-OES was performed on the samples to determine the actual metal loading of prepared catalysts. The results are shown in **Table 5.2.** As the previous set of experiments with different shapes it was found that the actual loading was lower than the theoretical loading expected on the basis of the synthesis procedure. Synthesis to produce catalysts with 1 wt % loading in all cases was attempted, but the loading of Au was, in the best case, slightly lower. It is possible that that Au was not fully digested while preparing the samples for analysis. In this chapter, the experimental loadings and metal ratios obtained by ICP will be used.

Catalyst Label	Synthesis	Theoretical loading (%)	ICP loading (%)
RHP-27	Citrate Spheres	1	0.92
RHP-35	Surf-free 1mM [Ag] (Stars)	1	0.83
RHP-36	Surf-free 1.5mM [Ag] (Stars)	1	0.91
RHP-37	Surf-free 2mM [Ag] (Stars)	1	0.79

Table 5.2. ICP-OES results of prepared AuNSs catalyst.

5.3.8 Reduction of 4-nitrophenol

In order to measure catalytic activity, supported AuNSs were tested for 4-nitrophenol reduction. The absorption peak at 400 nm was gradually decreased in intensity as a function of reaction time for all the solid catalysts run, at the same time a new absorption peak corresponding to 4-AP appeared at 300 nm as evident below in **Figure 5.16**. This is one example of the multiple reactions carried out, and in this case AuNSs/TiO_2 surfactant-free 1 mM [Ag] was used as catalyst.

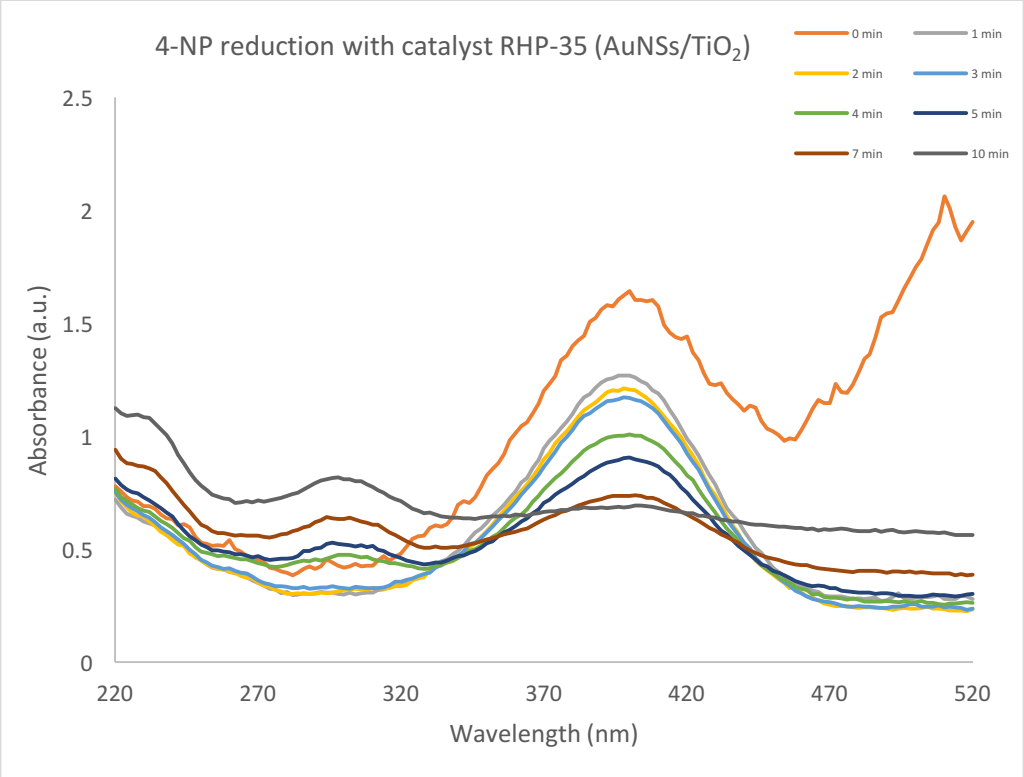

Figure 5.16. UV-Vis absorption spectra of 4-NP reduction with solid catalyst RHP-35, AuNSs/TiO_2 1mM [Ag].

Full conversion was obtained with all the catalyst tested. Catalytic efficiencies were determined from the apparent rate constants (kapp). The catalyst showed a linear relationship for $-\ln (C_t/C_0)$ as a function of reaction time (t) **Figure 5.17** below) confirming pseudo-first-order kinetics.

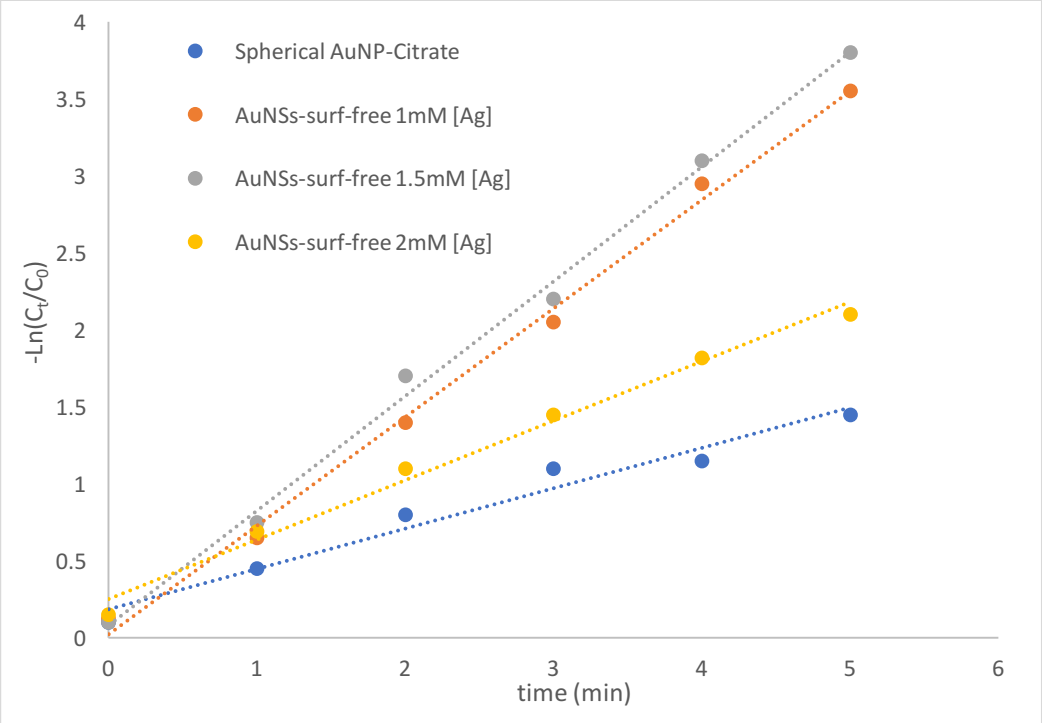

Figure 5.17. Plots of the natural logarithm of concentrations at 400 nm vs. the reduction time using different supported gold nanoparticles with the same molar ratio.

Table 5.3 below gives the apparent rate constants kapp values for the various reactions demonstrating the catalytic activity of the supported Au catalysts. In this case, AuNSs made via surfactant-free synthesis with 1.5 mM [Ag] presented the highest apparent rate constant value suggesting higher activity while the spherical AuNPs again, gave the lowest value, providing again that AuNSs nanoparticles supported could have potential catalytic applications.

Catalyst Label	Synthesis/Shape	Particle Size (nm)	Au/4-NP (molar ratio)	kapp (min^{-1})
RHP-27	Spherical Citrate Seeds	15	1/1.5	0.26
RHP-35	1 mM [Ag] _ Surfactant-free (Stars)	60	1/1.5	0.70
RHP-36	1.5 mM [Ag] _ Surfactant-free (Stars)	(unknow)	1/1.5	0.75
RHP-37	2 mM [Ag] _ Surfactant-free (Stars)	(unknow)	1/1.5	0.38

Table 5.3 (previous page) Comparison of the apparent rate constants (kapp) of supported gold nanostars with different size and spherical nanoparticles for the reduction of 4-NP with $NaBH_4$.

AuNSs made via surfactant-free method and supported via sol-immobilization have shown again to possess catalytic activity. Methyl Orange photodegradation in order to obtain further information about supported nanoparticle catalytic activity was also undertaken.

5.3.9 Methyl Orange Photodegradation

Photocatalytic degradation of the azo-dye Methyl Orange (MO) has been used to characterize and measure the catalytic activity of gold nanostars supported on titania under visible light.

Figure 5.18 shows representative UV-Vis spectra of methyl orange (MO) concentration initially and after photodegradation test (RHP-36 stars supported on titania 1.5mM [Ag], titania and citrate seeds spheres supported on titania too).

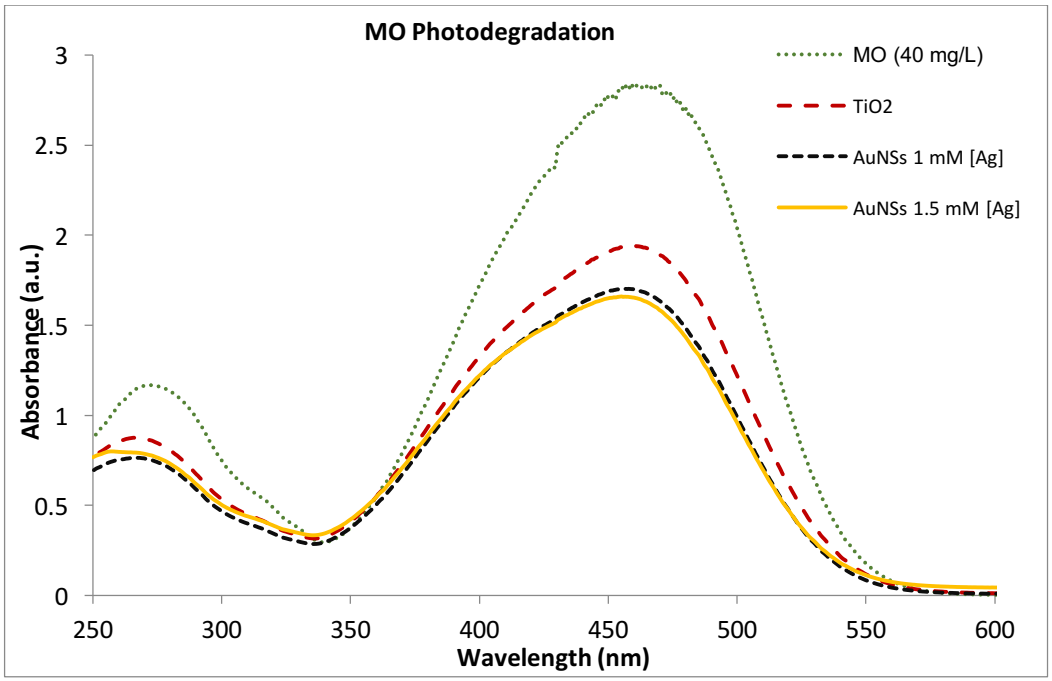

Figure 5.18. UV-Vis absorption spectra representative of Methyl Orange concentration before and after 3h of photoreaction with different catalyst. Typically, the vials were prepared with 10 ml of [MO] = 40 mg/L and 20 mg of catalyst or 1 ml of colloidal solution.

Table 5.4 shows the conversion values for supported nanoparticles catalysts and TiO_2. As it can be seen, in this case as occurred in the 4-nitropheno reduction, catalyst RHP-36 have shown better catalytic activity as 25.8 % conversion is the highest obtained.

Catalyst Label	Synthesis/Shape	Particle Size (nm)	Conversion (%)
TiO_2	---	---	21.4
RHP-27	Spherical Citrate Seeds	15	22.6
RHP-35	1 mM [Ag] _ Surfactant-free (Stars)	60	24.3
RHP-36	1.5 mM [Ag] _ Surfactant-free (Stars)	(unknow)	25.8
RHP-37	2 mM [Ag] _ Surfactant-free (Stars)	(unknow)	23.7

Table 5.4. Summary table of conversion values for catalysts tested in the photodegradation of Methyl Orange (MO) under visible light after 3 hours in the LuzChem ICH2, at 30℃.

Reproducibility tests showed that the experimental error was higher than the differences shown (around 10%) which prevents clear conclusion from being drawn. As observed, the conversion obtained in all the cases was superior to TiO_2 by a small amount, so it might seem there was a slightly promotion by the nanostars as had been expected. Therefore, further tests are needed to confirm this hypothesis. Alternatively, a more suitable and established probe reaction might be required, such as benzyl alcohol oxidation (108). This reaction has been well studied in the literature and it can be performed via both thermo- (158, 159) and photo-catalytic routes (160). Also, it allows one to follow not only conversion of the benzyl alcohol, but also selectivities to different products thus showing the effect upon various reaction pathways.

5.4 Conclusions

In conclusion, colloidal gold nanostars were prepared using seed-mediated growth by three different methods, and their catalytic activity was compared. Surfactant-free nanoparticles showed significantly better catalytic activity and colloidal gold nanostars were successfully supported on titania for the first time.

In the case of AuNSs made by the surfactant-free synthesis method, the citrate prepared spherical seed, were created by anisotropic growth and were also used as a catalyst in order to compare the catalytic activity with gold nanostars. The catalytic activity of differently-sized nanostars were compared using a model reaction (4-nitrophenol reduction by sodium borohydride) and also Methyl Orange photodegradation. Nanostars showed better catalytic activity than spherical particles and they could have promising applications for catalysis.

In this work, the synthesis of gold nanostars with different sizes and carried out by seed-mediated growth surfactant-free method has been successfully controlled. The nanostars of different sizes were synthesized using Ag^+ since increasing concentration of Ag^+ leads to larger nanoparticles with more branches.

Notwithstanding their interesting properties, not many studies on catalytic applications for metal nanostars have been carried out, especially on supported nanoparticles, and none of them with titania as support. For that reason, this work has provided an initial indication of the catalytic activity of gold nanostars catalysts supported on titania.

Chapter 6

Conclusions

&

Outlook

6 Conclusions and Outlook

6.1 Conclusions

This research outlined within this thesis initially aimed to study the size and shape control of anisotropic gold nanoparticles for their potential catalytic application.

In Chapter 3 the sonication-assisted precipitation-reduction was extended to the preparation of various mono- and bi-metallic catalysts supported on various support. The catalysts were applied for the photocatalytic degradation of MO and the PROX reaction. In general, there are three advantages for the sonication method as compared with the conventional methods, including the high dispersion of metal nanoparticles on the catalyst support, the much higher DE values than those of the DP and CP methods, and the very fast preparation as the deposition only takes 10-20 seconds. The photocatalytic degradation of MO over a series AuPd/TiO_2 showed that the AuPd(3:1)/TiO_2 catalyst was much more active than the other catalysts, mainly because of the high dispersion of the metal particles, the formation of Au-Pd alloy particles and the surface decoration of trace amounts of PdO on the Au-Pd alloy particles. It was found that, besides the solution pH, the addition of the metal solution into the $NaBH_4$ solution in the preparation (the inverse sonication method) and the separate deposition of Au or Pd led to the phase separation of Au and Pd, which was not conducive to the catalytic activity. For the PROX reaction, the highly dispersed Ru/TiO_2, Au-Cu/SBA-15 and Pt/γ-Al_2O_3 catalysts prepared by the sonication method were found to be very active. The Pt/γ-Al_2O_3 catalyst was also quite stable. Moreover, it was found that the Pt/γ-Al_2O_3 (SASOL) catalyst was able to lower the CO concentration to several ppm at a quite low reaction temperature (100 ^{o}C), indicating promise for practical application.

In Chapter 4, the focus was the knowledge and skills necessary to have better control of the morphology of the nanoparticles with successful results and their immobilization on titania in a “novel way”. This report demonstrates that the synthesis of variable shape and sized nanoparticles can be carried out precisely and also with subsequent immobilization. The first indication of success in the immobilization of

different morphologies was the catalyst's colour because after the nanoparticle immobilization on titania the initial colloidal nanoparticle colour was preserved. The preservation of the structure was also confirmed by UV-Vis diffuse reflectance spectra and TEM images of supported nanoparticles. Thus, for the first time, immobilization through the sol-immobilization method of anisotropy supported nanoparticles of variable morphology such as rods or stars on titania was performed.

In Chapter 5, colloidal gold nanostars were prepared using seed-mediated growth by three different methods, and their catalytic activity was compared. Surfactant-free nanoparticles showed a significant better catalytic activity and colloidal gold nanostars were successfully supported on titania for the first time. In the case of AuNSs made by the surfactant-free synthesis method, the citrate prepared spherical seed, was created by anisotropic growth and was also used as catalyst in order to compare its catalytic activity with gold nanostars. The catalytic activity of differently-sized nanostars was compared using a model reaction (4-nitrophenol reduction by sodium borohydride) and also methyl orange photodegradation. Nanostars showed a better catalytic activity than the spherical particles and they could have promising applications for catalysis. In this work, the synthesis of gold nanostars with different sizes and carried out by the seed-mediated growth surfactant-free method was successfully controlled. Nanostars of different sizes were synthesized using Ag^+ since the increase of concentration Ag^+ led to larger nanoparticles with more branches.

6.2 Outlook

It is noteworthy that the nanorods have shown to be active in both Methyl Orange photodegradation although the use of dye degradation is quite limited since it only evidences the loss of a chromophore and not complete mineralization. There is not a clear picture of its size-shape dependency and also in the selective oxidation of HMF, which has been deeply studied.

More research has to be undertaken in this field to obtain a clear outcome, although when compared with spherical nanoparticles it seems very obvious that gold nanorods have much lower activity.

In relation to obtaining a wider knowledge of the control possible in the synthesis of the nanoparticles in terms of both size and shape, more experiments must be done by

decisive modifying the different variables involved in the synthesis of noble metal nanoparticles.

Notwithstanding their interesting properties, not many studies on catalytic applications for metal nanostars have been carried out, especially on supported nanoparticles, and none of them with titania as the support. For that reason, the work herein provides an initial outcome on the catalytic activity of gold nanostars catalysts supported on titania.

References

7 References

1. Wittstock A, Zielasek V, Biener J, Friend CM, Baumer M. Nanoporous Gold Catalysts for Selective Gas-Phase Oxidative Coupling of Methanol at Low Temperature. Science. 2010;327(5963):319-22.

2. Campbell CT, Parker SC, Starr DE. The effect of size-dependent nanoparticle energetics on catalyst sintering. Science. 2002;298(5594):811-4.

3. Lei Y, Mehmood F, Lee S, Greeley J, Lee B, Seifert S, et al. Increased Silver Activity for Direct Propylene Epoxidation via Subnanometer Size Effects. Science. 2010;328(5975):224-8.

4. Daniel MC, Astruc D. Gold nanoparticles: assembly, supramolecular chemistry, quantum-size-related properties, and applications toward biology, catalysis, and nanotechnology. Chem Rev. 2004;104(1):293-346.

5. Marangoni VS, Cancino-Bernardi J, Zucolotto V. Synthesis, Physico-Chemical Properties, and Biomedical Applications of Gold Nanorods-A Review. J Biomed Nanotechnol. 2016;12(6):1136-58.

6. Wiley BJ, Xiong Y, Li ZY, Yin Y, Xia Y. Right bipyramids of silver: a new shape derived from single twinned seeds. Nano Lett. 2006;6(4):765-8.

7. Personick ML, Langille MR, Zhang J, Wu J, Li S, Mirkin CA. Plasmon-mediated synthesis of silver cubes with unusual twinning structures using short wavelength excitation. Small. 2013;9(11):1947-53.

8. Judith L, Sergey MN, Luis ML-M. Sensing using plasmonic nanostructures and nanoparticles. Nanotechnology. 2015;26(32):322001.

9. Fujishima A, Honda K. Electrochemical Photolysis of Water at a Semiconductor Electrode. Nature. 1972;238(5358):37-+.

10. Zou ZG, Ye JH, Sayama K, Arakawa H. Direct splitting of water under visible light irradiation with an oxide semiconductor photocatalyst. Nature. 2001;414(6864):625-7.

11. Claus P, Bruckner A, Mohr C, Hofmeister H. Supported gold nanoparticles from quantum dot to mesoscopic size scale: Effect of electronic and structural properties on catalytic hydrogenation of conjugated functional groups. J Am Chem Soc. 2000;122(46):11430-9.

12. Maier SA, Kik PG, Atwater HA, Meltzer S, Harel E, Koel BE, et al. Local detection of electromagnetic energy transport below the diffraction limit in metal nanoparticle plasmon waveguides. Nat Mater. 2003;2(4):229-32.

13. Hazra B, Das K, Das Chakraborty S, Verma MS, Devi MM, Katiyar NK, et al. Hollow Gold Nanoprism as Highly Efficient "Single" Nanotransducer for Surface-Enhanced Raman Scattering Applications. J Phys Chem C. 2016;120(44):25548-56.

14. Sarathy KV, Kulkarni GU, Rao CNR. A novel method of preparing thiol-derivatised nanoparticles of gold, platinum and silver forming superstructures. Chem Commun. 1997(6):537-8.

15. Jin RC, Cao YW, Mirkin CA, Kelly KL, Schatz GC, Zheng JG. Photoinduced conversion of silver nanospheres to nanoprisms. Science. 2001;294(5548):1901-3.

16. An BZ, Li MJ, Wang JL, Li CX. Shape/size controlling syntheses, properties and applications of two-dimensional noble metal nanocrystals. Frontiers of Chemical Science and Engineering. 2016;10(3):360-82.

17. Murphy CJ, San TK, Gole AM, Orendorff CJ, Gao JX, Gou L, et al. Anisotropic metal nanoparticles: Synthesis, assembly, and optical applications. J Phys Chem B. 2005;109(29):13857-70.

18. Stephen A, Hashmi K. Homogeneous catalysis by gold. Gold Bull.37(1):51-65.

19. Haruta M, Yamada N, Kobayashi T, Iijima S. Gold Catalysts Prepared by Coprecipitation for Low-Temperature Oxidation of Hydrogen and of Carbon-Monoxide. J Catal. 1989;115(2):301-9.

20. Zhong Z, Lin J, Teh SP, Teo J, Dautzenberg FM. A Rapid and Efficient Method to Deposit Gold Particles onto Catalyst Supports and Its Application for CO Oxidation at Low Temperatures. Adv Funct Mater. 2007;17(8):1402-8.

21. Zhang QF, Han LL, Jing H, Blom DA, Lin Y, Xing HLL, et al. Facet Control of Gold Nanorods. Acs Nano. 2016;10(2):2960-74.

22. Budy SM, Hamilton DJ, Cai YH, Knowles MK, Reed SM. Polymer mediated layer-by-layer assembly of different shaped gold nanoparticles. J Colloid Interf Sci. 2017;487:336-47.

23. Chen X, Zhu H, Groarke RJ. Catalysis by Supported Gold Nanoparticles. Reference Module in Materials Science and Materials Engineering: Elsevier; 2016.

24. Sathishkumar G, Jha PK, Vignesh V, Rajkuberan C, Jeyaraj M, Selvakumar M, et al. Cannonball fruit (Couroupita guianensis, Aubl.) extract mediated synthesis of gold nanoparticles and evaluation of its antioxidant activity. J Mol Liq. 2016;215:229-36.

25. Thorkelsson K, Bai P, Xu T. Self-assembly and applications of anisotropic nanomaterials: A review. Nano Today. 2015;10(1):48-66.

26. Yi CL, Zhang SY, Webb KT, Nie ZH. Anisotropic Self-Assembly of Hairy Inorganic Nanoparticles. Accounts Chem Res. 2017;50(1):12-21.

27. Giner-Casares JI, Henriksen-Lacey M, Garcia I, Liz-Marzan LM. Plasmonic Surfaces for Cell Growth and Retrieval Triggered by Near-Infrared Light. Angew Chem Int Edit. 2016;55(3):974-8.

28. Zhao P, Li N, Astruc D. State of the art in gold nanoparticle synthesis. Coordin Chem Rev. 2013;257(3–4):638-65.

29. Santos JJ, Ando RA, Toma SH, Corio P, Araki K, Toma HE. Surface enhanced Raman spectroelectrochemistry of a mu-oxo triruthenium acetate cluster: an experimental and theoretical approach. Inorg Chem. 2015;54(19):9656-63.

30. Moores A, Goettmann F, eacute, eacute, ric, Moores A, et al. The plasmon band in noble metal nanoparticles: an introduction to theory and applications. New J Chem. 2006;30(8):1121-32.

31. Simon S, Olumorin TI, Guo B, Burgess IJ. Role of Au(I) Intermediates in the Electrochemical Formation of Highly Anisotropic Gold Nanostructures with Near-IR SERS Applications. J Phys Chem C. 2016;120(45):26150-8.

32. El-Sayed MA. Some interesting properties of metals confined in time and nanometer space of different shapes. Accounts Chem Res. 2001;34(4):257-64.

33. Hu H, Zhou J, Kong Q, Li C. Two-Dimensional Au Nanocrystals: Shape/Size Controlling Synthesis, Morphologies, and Applications. Part Part Syst Char. 2015;32(8):796-808.

34. Ndokoye P, Li X, Zhao Q, Li T, Tade MO, Liu S. Gold nanostars: Benzyldimethylammonium chloride-assisted synthesis, plasmon tuning, SERS and catalytic activity. J Colloid Interf Sci. 2016;462:341-50.

35. Xiong W, Sikdar D, Yap LW, Guo P, Premaratne M, Li X, et al. Matryoshka-caged gold nanorods: Synthesis, plasmonic properties, and catalytic activity. Nano Res. 2016;9(2):415-23.

36. Liu LQ, Ouyang SX, Ye JH. Gold-Nanorod-Photosensitized Titanium Dioxide with Wide-Range Visible-Light Harvesting Based on Localized Surface Plasmon Resonance. Angew Chem Int Edit. 2013;52(26):6689-93.

37. Pallares RM, Su XD, Lim SH, Thanh NTK. Fine-tuning of gold nanorod dimensions and plasmonic properties using the Hofmeister effects. J Mater Chem C. 2016;4(1):53-61.

38. Jiang T, Jia C, Zhang L, He S, Sang Y, Li H, et al. Gold and gold-palladium alloy nanoparticles on heterostructured TiO2 nanobelts as plasmonic photocatalysts for benzyl alcohol oxidation. Nanoscale. 2015;7(1):209-17.

39. Gan QQ, Bartoli FJ, Kafafi ZH. Plasmonic-Enhanced Organic Photovoltaics: Breaking the 10% Efficiency Barrier. Adv Mater. 2013;25(17):2385-96.

40. Barbosa S, Agrawal A, Rodriguez-Lorenzo L, Pastoriza-Santos I, Alvarez-Puebla RA, Kornowski A, et al. Tuning size and sensing properties in colloidal gold nanostars. Langmuir. 2010;26(18):14943-50.

41. Hallett-Tapley GL, Silvero MJ, Bueno-Alejo CJ, Gonzalez-Bejar M, McTiernan CD, Grenier M, et al. Supported Gold Nanoparticles as Efficient Catalysts in the Solvent less Plasmon Mediated Oxidation of sec-Phenethyl and Benzyl Alcohol. J Phys Chem C. 2013;117(23):12279-88.

42. Choi S, Moon Y, Yoo H. Finely tunable fabrication and catalytic activity of gold multipod nanoparticles. J Colloid Interf Sci. 2016;469:269-76.

43. Shelby RA, Smith DR, Schultz S. Experimental verification of a negative index of refraction. Science. 2001;292(5514):77-9.

44. Hornyak GL, Patrissi CJ, Martin CR. Fabrication, Characterization, and Optical Properties of Gold Nanoparticle/Porous Alumina Composites: The Nonscattering Maxwell−Garnett Limit. The Journal of Physical Chemistry B. 1997;101(9):1548-55.

45. Link S, El-Sayed MA. Shape and size dependence of radiative, non-radiative and photothermal properties of gold nanocrystals. International Reviews in Physical Chemistry. 2000;19(3):409-53.

46. Spesyvtseva SES, Dholakia K. Trapping in a Material World. ACS Photonics. 2016;3(5):719-36.

47. Hermoso W, Alves TV, de Oliveira CCS, Moriya EG, Ornellas FR, Camargo PHC. Triangular metal nanoprisms of Ag, Au, and Cu: Modeling the influence of size, composition, and excitation wavelength on the optical properties. Chem Phys. 2013;423:142-50.

48. Tu W, Zhou Y, Li H, Li P, Zou Z. Au@TiO2 yolk-shell hollow spheres for plasmon-induced photocatalytic reduction of CO2 to solar fuel via a local electromagnetic field. Nanoscale. 2015;7(34):14232-6.

49. Wu ZH, Yang SL, Wu W. Shape control of inorganic nanoparticles from solution. Nanoscale. 2016;8(3):1237-59.

50. Cennamo N, D'Agostino G, Donà A, Dacarro G, Pallavicini P, Pesavento M, et al. Localized Surface Plasmon Resonance with Five-Branched Gold Nanostars in a Plastic Optical Fiber for Bio-Chemical Sensor Implementation. Sensors-Basel. 2013;13(11):14676-86.

51. Lukosi M, Zhu H, Dai S. Recent advances in gold-metal oxide core-shell nanoparticles: Synthesis, characterization, and their application for heterogeneous catalysis. Frontiers of Chemical Science and Engineering. 2016;10(1):39-56.

52. Castiello FR, Romo-Herrera JM, Farias MH, Guerra ED, Contreras OE, Berhault G, et al. "Green" seed-mediated synthesis and morphology of Au nanoparticles using beta-cyclodextrin. Gold Bull. 2016;49(1-2):45-51.

53. Mie G. Beiträge zur Optik trüber Medien, speziell kolloidaler Metallösungen. Annalen der physik. 1908;330(3):377-445.

54. Perez-Juste J, Pastoriza-Santos I, Liz-Marzan LM, Mulvaney P. Gold nanorods: Synthesis, characterization and applications. Coordin Chem Rev. 2005;249(17-18):1870-901.

55. Gans R. Über die Form ultramikroskopischer Goldteilchen. Annalen der Physik. 1912;342(5):881-900.

56. Zimbone M, Calcagno L, Messina G, Baeri P, Compagnini G. Dynamic light scattering and UV–vis spectroscopy of gold nanoparticles solution. Mater Lett. 2011;65(19–20):2906-9.

57. Huang YJ, Dai LW, Song LP, Zhang L, Rong Y, Zhang JW, et al. Engineering Gold Nanoparticles in Compass Shape with Broadly Tunable Plasmon Resonances and High-Performance SERS. Acs Appl Mater Inter. 2016;8(41):27949-55.

58. Li N, Zhao P, Astruc D. Anisotropic Gold Nanoparticles: Synthesis, Properties, Applications, and Toxicity. Angewandte Chemie International Edition. 2014;53(7):1756-89.

59. Nikoobakht B, El-Sayed MA. Preparation and growth mechanism of gold nanorods (NRs) using seed-mediated growth method. Chem Mater. 2003;15(10):1957-62.

60. Vankayala R, Huang Y-K, Kalluru P, Chiang C-S, Hwang KC. First Demonstration of Gold Nanorods-Mediated Photodynamic Therapeutic Destruction of Tumors via Near Infra-Red Light Activation. Small. 2014;10(8):1612-22.

61. Alfranca G, Artiga A, Stepien G, Moros M, Mitchell SG, de la Fuente JM. Gold nanoprism-nanorod face off: comparing the heating efficiency, cellular internalization and thermoablation capacity. Nanomedicine-Uk. 2016;11(22):2903-16.

62. Rodríguez-Oliveros R, Sánchez-Gil Ja. Gold nanostars as thermoplasmonic nanoparticles for optical heating. Opt Express. 2012;20(1):621-.

63. Chandra K, Culver KSB, Werner SE, Lee RC, Odom TW. Manipulating the Anisotropic Structure of Gold Nanostars using Good's Buffers. Chem Mater. 2016;28(18):6763-9.

64. Liu Y, Yuan HK, Kersey FR, Register JK, Parrott MC, Vo-Dinh T. Plasmonic Gold Nanostars for Multi-Modality Sensing and Diagnostics. Sensors-Basel. 2015;15(2):3706-20.

65. Dickerson EB, Dreaden EC, Huang X, El-Sayed IH, Chu H, Pushpanketh S, et al. Gold nanorod assisted near-infrared plasmonic photothermal therapy (PPTT) of squamous cell carcinoma in mice. Cancer Letters. 2008;269:57-66.

66. Hill EH, Claes N, Bals S, Liz-Marzan LM. Layered Silicate Clays as Templates for Anisotropic Gold Nanoparticle Growth. Chem Mater. 2016;28(14):5131-9.

67. Niu CX, Song QW, He G, Na N, Ouyang J. Near-Infrared-Fluorescent Probes for Bioapplications Based on Silica-Coated Gold Nanobipyramids with Distance-Dependent Plasmon-Enhanced Fluorescence. Anal Chem. 2016;88(22):11062-9.

68. Rajeshwar K. Solar Energy Conversion and Environmental Rennediation Using Inorganic Semiconductor-Liquid Interfaces: The Road Traveled and the Way Forward. J Phys Chem Lett. 2011;2(11):1301-9.

69. Martinsson E, Shahjamali MM, Large N, Zaraee N, Zhou Y, Schatz GC, et al. Influence of Surfactant Bilayers on the Refractive Index Sensitivity and Catalytic Properties of Anisotropic Gold Nanoparticles. Small. 2016;12(3):330-42.

70. Lan JY, Zhou XM, Liu G, Yu JG, Zhang JC, Zhi LJ, et al. Enhancing photocatalytic activity of one-dimensional KNbO3 nanowires by Au nanoparticles under ultraviolet and visible-light. Nanoscale. 2011;3(12):5161-7.

71. Yoo H, Millstone JE, Li S, Jang JW, Wei W, Wu J, et al. Core-shell triangular bifrustums. Nano Lett. 2009;9(8):3038-41.

72. Schmid G, Corain B. Nanoparticulated Gold: Syntheses, Structures, Electronics, and Reactivities. Eur J Inorg Chem. 2003;2003(17):3081-98.

73. Hutter E, Fendler JH. Exploitation of localized surface plasmon resonance. Adv Mater. 2004;16(19):1685-706.

74. Faraday M. The Bakerian Lecture: Experimental Relations of Gold (and Other Metals) to Light. Philosophical Transactions of the Royal Society of London. 1857;147:145-81.

75. Turkevich J, Stevenson PC, Hillier J. A study of the nucleation and growth processes in the synthesis of colloidal gold. Discuss Faraday Soc. 1951;11(0):55-75.

76. Turkevich J, Stevenson PC, Hillier J. A Study of the Nucleation and Growth Processes in the Synthesis of Colloidal Gold. Discuss Faraday Soc. 1951(11):55-&.

77. Possin GE. A Method for Forming Very Small Diameter Wires. Review of Scientific Instruments. 1970;41(5):772-4.

78. Tong W, Ye HP, Zhu HH, Dsouza VT. Photooxidation of Substituted Benzyl Alcohol by Riboflavin. Theochem-J Mol Struc. 1995;333(1-2):19-27.

79. Cooper E, Leggett GJ. Static secondary ion mass spectrometry studies of self-assembled monolayers: Influence of adsorbate chain length and terminal functional group on rates of photooxidation of alkanethiols on gold. Langmuir. 1998;14(17):4795-801.

80. Fukuzumi S, Kuroda S. Photooxidation of benzyl alcohol derivatives by oxygen, catalyzed by protonated flavin analogues. Res Chem Intermediat. 1999;25(8):789-811.

81. Drizhd LP, Bondarenko LI, Litvinenko LM, Savelova VA, Kirichenko AI. Mechanism of Catalysis of 4-N-N-Dimethylaminopyridine in the Reaction of 4-N,N-Dimethylaminobenzoylchloride with Benzyl Alcohol in Methylene-Chloride. Zh Org Khim+. 1984;20(11):2394-400.

82. Sardar R, Funston AM, Mulvaney P, Murray RW. Gold Nanoparticles: Past, Present, and Future. Langmuir. 2009;25(24):13840-51.

83. Zhao PX, Li N, Astruc D. State of the art in gold nanoparticle synthesis. Coordin Chem Rev. 2013;257(3-4):638-65.

84. Niidome Y, Haine AT, Niidome T. Anisotropic Gold-based Nanoparticles: Preparation, Properties, and Applications. Chem Lett. 2016;45(5):488-98.

85. Zheng J, Zhang CW, Dickson RM. Highly fluorescent, water-soluble, size-tunable gold quantum dots. Phys Rev Lett. 2004;93(7).

86. Zhong C-J, Maye M, Luo J, Han L, Kariuki N. Nanoparticles in Catalysis. In: Rotello V, editor. Nanoparticles. Nanostructure Science and Technology: Springer US; 2004. p. 113-43.

87. Kunkely H, Vogler A. Photolysis of XeF2 in CH3CN in the presence of colloidal gold: photooxidation of the elemental metal. Inorg Chim Acta. 2004;357(8):2407-9.

88. Eustis S, El-Sayed MA. Why gold nanoparticles are more precious than pretty gold: Noble metal surface plasmon resonance and its enhancement of the radiative and nonradiative properties of nanocrystals of different shapes. Chem Soc Rev. 2006;35(3):209-17.

89. Kimling J, Maier M, Okenve B, Kotaidis V, Ballot H, Plech A. Turkevich method for gold nanoparticle synthesis revisited. J Phys Chem B. 2006;110(32):15700-7.

90. Cha S-H, Kim J-U, Kim K-H, Lee J-C. Preparation of gold nanosheets using poly(ethylene oxide)–poly(propylene oxide)–poly(ethylene oxide) block copolymers via photoreduction. Materials Science and Engineering: B. 2007;140(3):182-6.

91. Zanella R, Giorgio S, Henry CR, Louis C. Alternative Methods for the Preparation of Gold Nanoparticles Supported on TiO2. The Journal of Physical Chemistry B. 2002;106(31):7634-42.

92. Bond GC, Louis C, Thompson D. Catalysis by gold (Catalytic Science Series, vol. 6). Ed GJ Hutchings, Imperial College Press, London. 2006.

93. Grunwaldt J-D, Kiener C, Wögerbauer C, Baiker A. Preparation of Supported Gold Catalysts for Low-Temperature CO Oxidation via "Size-Controlled" Gold Colloids. J Catal. 1999;181(2):223-32.

94. Rodríguez-Fernández J, Pérez−Juste J, Liz−Marzán LM, Lang PR. Dynamic Light Scattering of Short Au Rods with Low Aspect Ratios. The Journal of Physical Chemistry C. 2007;111(13):5020-5.

95. Xia Y, Xia X, Peng HC. Shape-Controlled Synthesis of Colloidal Metal Nanocrystals: Thermodynamic versus Kinetic Products. J Am Chem Soc. 2015;137(25):7947-66.

96. Yu YY, Chang SS, Lee CL, Wang CRC. Gold nanorods: Electrochemical synthesis and optical properties. J Phys Chem B. 1997;101(34):6661-4.

97. Jana NR, Gearheart L, Murphy CJ. Wet chemical synthesis of high aspect ratio cylindrical gold nanorods. J Phys Chem B. 2001;105(19):4065-7.

98. Helgeson ME, Hodgdon TK, Kaler EW, Wagner NJ. A systematic study of equilibrium structure, thermodynamics, and rheology of aqueous CTAB/NaNO3 wormlike micelles. J Colloid Interf Sci. 2010;349(1):1-12.

99. Gao JX, Bender CM, Murphy CJ. Dependence of the gold nanorod aspect ratio on the nature of the directing surfactant in aqueous solution. Langmuir. 2003;19(21):9065-70.

100. Osinkina L, Lohmuller T, Jackel F, Feldmann J. Synthesis of Gold Nanostar Arrays as Reliable, Large-Scale, Homogeneous Substrates for Surface-Enhanced Raman Scattering Imaging and Spectroscopy. J Phys Chem C. 2013;117(43):22198-202.

101. Kumar PS, Pastoriza-Santos I, Rodriguez-Gonzalez B, Garcia de Abajo FJ, Liz-Marzan LM. High-yield synthesis and optical response of gold nanostars. Nanotechnology. 2008;19(1).

102. Yuan HK, Khoury CG, Hwang H, Wilson CM, Grant GA, Vo-Dinh T. Gold nanostars: surfactant-free synthesis, 3D modelling, and two-photon photoluminescence imaging. Nanotechnology. 2012;23(7).

103. Zhong Z, Ho J, Teo J, Shen S, Gedanken A. Synthesis of Porous α-Fe₂O₃ Nanorods and Deposition of Very Small Gold Particles in the Pores for Catalytic Oxidation of CO. Chem Mater. 2007;19(19):4776-82.

104. Zhong Z, Teo J, Lin M, Ho J. Synthesis of Porous α-Fe2O3 Nanorods as Catalyst Support and A Novel Method to Deposit Small Gold Colloids on Them. Top Catal. 2008;49(3):216-26.

105. Zhong ZY, Lin JY, Teh SP, Teo J, Dautzenberg FM. A rapid and efficient method to deposit gold particles on catalyst supports and its application for CO oxidation at low temperatures. Adv Funct Mater. 2007;17(8):1402-8.

106. Lin C, Tao K, Hua DY, Ma Z, Zhou SH. Size Effect of Gold Nanoparticles in Catalytic Reduction of p-Nitrophenol with NaBH4. Molecules. 2013;18(10):12609-20.

107. bin Saiman MI, Brett GL, Tiruvalam R, Forde MM, Sharples K, Thetford A, et al. Involvement of Surface-Bound Radicals in the Oxidation of Toluene Using Supported Au-Pd Nanoparticles. Angew Chem Int Edit. 2012;51(24):5981-5.

108. Lopez-Sanchez JA, Dimitratos N, Miedziak P, Ntainjua E, Edwards JK, Morgan D, et al. Au-Pd supported nanocrystals prepared by a sol immobilisation technique as catalysts for selective chemical synthesis. Phys Chem Chem Phys. 2008;10(14):1921-30.

109. Huang XM, Wang XG, Wang XS, Wang XX, Tan MW, Ding WZ, et al. P123-stabilized Au-Ag alloy nanoparticles for kinetics of aerobic oxidation of benzyl alcohol in aqueous solution. J Catal. 2013;301:217-26.

110. Lopez-Sanchez JA, Dimitratos N, Hammond C, Brett GL, Kesavan L, White S, et al. Facile removal of stabilizer-ligands from supported gold nanoparticles. Nat Chem. 2011;3(7):551-6.

111. Graf C, Vossen DLJ, Imhof A, van Blaaderen A. A general method to coat colloidal particles with silica. Langmuir. 2003;19(17):6693-700.

112. Verma MS, Chen PZ, Jones L, Gu FX. Branching and size of CTAB-coated gold nanostars control the colorimetric detection of bacteria. Rsc Adv. 2014;4(21):10660-8.

113. Lu WT, Singh AK, Khan SA, Senapati D, Yu HT, Ray PC. Gold Nano-Popcorn-Based Targeted Diagnosis, Nanotherapy Treatment, and In Situ Monitoring of Photothermal Therapy Response of Prostate Cancer Cells Using Surface-Enhanced Raman Spectroscopy. J Am Chem Soc. 2010;132(51):18103-14.

114. Ye W, Yu J, Zhou Y, Gao D, Wang D, Wang C, et al. Green synthesis of Pt–Au dendrimer-like nanoparticles supported on polydopamine-functionalized graphene and their high performance toward 4- nitrophenol reduction. Applied Catalysis B: Environmental. 2016;181:371-8.

115. Xu D, Bliznakov S, Liu Z, Fang J, Dimitrov N. Composition-Dependent Electrocatalytic Activity of Pt-Cu Nanocube Catalysts for Formic Acid Oxidation. Angewandte Chemie International Edition. 2010;49(7):1282-5.

116. Fu Q, Yang F, Bao X. Interface-Confined Oxide Nanostructures for Catalytic Oxidation Reactions. Accounts Chem Res. 2013;46(8):1692-701.

117. Khoudiakov M, Gupta MC, Deevi S. Au/Fe2O3 nanocatalysts for CO oxidation: A comparative study of deposition–precipitation and coprecipitation techniques. Applied Catalysis A: General. 2005;291(1):151-61.

118. Gedanken A, Tang X, Wang Y, Perkas N, Koltypin Y, Landau MV, et al. Using Sonochemical Methods for the Preparation of Mesoporous Materials and for the

Deposition of Catalysts into the Mesopores. Chemistry – A European Journal. 2001;7(21):4546-52.

119. Bhattacharyya S, Gabashvili A, Perkas N, Gedanken A. Sonochemical Insertion of Silver Nanoparticles into Two-Dimensional Mesoporous Alumina. The Journal of Physical Chemistry C. 2007;111(30):11161-7.

120. Suslick KS, Price GJ. APPLICATIONS OF ULTRASOUND TO MATERIALS CHEMISTRY. Annual Review of Materials Science. 1999;29(1):295-326.

121. Suslick KS, Choe S-B, Cichowlas AA, Grinstaff MW. Sonochemical synthesis of amorphous iron. Nature. 1991;353:414.

122. Grunwaldt J-D, Maciejewski M, Becker OS, Fabrizioli P, Baiker A. Comparative Study of Au/TiO2 and Au/ZrO2 Catalysts for Low-Temperature CO Oxidation. J Catal. 1999;186(2):458-69.

123. Porta F, Prati L, Rossi M, Scari G. New Au(0) Sols as Precursors for Heterogeneous Liquid-Phase Oxidation Catalysts. J Catal. 2002;211(2):464-9.

124. Risse T, Shaikhutdinov S, Nilius N, Sterrer M, Freund HJ. Gold supported on thin oxide films: From single atoms to nanoparticles. Accounts Chem Res. 2008;41(8):949-56.

125. Brown GE, Henrich VE, Casey WH, Clark DL, Eggleston C, Felmy A, et al. Metal oxide surfaces and their interactions with aqueous solutions and microbial organisms. Chem Rev. 1999;99(1):77-174.

126. Ma Z, Dai S, Chen YW, Jin R, Kang Y, Han YF, et al. Heterogeneous Gold Catalysts and Catalysis: Royal Society of Chemistry; 2014.

127. Zhong ZY, Luo JZ, Ang TP, Highfield J, Lin JY, Gedanken A. Controlled organization of Au colloids into linear assemblies. J Phys Chem B. 2004;108(47):18119-23.

128. Zhong ZY, Patskovskyy S, Bouvrette P, Luong JHT, Gedanken A. The surface chemistry of Au colloids and their interactions with functional amino acids. J Phys Chem B. 2004;108(13):4046-52.

129. Perkas N, Teo J, Shen S, Wang Z, Highfield J, Zhong Z, et al. Supported Ru catalysts prepared by two sonication-assisted methods for preferential oxidation of CO in H2. Phys Chem Chem Phys. 2011;13(34):15690-8.

130. Linic S, Christopher P, Ingram DB. Plasmonic-metal nanostructures for efficient conversion of solar to chemical energy. Nat Mater. 2011;10(12):911-21.

131. Rajeshwar K, Thomas A, Janaky C. Photocatalytic Activity of Inorganic Semiconductor Surfaces: Myths, Hype, and Reality. J Phys Chem Lett. 2015;6(1):139-47.

132. Veres A, Menesi J, Janaky C, Samu GF, Scheyer MK, Xu QS, et al. New insights into the relationship between structure and photocatalytic properties of TiO2 catalysts. Rsc Adv. 2015;5(4):2421-8.

133. Cybula A, Priebe JB, Pohl M-M, Sobczak JW, Schneider M, Zielińska-Jurek A, et al. The effect of calcination temperature on structure and photocatalytic properties of Au/Pd nanoparticles supported on TiO2. Applied Catalysis B: Environmental. 2014;152-153:202-11.

134. Gao H, McMahon JM, Lee MH, Henzie J, Gray SK, Schatz GC, et al. Rayleigh anomaly-surface plasmon polariton resonances in palladium and gold subwavelength hole arrays. Opt Express. 2009;17(4):2334-40.

135. Pakizeh T, Langhammer C, Zorić I, Apell P, Käll M. Intrinsic fano interference of localized plasmons in Pd nanoparticles. Nano Lett. 2009;9(2):882-6.

136. Lee YW, Kim NH, Lee KY, Kwon K, Kim M, Han SW. Synthesis and characterization of flower-shaped porous Au-Pd alloy nanoparticles. J Phys Chem C. 2008;112(17):6717-22.

137. Hu W, Chen H, Li CM. One-step synthesis of monodisperse gold dendrite@polypyrrole core-shell nanoparticles and their enhanced catalytic durability. Colloid Polym Sci. 2014;293(2):505-12.

138. Lang XF, Yin PG, You TT, Guo L. Chemical Effects in SERS of Pyrazine Adsorbed on Au–Pd Bimetallic Nanoparticles: A Theoretical Investigation. Chemphyschem. 2012;13(1):237-44.

139. Zhang Q, Guo X, Liang Z, Zeng J, Yang J, Liao S. Hybrid PdAg alloy-Au nanorods: Controlled growth, optical properties and electrochemical catalysis. Nano Res. 2013;6(8):571-80.

140. Nakagawa T, Nitani H, Tanabe S, Okitsu K, Seino S, Mizukoshi Y, et al. Structural analysis of sonochemically prepared Au/Pd nanoparticles dispersed in porous silica matrix. Ultrason Sonochem. 2005;12(4):249-54.

141. Kahlich MJ, Gasteiger HA, Behm RJ. Kinetics of the Selective CO Oxidation in H2-Rich Gas on Pt/Al2O3. J Catal. 1997;171(1):93-105.

142. Mariño F, Descorme C, Duprez D. Noble metal catalysts for the preferential oxidation of carbon monoxide in the presence of hydrogen (PROX). Applied Catalysis B: Environmental. 2004;54(1):59-66.

143. Yoshihara J, Campbell CT. Methanol Synthesis and Reverse Water–Gas Shift Kinetics over Cu(110) Model Catalysts: Structural Sensitivity. J Catal. 1996;161(2):776-82.

144. Tiruvalam RC, Pritchard JC, Dimitratos N, Lopez-Sanchez JA, Edwards JK, Carley AF, et al. Aberration corrected analytical electron microscopy studies of sol-immobilized Au plus Pd, Au{Pd} and Pd{Au} catalysts used for benzyl alcohol oxidation and hydrogen peroxide production. Faraday Discussions. 2011;152:63-86.

145. Link S, Mohamed MB, El-Sayed MA. Simulation of the Optical Absorption Spectra of Gold Nanorods as a Function of Their Aspect Ratio and the Effect of the

Medium Dielectric Constant. The Journal of Physical Chemistry B. 1999;103(16):3073-7.

146. Kim F, Song JH, Yang P. Photochemical synthesis of gold nanorods. J Am Chem Soc. 2002;124(48):14316-7.

147. John CL, Strating SL, Shephard Ka, Zhao JX. Reproducibly synthesize gold nanorods and maintain their stability. Rsc Adv. 2013;3(27):10909-.

148. Priecel P, Salami HA, Padilla RH, Zhong ZY, Lopez-Sanchez JA. Anisotropic gold nanoparticles: Preparation and applications in catalysis. Chinese J Catal. 2016;37(10):1619-50.

149. Link S, El-Sayed MA, Link S, El-Sayed MA. Spectral Properties and Relaxation Dynamics of Surface Plasmon Electronic Oscillations in Gold and Silver Nanodots and Nanorods. The Journal of Physical Chemistry B. 1999;103(40):8410-26.

150. Limmer SJ, Chou TP, Cao GZ. Formation and optical properties of cylindrical gold nanoshells on silica and titania nanorods. P Soc Photo-Opt Ins. 2002;4809:222-30.

151. Li X, Yang Y, Zhou G, Han S, Wang W, Zhang L, et al. The unusual effect of AgNO3 on the growth of Au nanostructures and their catalytic performance. Nanoscale. 2013;5(11):4976-85.

152. Yu, Chang S-S, Lee C-L, Wang CRC. Gold Nanorods: Electrochemical Synthesis and Optical Properties. The Journal of Physical Chemistry B. 1997;101(34):6661-4.

153. Manna A, Chen PL, Akiyama H, Wei TX, Tamada K, Knoll W. Optimized photoisomerization on gold nanoparticles capped by unsymmetrical azobenzene disulfides. Chem Mater. 2003;15(1):20-8.

154. Mitamura K, Imae T. Functionalization of Gold Nanorods Toward Their Applications. Plasmonics. 2008;4(1):23-30.

155. Jana NR, Gearheart L, Murphy CJ. Seed-Mediated Growth Approach for Shape-Controlled Synthesis of Spheroidal and Rod-like Gold Nanoparticles Using a Surfactant Template. Adv Mater. 2001;13(18):1389-93.

156. Ohtani B, Prieto-Mahaney OO, Li D, Abe R. What is Degussa (Evonik) P25? Crystalline composition analysis, reconstruction from isolated pure particles and photocatalytic activity test. J Photoch Photobio A. 2010;216(2-3):179-82.

157. Primo A, Corma A, Garcia H. Titania supported gold nanoparticles as photocatalyst. Phys Chem Chem Phys. 2011;13(3):886-910.

158. Alhumaimess M, Lin ZJ, He Q, Lu L, Dimitratos N, Dummer NF, et al. Oxidation of Benzyl Alcohol and Carbon Monoxide Using Gold Nanoparticles Supported on MnO2 Nanowire Microspheres. Chem-Eur J. 2014;20(6):1701-10.

159. Choudhary VR, Dumbre DK. Supported Nano-Gold Catalysts for Epoxidation of Styrene and Oxidation of Benzyl Alcohol to Benzaldehyde. Top Catal. 2009;52(12):1677-87.

160. Zhang XG, Ke XB, Zhu HY. Zeolite-Supported Gold Nanoparticles for Selective Photooxidation of Aromatic Alcohols under Visible-Light Irradiation. Chem-Eur J. 2012;18(26):8048-56.

161. DeJong E, Dam R, Sipos L, Den Ouden D, Gruter GJ. Furandicarboxylic acid (FDCA) a versatile building block for a very interesting class of polyesters. Abstr Pap Am Chem S. 2011;241.

162. Gruter GJM, Sipos L, Dam MA. Accelerating Research into Bio-Based FDCA-Polyesters by Using Small Scale Parallel Film Reactors. Comb Chem High T Scr. 2012;15(2):180-8.

163. Hrelescu C, Sau TK, Rogach AL, Jäckel F, Feldmann J. Single gold nanostars enhance Raman scattering. Appl Phys Lett. 2009;94(15):153113.

164. Giorgetti E, Trigari S, Rindi A, Margheri G, Sottini S, Dellepiane G, et al. Tunable gold nanostars for surface enhanced Raman spectroscopy. Physica Status Solidi (B). 2012;249(6):1188-92.

165. Guerrero-Martínez A, Barbosa S, Pastoriza-Santos I, Liz-Marzán LM. Nanostars shine bright for you: Colloidal synthesis, properties and applications of branched metallic nanoparticles. Current Opinion in Colloid & Interface Science. 2011;16(2):118-27.

166. Cui Q, Xia B, Mitzscherling S, Masic A, Li L, Bargheer M, et al. Preparation of gold nanostars and their study in selective catalytic reactions. Colloids and Surfaces A: Physicochemical and Engineering Aspects. 2015;465:20-5.

m